A DFT STUDY OF ETHYLENE ADSORPTION AND HYDROGENATION MECHANISMS ON NICKEL

A THESIS SUBMITTED TO
THE GRADUATE SCHOOL OF NATURAL AND APPLIED SCIENCES
OF
MIDDLE EAST TECHNICAL UNIVERSITY

BY

NUSRET DUYGU YILMAZER

IN PARTIAL FULFILLMENT OF THE REQUIREMENTS
FOR
THE DEGREE OF MASTER OF SCIENCE
IN
CHEMICAL ENGINEERING

MAY 2010

Approval of the thesis:

A DFT STUDY OF ETHYLENE ADSORPTION AND HYDROGENATION MECHANISMS ON NICKEL

Submitted by **NUSRET DUYGU YILMAZER** in partial fulfillment of the requirements for the degree of **Master of Science in Chemical Engineering Department, Middle East Technical University** by,

Prof. Dr. Canan Özgen _____
Dean, Graduate School of **Natural and Applied Sciences**

Prof. Dr. Gürkan Karakaş _____
Head of Department, **Chemical Engineering**

Prof. Dr. Işık Önal _____
Supervisor, **Chemical Engineering Dept., METU**

Examining Committee Members:

Prof. Dr. Hayrettin Yücel _____
Chemical Engineering Department, METU

Prof. Dr. Işık Önal _____
Chemical Engineering Department, METU

Prof. Dr. Saim Özkar _____
Chemistry Department, METU

Prof. Dr. Şinasi Ellialtıoğlu _____
Physics Department, METU

Prof. Dr. Mehmet Çakmak _____
Physics Department, Gazi University

Date: 4th May, 2010

I hereby declare that all information in this document has been obtained and presented in accordance with academic rules and ethical conduct. I also declare that, as required by these rules and conduct, I have fully cited and referenced all material and results that are not original to this work.

Name, Last name: Nusret Duygu YILMAZER

Signature:

ABSTRACT

A DFT STUDY OF ETHYLENE ADSORPTION AND HYDROGENATION MECHANISMS ON NICKEL

Yılmazer, Nusret Duygu

M.Sc., Department of Chemical Engineering

Supervisor: Prof. Dr. Işık Önal

May 2010, 115 pages

Ethylene adsorption was studied by use of DFT/B3LYP with basis set 6-31G(d,p) in Gaussian'03 software. It was found that ethylene adsorbs molecularly on the Ni_{13} nanocluster with π adsorption mode. π adsorption mode is studied for the Ni_{10} (1 1 1), Ni_{13} (1 0 0) and Ni_{10} (1 1 0) surface cluster as well. Relative energy values were calculated as −50.86 kcal/mol, −20.48 kcal/mol, −32.44 kcal/mol and −39.27 kcal/mol for Ni_{13} nanocluster, Ni_{10} (1 1 1), Ni_{13} (1 0 0) and Ni_{10} (1 1 0) surface cluster models, respectively. Ethylene adsorption energy was found inversely proportional to Ni coordination number when Ni_{10} (1 1 1), Ni_{13} (1 0 0) and Ni_{10} (1 1 0) cluster models and Ni_{13} nanocluster were compared with each other.

DFT/B3LYP and basis set of 86-411(41d)G in Gaussian'03 was used to investigate Ni_{55} nanocluster. Ethylene adsorption on Ni_{55} nanocluster was studied by means of equilibrium geometry calculations with π adsorption modes for two different coordination numbers as 6 and 8. The related adsorption energies were

approximately found as -22.07 and -14.82 kcal/mol for these coordination numbers of surfaces, respectively.

In addition, the binding energies stated in literature that are for Ni_2 dimer and Ni_{13} nanoclusters were considered together with our binding energy results for Ni_{55} nanocluster. Accordingly, when a correlation line was drawn and the intercept of binding energies was obtained against the value of "$n^{-1/3}$" ;where n is the number of atoms in the cluster; the result of interception gives a good estimation for bulk nickel binding energy at infinite "n". This interception result was found as 4.58 eV/atom where the experimental value is reported as 4.45 eV/atom for bulk in the literature.

Ehtylene hydrogenation mechanisms were also investigated in terms of the resultant geometries and total energy required for the related mechanism steps.

Keywords: Ethylene adsorption, ethylene hydrogenation mechanism, binding energy, nickel nanocluster, nanosurface, DFT.

ÖZ

NİKEL ÜZERİNDE ETİLEN ADSORPSİYONUNUN VE HİDROJENLENME MEKANİZMALARININ DFT ÇALIŞMASI

Nusret Duygu Yılmazer
Yüksek Lisans, Kimya Mühendisliği Bölümü
Tez Yöneticisi: Prof. Dr. Işık Önal

Mayıs 2010, 115 sayfa

Etilen adsorpsiyonu, DFT/B3LYP ile 6-31G(d,p) basis set'ini kullanarak Gaussian'03 yazılımı ile çalışılmıştır. Etilenin Ni_{13} nanokümesi üzerinde moleküler olarak π adsorpsiyon moduyla adsorbe olduğu gözlemlenmiştir. π adsorpsiyon modu aynı zamanda Ni_{10} (1 1 1), Ni_{13} (1 0 0) and Ni_{10} (1 1 0) yüzey kümeleri için de çalışılmıştır. Bağıl enerji değerleri sırasıyla Ni_{13} nanokümesi, Ni_{10}(1 1 1), Ni_{13}(1 0 0) ve Ni_{10}(1 1 0) yüzey küme modelleri için −50.86 kcal/mol, −20.48 kcal/mol, −32.44 kcal/mol ve −39.27 kcal/mol olarak hesaplanmıştır. Etilen adsorpsiyon enerjisi için, Ni_{10} (1 1 1), Ni_{13} (1 0 0) and Ni_{10} (1 1 0) yüzey küme modelleri ve Ni_{13} nanokümesi birbirleriyle kıyaslandığında ise, Ni koordinasyon sayısıyla ters orantılıdır.

DFT/B3LYP ve Gaussian'03'teki 86-411(41d)G basis seti Ni_{55} nanokümesini incelemek için kullanılmıştır. Ni_{55} nanokümesi üzerindeki etilen adsorpsiyonu denge geometrisi hesaplarıyla "6 ve 8" gibi iki farklı koordinasyon sayısı için π adsorpsiyon moduyla çalışılmıştır. Bahsedilen adsorpsiyon enerjileri, sırasıyla bu yüzey koordinasyon sayıları için yaklaşık olarak -22.07 ve -14.82 kcal/mol olarak bulunmuştur.

Buna ek olarak, literatürde Ni_2 dimer ve Ni_{13} nanokümesi için yer alan bağlanma enerjisi değerleri, bu çalışmadaki Ni_{55} nanokümesi için hesapladığımız bağlanma enerjisi değerleri ile beraber değerlendirilmiştir. Burada, bahsi geçen "n" sayısının kümedeki atom sayısını tanımlayan bir nicelik olduğu belirtilirse, sözü geçen bağlanma enerjisi değerlerinin, "$n^{-1/3}$" niceliğine göre bir korelasyon doğrusu çizildiğinde, sonsuz "n" değeri için denk gelen kesişme noktası, deneysel literatür göz önünde bulundurulduğunda yığın nikel için iyi bir yakınsama sonucu çıkarmaktadır. Bu kesişme noktasının bahsedilen deneysel literatür değeri 4.45 eV/atom olarak belirtlmiştir ve bizim çalışmamızda bu değer 4.58 eV/atom olarak hesaplanmıştır.

Ni_{13} nanokümesinin üzerindeki etilen adsorpsiyonu çalışmasının devamı olarak etilen hidrojenlenme mekanizmaları da incelenmiş, sonuç geometrileri ve ilgili mekanizma basamakları için gereken toplam enerjiler cinsinden değerlendirilmiştir.

Anahtar Kelimeler: Etilen adsorpsiyonu, etilen hidrojenlenme mekanizma, bağlanma enerjisi, nikel nanoküme, nanoyüzey, DFT

To My Family

ACKNOWLEDGEMENTS

Firstly, I would like to express my sincere gratitude to my supervisor, Prof. Dr. Işık Önal for his guidance, advice and support throughout this research.

Foremost, I would like to express my sincere thanks to Dr. Mehmet Ferdi Fellah for his endless support, kindness and great contribution to this study.

I sincerely would like to thank to my dear instructers Prof. Dr. Volkan Ş. Ediger, Prof. Dr. Canan Özgen, Prof. Dr. Hayrettin Yücel and Dr. Cevdet Öztin for their great care throughout my academic programs.

I would like to thank so much to my examining committee members, Prof. Dr. Saim Özkar, Prof. Dr. Şinasi Ellialtıoğlu and Prof. Dr. Mehmet Çakmak for their great kindness.

I would like to express my sincere thanks to T.R. Prime Ministry State Planning Organization together with EDAM members; Niyazi İlter, Dr. Sema Bayazıt and Sinan Ülgen especially for their support, understanding and kindness throughout my academic program.

I am grateful to my dear friends Hale Ay, Güzide Aydın, Dominic Deo Androga, Elif Aydın, Murat Cengiz, Süleyman Cincioğlu, Rezan Erdoğan, Murat Erdoğan, Martin Hillenga, Deniz İşcen, H. Murat İşler, Ersin Murad, Ahmet Naiboğlu, Saltuk Pirgalıoğlu, A. Ceren Satıoğlu, Tamer Sarıoğlu, Canan Turgut and Murat Yükselen for their great care and friendship giving me strength and encouragement all the time.

Lastly, I deeply thank my family for their great support and love. I cordially thank E. Canan Yılmazer, Servet Yılmazer, Nuran Ergün, Nusret Durak, Nevzat Oruç, B. Yılmaz Durak, Nevin Kadı, F. Nuran Durak, Derya Emirleroğlu, Fatma Kadı,for their endless love and encouragement.

This research was supported in part by TUBITAK through TR-Grid e-Infrastructure Project. TR-Grid systems are hosted by TUBITAK ULAKBIM and Middle East Technical University.

TABLE OF CONTENTS

LIST OF TABLES

TABLES

LIST OF FIGURES

FIGURES

LIST OF SYMBOLS AND ABBREVIATIONS

ADF:	Amsterdam Density Functional
B3LYP:	Becke's three-parameter exchange functional (B3) with the Lee, Yang, and Parr (LYP) correlation functional
CEM:	Corrected effective medium
CN:	Coordination number
DBF:	Daw, Baskes and Foiles
DFT:	Density Functional Theory
EAM:	Embedded-atom method
EG:	Equilibrium geometry
FS:	Fusion sensitivity
GGA:	Generalized gradient approximation
GSA:	Generalized Simulated Annealing
HREEL:	High-resolution Electron Energy Loss
IC, ICO:	Icosahedral
LCGTO-LDF:	Linear combination of gaussian-type orbitals-local density functional
MD/MC-CEM:	Molecular Dynamics/Monte Carlo-Corrected Effective Medium.
MIC:	Mackay Icosahedral
QC:	Quantum Chemistry
RPBE:	Revised Perdew-Burke-Ernzerhof
SPE:	Single Point Energy Calculations
TB:	Tight Binding
TBMD:	Tight-binding Molecular Dynamics
USPP:	Ultra-soft pseudopotentials
VASP:	Vienna ab initio simulation package

CHAPTER 1

INTRODUCTION

1.1 Nanotechnology and quantum chemistry in the field of catalysis

Research efforts in nano-science and nanotechnology have grown worldwide where atoms, molecules, clusters and nano-particles are used as the functional building blocks for developing advanced and new phases of condensed matter on the nanometer length scale. The optimal size of these unit components depend on the particular property to be engineered; altering the dimensions of the building blocks, controlling their surface geometry, chemistry and assembly. The major focus is miniaturization of particles to be used in different fields such as the semiconductor and biomedical industries. The development of this multidisciplinary field has been accelerated by the advent of recent technologies that allow the visualization, design, characterization and manipulation of nanoscale systems. Techniques such as scanning probe microscopy (SPM), scanning tunnelling microscopy (STM), atomic force microscopy (AFM), scanning near-field optical microscopy (SNOM), magnetic force microscopy (MFM) and piezo-response force microscopy (PFM) are largely responsible for the emergence of nano-science as a novel field of research. (Rosei, 2004)

Many of the current experimental and industrially applied catalytic processes require funding and lead to the release of poisonous volatile organics, chlorofluorocarbons and sulfur compounds which are malignant to the environment. However, the use of advanced softwares for theoretical modeling and simulation of nanocluster structures are cost efficient and environmental

friendly. They also enable better control of matter organization at the nano scale science thus lead to production of highly efficient catalysts.

Among these theoretical developments, mainly two directions are emerging in the catalysis field, such as *the creation of metal clusters with controllable sizes and shapes*, and *the spontaneous formation of organized nanopatterns at surfaces* to increase the rate of numerous reactions that even sometimes would not occur at the human time scale (Filhol et al., 2004). As a result such improvements provide new insights into the nature of chemical bonds and surface reactivity which provides the ability to manipulate matter with atomic scale precision.

Quantum chemistry (QC), is a powerful tool that is used to complement experimental efforts for providing reliable energetic and kinetic data of complex reaction systems. Primarily focusing on the adsorbate-surface interaction at specific sites on model catalytic systems, QC calculations are employed to predict binding energies and energies of activation for elementary steps at active sites, where this data can also be used to help construct more robust molecular simulation algorithms. (Neurock and Hansen, 1998)

Throughout the calculations the appropriate choice of the model cluster or surface, along with careful optimization of geometry and the electronic spin-state can typically yield bond and adsorption energies that are within known experimental values by 5 kcal/mol where the optimization is achieved by manipulating the overall process parameters to meet the desired performance measures. (Neurock and Hansen, 1998)

1.2 Scope of Thesis

The aim of this study was first to perform equilibrium geometry calculations for ethylene adsorption on optimized nickel Ni_{13} nanocluster and $Ni_{10}(111)$, $Ni_{13}(100)$ and $Ni_{10}(110)$ surface cluster models by using Density Functional Theory (DFT) with B3LYP basis set and 6-31G(d,p) method. A comparison for ethylene adsorption energy is made as a function of the coordination number of Ni atom of the active site.

Equilibrium geometry calculations for ethylene adsorption on nickel Ni_{55} nanocluster is also performed by using DFT/B3LYP/86-411(41d)G method. A comparison for ethylene adsorption energy with Ni_{55} nanocluster is made as a function of the coordination number of Ni atom of the active site with two different coordination numbers for the Ni_{55} nanocluster.

In addition, for Ni_{13} nanocluster, after ethylene adsorption is studied, different types of ethylene hydrogenation mechanisms are also investigated on a molecular basis in order to have an assessment of knowledge for nanocluster behaviors as a model in reaction kinetics.

CHAPTER 2

LITERATURE SURVEY

2.1 Nickel as a Catalyst

The development of efficient catalysts that are reliable and cost effective depends on the choice of metals to be used in the design. The choice of the substrate, as well as the support, influence catalyst performance through electronic interactions, spillover and migration effects (Park and Keane, 2004).

It is also known that, the adsorption structure and geometry of small hydrocarbons on transition metal surfaces is of great importance in order to understand surface kinetics and detailed reaction mechanisms in heterogeneous catalysis. The metals of group 10 (Ni, Pd and Pt) are very important catalysts in a large variety of chemical reactions such as hydrogenations/dehydrogenations, isomerizations and total oxidations (Bernardo and Gomes, 2001b). Ni nanocluster catalysts have a potential of having high activity and selectivity particularly in hydrocarbon hydrogenation reactions as compared to traditional supported Ni catalysts. (Schmid et al., 1996)

2.2 Ethylene Adsorption Reactions on Nickel Nanoclusters and Surfaces

2.2.1 Ethylene in Hydrocarbon Reactions

Among the hydrocarbons, ethylene is a crucial intermediate in many industrial reactions. One of the most important of these reactions is ethylene polymerization. Ethylene is produced by thermal or catalytic cracking of higher hydrocarbons, which also generates impurities, such as acetylene, that can poison

traditional polymerization catalysts as an industrial case (Huang et al., 2007). In addition to these, in terms of theoretical calculation studies, ethylene provides a great model for quantum chemical computations while investigating some main hydrocarbon reactions.

2.2.2 Ethylene Adsorption Reaction on Nickel

2.2.2.1 Ethylene Adsorption Modes and the Hydrogenation Mechanism

In Egawa's study (Egawa et al., 2000) it is stated that, on transition metal single crystal surfaces there are two ethylene adsorption modes generally agreed by many researchers, which are named as **π** and **di-σ adsorption modes.** However, in case of ethylene adsorption on nickel surfaces, there are some different favorings among these referred adsorption sites.

For instance, according to the notice of Huang's study (Huang et al., 2007), it has been found that there is a *cluster size dependency* for the adsorption of the ethylene molecules since they preferentially adsorb in the di-σ configuration on the larger particles, whereas π binding is favored for the small particles. The reason is associated with the π-bonded ethylene which is generally considered as the intermediate of hydrogenation species and also with the smaller particles promoting the hydrogenation of ethylene over larger particles.

However, it is emphasized in Neurock and van Santen's work (Neurock and van Santen, 2000) that ethylene is thought to be adsorbed on single-crystal transition metal surfaces in one of the following three modes; π, di-σ or the physisorbed mode. It is explained that in the π-bound chemisorption and in the physisorption modes, ethylene sits atop a single metal atom, whereas, in the di-σ-mode, ethylene binds parallel to one of the bridge metal-metal bonds forming two σ-metal-carbon bonds. However, among all these types, it is stated that the favored adsorption site is "*strongly dependent upon the electronic and the geometric structure of the exposed metal surface as well as the reaction conditions."*

Referring to Yagasaki and Masel's study (Yagasaki and Masel, 1994) it is reported that the ethylene bond orders were subsequently used to characterize whether ethylene chemisorbs in either the π- or di-σ adsorption modes depending upon the specific degree of hybridization. The π-bound intermediate is mostly sp^2 hybridized (bond order 1.5-2.0) whereas the di-σ intermediate is nearly sp^3 (bond order 1.0-1.5). Thus, in general, ethylene is thought to bind in the π-adsorption mode for metals to the far left and far right of the periodic table, whereas the di-σ mode appears to be most prevalent mode for metals that are located at the center of the transition metal series.

Moreover, Neurock and van Santen (Neurock and van Santen, 2000) suggested that the π-intermediate is more readily to react with hydrogen. They reported that according to the study of Janssens' and Zaera's (Janssens et al., 1998; Zaera, 1996) ethylene adsorbs in both π- and di-σ adsorption states. However, the π-bound exists at very low temperatures and at higher temperatures in the presence of other coadsorbates. The π-bound intermediate is stated to lead to hydrogenated products whereas the di-σ bound species is explained to lead to the formation of ethylidyne. Moreover, it is also reported in literature that (Zaera, 1996; Zaera et al., 1996; Yata and Madix, 1995; Cremer et al., 1995) the adsorbed ethylene can either hydrogenate to form ethyl and subsequently ethane or decompose to form vinyl or ethylidene. In terms of experimental conditions, reactions of ethylene to form ethylidene and ethylidene to ethylidyne are reported to occur at higher temperatures and have activation barriers that are on the order of 15-18 kcal/mol. The barriers are mentioned to be about 3-7 kcal/mol higher than that for the hydrogenation of ethylene to ethyl. Then it was there concluded that *the surface chemistry was strongly dependent upon the surface coverage and reaction conditions and so that the results depend not only upon the coverage but on the specific surface structures that form* (Land, 1992).

2.2.2.2 Ethylene Adsorption Reactions on Ni_{13} Nanocluster and Ni(111), Ni(100) and Ni(110) Surface Clusters

In the perspective mentioned above, in an experimental surface study done by Brown (Brown et al., 1999) single-crystal adsorption calorimetry is used in order to measure the heats of adsorption for hydrocarbons on single-crystal surfaces. The measured energy of adsorption of ethene on Ni(1 1 0) surface is reported as −28.68 kcal/mol. It is also concluded that π bonding is an important contribution.

In theoretical literature, spin-polarized DFT calculations on Ni(1 1 1) and Ni(2 1 1) surfaces were carried out by using DACAPO code in a study by Vang (Vang et al, 2006). They employed the RPBE generalized gradient correction self-consistently, and the core electrons of all the atoms were treated with Vanderbilt ultra-soft pseudopotentials (USPPs). The Ni(1 1 1) terrace was made out of a three-atomic-layer thick slab with a (3×2) unit cell where it gives a six-atom Ni surface unit cell. The sampling of 12 Ni(1 1 1) Monkhorst-Pack k-points was used. The topmost metal layer and chemisorbed species were relaxed in all calculations whereas the other substrate layers were kept fixed to the fcc ideal slab positions. Adsorbates were positioned only on one side of the slab. They applied two different methods to determine the transition states. In some cases the transition state was localized constraining the C–C distances or C–H distances and relaxing all other degrees of freedom. In cases where the location of transition state was not known, they used nudged elastic band method to determine transition states. According to the DFT calculations they performed, the most stable binding geometry of ethylene on both the terrace and the step edge sites was the top site.

Fahmi and van Santen (Fahmi and van Santen, 1997) presented a DFT study of the molecular adsorption of ethylene on Ni(1 1 1). They used Ni_4 and Ni_{14} clusters as models for the metal surface. For each adsorbate, they compared the di-σ and μ-bridging adsorption modes. Their method of calculation was

Amsterdam Density Functional (ADF) program in order to determine geometries and adsorption energies of C_2H_4 on Ni_4 and Ni_{14} clusters.

Bernardo and Gomes (Bernardo and Gomes, 2001a) studied the interaction of ethylene molecule with the (1 0 0) surface of nickel using the cluster model approach. Ni having an fcc crystal structure was modeled by a 2-layer $M_9(5,4)$ cluster of C_{4v} symmetry, where "5 and 4" in paranthesis indicate the first layer and the second layer, respectively. In the theoretical method, metal atoms were described by a large LANL2DZ basis set, and the non-metallic atoms (C and H) were described by the 6–31G(d,p) basis set. For the cluster, nearest neighbor distances were taken from the bulk for the nickel. DFT/B3LYP hybrid method was used in Gaussian'98 package. In all their calculations the metal cluster geometry was kept frozen. They calculated optimized geometrical and electronic parameters obtained for the di-σ and π adsorption modes for Ni(1 0 0) and reported the related distances for both adsorption modes.

A 16-atom cluster was chosen to model the nickel surface Ni(1 0 0) by Crispin (Crispin et al., 1999). According to their point, Ni (1 0 0) surface has a surface atomic density intermediate between that of the compact (1 1 1) surface and that of the open (1 1 0) surface. Since reactivity of the surface depends on the surface atomic density, Ni (1 0 0) surface can be considered as possessing an average reactivity of different phases of the polycrystalline nickel surface. The interatomic distances in Ni_{16} (1 0 0) were kept fixed at the bulk interatomic distances in their work also. The cluster was made of two layers each containing 8 atoms. The adsorption of solvent or monomer molecules onto the metal surface was modeled by a complex composed of the organic molecule interacting with Ni_{16} (1 0 0) cluster. After optimizing the geometry of the complex with the nickel cluster structure kept fixed, the binding energy was evaluated. Their calculations were performed using DFT method with DNP basis set. In order to evaluate the capacity of the metal cluster to model the adsorption of molecules likely to be π-bonded, they carried out a preliminary study of the surface reactivity of Ni_{16} (1 0 0) for ethylene adsorption. Some different positions of ethylene on the

Ni_{16} (1 0 0) surface were considered. Different adsorption energies were reported for di-σ adsorption and π adsorption modes.

Onal and co-workers (Onal et al., 2009) investigated Ni_2 and Ni_{13} clusters quantum mechanically in terms of their structures, binding energies and bond lengths by use of DFT/B3LYP method with three different basis sets.

2.2.2.3 Ethylene Adsorption Reactions on Ni_{55} Nanocluster

According to study of Fulton and Crosser (Fulton and Crosser, 1965), the variation behavior in chemical reaction with changing particle size causes a change in character of the reaction kinetics. Therefore, changing the particle size will have an effect upon the behavior of the reacting system.

In addition, developments in nanoscale science are known to enable scientists to atomically engineer and characterize clusters of any size and composition. The importance of these developments lies in the fact that clusters offer a novel class of materials with electronic, catalytic and magnetic properties which are different from the bulk and change with size or composition. According to Grigoryan and Springborg's study (Grigoryan and Springborg, 2001), clusters are important materials, both for the basic research and for the applications between those of molecules and solids. It is reported that for the clusters having number of atoms; N; in the range of 10–10 000, usually consisting of one or only a few types of atoms, have interesting properties. These are stated to originate partly from the fact that the number of atoms at the surface relative to N is large and partly from finite-size or quantum-confinement effects. The first feature is explained to be responsible for the excellent catalytic properties of small and medium-sized clusters, e.g., nano-scaled metallic catalysts are widely used in the petroleum industry. Therefore, it is claimed that clusters are excellent objects for a systematic study of the evolution of the physical/chemical properties with N and, hence, are of importance for an understanding of the transition from the molecular to condensed matter regimes. It is expressed that one of the central issues held today is about how the structure and properties of a cluster depend on N.

Besides, it is emphasized by Schmid's study (Schmid et al., 1996) that the basic reason for producing nanoparticle-based catalysts was to improve the active surface to total metal volume ratio where the catalytic properties changed qualitatively with change of the metal particle size. This change was regarded not surprising in retrospect since electronic properties are strongly dependent on particle size as they approach the atomic scale. Ni nanocluster catalysts are explained to have a potential of having high activity and selectivity particularly in hydrocarbon hydrogenation reactions as compared to traditional supported Ni catalysts.

There are many calculations on nickel clusters by a variety of techniques which include methods developed based upon the density functional formalism such as the embedded atom method as in Daw's study (Daw et al., 1993); the effective medium theory as in Norskov's work (Norskov, 1994); the corrected effective medium (CEM) as in Christensen's research (Christensen et al., 1995) and tight-binding molecular dynamics (TBMD) and LCGTO-LDF method in the work of Lathiotakis' (Lathiotakis et al., 1996).

In this perspective, Parks and co-workers have reported experimental studies investigating the structure of nickel clusters by use of ammonia (Parks et al., 1991) and nitrogen (Parks et al., 1994) and (Parks et al., 1995) adsorption on neutral nickel gas clusters with different sizes ranging from 3 to 120 atoms. They reported that all of the nickel nanoclusters, including Ni_{55}, have Mackay icosahedral structure and the magic number clusters, such as Ni_{13} and Ni_{55}, have been observed experimentally. Icosahedral structure was first identified for nickel clusters by looking at the size dependence of the chemical reactivity with various probe molecules (Parks et al., 2001; Winter et al., 1991; Klots et al., 1991).

Similarly, the icosahedral structure of Ni_{55} was found by a large mass range with threshold photoionization experiments and standard mass spectrometry by Pellarin (Pellarin et al., 1994). Also, as reported in their work, for Ni nanoclusters having the atom numbers N=55, 147, 309, and 561 which correspond

to perfect icosahedra showed strong effects for these atoms with performing near-threshold photo-ionization and time-of-flight mass spectroscopy.

Lathiotakis and co-workers (Lathiotakis et al., 1996) studied Ni clusters with N=13 and N=55 with the tight-binding (semi-empirical) MD method. Among these clusters the most stable structure is reported as the icosahedral structure. Moreover, it is explained that for the open-shell clusters in the range $13<N<55$, that relaxed fcc clusters are the most stable structures. Moreover, as stated by Vlachos (Vlachos et al., 1992) there are also semi-empirical model potentials used for Ni clusters.

In addition, Stave and DePristo (Stave and DePristo, 1992) and also Wetzel and DePristo (Wetzel and DePristo, 1996) had systematically computed energies and structures of nickel clusters containing 3–23, 24–55 atoms by employing the CEM and MD/MC-CEM theories.

Grigoryan and Springborg (Grigoryan and Springborg, 2001) optimized nickel clusters in the size range: N=2–100, using the combination EAM (DBF-version) and quasi-Newton optimization method, for each size and without any restrictions on the symmetry and bond lengths. The optimized binding energy results for clusters of certain sizes: N=13, 19, 43, 55, … , 603, 627 are plotted. It is reported that, "the binding energy per atom increases with increasing cluster size, but the increase is non-monotonic. The non-monotonic dependence of the binding energy arises from the competition between the bulk and surface parts of the cluster energy, and that generally, the role of the surface effects should decrease with increasing cluster size". It is concluded that the surface effects are essential for the medium clusters ($N\approx400$), whereas, for larger cluster sizes the dependence becomes almost monotonic and the bulk atoms inside the clusters play the main role.

Grigoryan and Springborg (Grigoryan and Springborg, 2003) also utilized EAM method in their calculations for the Ni_N clusters in the size range of 2 to 150, where electronic effects i.e. Jahn-Teller distortions were not included and Mackay icosahedron for Ni_{55} cluster is concluded as the structure.

Montejano-Carrizales (Montejano-Carrizales et al., 1994) studied the stabilities of perfect cuboctahedral and also in their work icosahedral closed-shell clusters with N=13, 55, 147, 309, …, 5083 were considered relatively. It was concluded that the icosahedral structures are more stable up to atom number N=1415, which corresponds to the seven full layers around the central atom of the icosahedron structure.

In another study of Montejano-Carrizales (Montejano-Carrizales et al., 1996) Ni clusters of the size range from 13 to 147 are studied with EAM keeping the cluster structure relaxed only up to N=78 where Jahn-Teller distortions were not included. In their work, two different types of structures based on icosahedral growth were considered and Mackay icosahedron for Ni_{55} cluster is concluded as a result.

Doye and Wales (Doye and Wales, 1998) used Monte Carlo minimization approach to model different metal clusters up to 80 atoms without using Jahn-Teller distortions. They also reported Ni_{55} cluster as for having Mackay IC (icosahedral) structure.

Cleveland and Landman (Cleveland and Landman, 1991) worked on the energetics of nickel clusters studied by various cube or octahedron truncations. For the Ni clusters containing less than 2300 atoms, optimal structures of clusters are predicted as the icosahedral sequence.

In Qi's study (Qi et al., 2001) Ni nanoclusters are studied by MD with the quantum-Sutten-Chen many-body force field. For the clusters with less than ≈400 atoms the most stable structure is reported as icosahedron.

Chemical probe experiments on Ni clusters by Parks, (Parks et al., 1991; Parks et al., 1994; Parks et al., 1995; Parks and Riley, 1995) showed icosahedral symmetry for N>48. Parks and Riley (Parks and Riley, 1995) stated that Ni_N indicated bare nickel clusters in the $49 \leq N \leq 105$ size region preferentially adopt icosahedral-based structure, and more specifically, the experiments showed evidence for regular icosahedra and icosahedra with closed subshells.

In the study of Wang's (Wang et al., 2010) distances of icosahedral Ni_{13} and Ni_{55} nanoclusters are discussed. Starting from the smaller cluster, it is reported that Ni_{13} has one atom at the center and other 12 identical atoms on the spherical shell surface with a coordination number of 6. The distance between the spherical shell and the central atom is 2.32 **Å.** The surface Ni–Ni bond length is 2.44 **Å**. As they indicated, based on the Ni_{13} icosahedral structure, the Ni_{55} is built by adding 30 atoms on the top of Ni_{13} ''edge atoms'' with a coordination number of 8 (denoted as ''edge atoms'' for Ni_{55}), and additional 12 atoms on the top of Ni_{13} vertex positions with a coordination number of 6 (denoted as ''top atoms'' for Ni_{55}). The ''top atoms'' are reported to be 4.65 **Å** away to the cluster center, while the ''edge atoms'' are 4.07 **Å** to the cluster center. The surface bond lengths are stated as 2.52 **Å** between two ''edge atoms'' and 2.45 **Å** for two adjacent ''top atom'' and ''edge atom'' where Ni_{55} sublayer is 2.36 **Å** to the cluster center, this layer is suggested to be slightly enlarged compared to the original Ni_{13} clusters, due to addition of surface atoms.

Luo (Luo, 2002) adopted the TB approximation and MD technique to compute the energies and structural properties of nickel clusters containing 4–55 atoms and obtained an IC structure for Ni_{13} and Ni_{55} as well. In their work, it is stated that, theory only assumes spherically symmetric nickel atoms (i.e. no directional bonding) and does not take into account possible Jahn–Teller distortions of electronically degenerate configurations, and it is known that ignoring directional bonding in the d manifold in structure calculations could yield a wrong structure for some nickel clusters. Luo claimed that their results show an important conclusion, i.e. Jahn–Teller distortions do play a leading role in cluster geometry, and should be considered in any realistic calculations.

Kar'kin and co-workers (Kar'kin et al., 2008) reported that in their study the Ni clusters with magic numbers N= 55 and N= 147 are energetically preferable within the chosen ranges of N; in this case, the structure of the ground state which is achieved during cooling corresponds to the Mackay icosahedron. For the Ni cluster interval N = 50–60, the dependence of the energy of the ground state of clusters on the number of atoms is reported and local energy minimum

upon N magnitudes is corresponded to "magic" number 55. The energy of Ni_{55} nanocluster is read from the related figure in Kar'kin's study as around 3.694 eV/atom.

In Xiang's work (Xiang et al., 2000) the Stariolo-Tsallis form of GSA is applied to the nickel clusters in order to determine the structures of Ni_N clusters (N = 2–55), in which the inter-atomic potentials are modeled by the Sutton-Chen version of FS potential. The structural and some physical properties of Ni from N = 52 to N = 55 are investigated, and it is reported that the clusters with N = 52–55 have the icosahedral structure and at where N = 55 a perfect icosahedron is formed. Binding energy is explained as 3.77 eV for $Ni_{55.}$ In addition, structures of N = 13, 38, and 55 with a high symmetry are concluded to be very stable, that is also confirmed by the binding energy and their differentials.

Doye and Wales (Doye and Wales, 1998) also concluded that features at N=13 and 55 indicate an icosahedral structure.

In their study, Singh and Kroll, (Singh and Kroll, 2008) performed *ab initio* geometry optimization of icosahedral (ico), cuboctahedral (cubo), and anticuboctahedral (anticubo) clusters of 13, 55, and 147 atoms of Fe, Co, and Ni using the spin-polarized density functional theory (DFT) and the generalized gradient approximation (GGA) as implemented in Vienna *ab initio* simulation package (VASP). It is reported that the groundstate ico-Ni_{55} cluster exhibits an interatomic distance of 2.35 **Å** between center atom and surrounding 12 neighbors in first shell. In ico-Ni_{55} computations, the nearest-neighbor bond length between atoms in first shell is found to be 2.47 **Å** where between atoms in second shell it is noted as 2.41 **Å**. Moreover it is indicated that, in its ground-state ico-Ni_{55} has significantly shorter Ni-Ni distance in the core of the cluster in comparison to the bulk where bulk is calculated as Ni-Ni =2.48 **Å** for fcc Ni. It is also reported that icosahedral structures are lower in energy than other structures at all total magnetic moments where it is calculated as -4.541 eV/atom for ico-Ni_{55} nanocluster. It is implied that the cohesive energy of a cluster increases as size of cluster is increased. Reason is claimed due the fact that energy of a surface in Fe,

Co, and Ni is positive and consequently the surface energy tends to decrease the cohesive of a cluster and so that the surface to volume ratio decreases as size of cluster is increased and consequently the cohesive energy increases. It is specified that as the size of cluster is increased, the nearest-neighbor bond length is increased toward bulk value and also that the magnetic and electronic structures of a cluster are dependent on its size, intrastructure, and geometrical structure symmetries.

2.2.2.4 Relation Between Coordination Number of Metal Surfaces and Activation Energies

A relation between the coordination number of metal surfaces and activation energies are stated previously in literature. However, in terms of specific studies among this subject, Lopez and co-workers (Lopez et al., 2004) worked on quantum mechanically carbon monoxide and oxygen adsorption on nano-sized gold particles (Au_{10} nanocluster) and on Au(1 1 1) and Au(2 1 0) single crystal surfaces. Their DFT calculations indicated that CO and O_2 adsorption energies increased proportionately with decreasing coordination numbers of surface gold atoms. As a result, it is stated that the chemical activity of gold was strongly dependent on the coordination number of the gold atoms.

Van Santen and Neurock (van Santen and Neurock, 2006) have emphasized also that metal atoms in the cluster which have very low coordination numbers form very strong bonds with the adsorbate to compensate for the smaller number of metal-metal bonds. This increases binding energy between the metal and the adsorbate.

2.3 Ethylene Hydrogenation Reactions on Nickel

2.3.1 General View of Ethylene Hydrogenation Mechanisms

Hydrogenation and dehydrogenation reactions of simple hydrocarbons have been of considerable research interest ever since the original Nobel Prize winning work of Sabatier (Moors et al., 2007). As also Harinipriya and Sangaranarayanan (Harinipriya and Sangaranarayanan, 2004) states, the hydrogenation of alkenes plays a central role in petroleum cracking and there "ethylene" being the lowest member in the alkene series; it serves as a prototype compound for comprehending the mechanism of hydrogenation. In addition, as similarly Neurock and van Santen (Neurock and van Santen, 2000) notes, the hydrogenation of ethylene has served as the classic model for understanding the hydrogenation of olefins and aromatics for nearly 75 years, since afterwards olefin hydrogenation is at the heart of petroleum hydro-treating and upgrading processes as well as saturated oil hydrogenation processes in the food industry and that bulk chemical processes, many current pharmaceutical and fine chemical syntheses target the selective the hydrogenation of specific olefin bonds.

As indicated in Pirard's work (Pirard et al., 2008) ethylene hydrogenation on a variety of catalytic surfaces has been extensively studied over years, where the numerous efforts have been devoted to the study of ethylene hydrogenation on well-defined crystallographic planes of transition metal catalysts (group VIII). It is also expressed there that, some authors suggest such a reaction mechanism which is based on *molecular adsorption of ethylene, dissociative adsorption of hydrogen, and the stepwise addition of hydrogen atoms to ethylene on the surface of the catalyst* (Horuiti and Polanyi, 1934; van Santen and Niematsverdriet, 1995; Dumesic et al., 1993; Bond, 1962) here *C_2H_4 and H_2 adsorbing either competitively* (Horuiti and Polanyi, 1934; van Santen and Niematsverdriet, 1995; Dumesic et al., 1993; Ghiotti et al., 1989) *or non-competitively as an example.* (Horuiti and Polanyi, 1934; Dumesic et al., 1993; Ghiotti et al., 1989; Heinrichset al., 2001). Moreover, according to some studies on metals from group VIII, the apparent activation energy of ethylene hydrogenation is reported to be in the range from 30 to 45 kJ mol^{-1} (Dumesic et al., 1993; Bond, 1962).

According to Harinipriya and Sangaranarayanan, (Harinipriya and Sangaranarayanan, 2004) several investigations using ultrahigh vacuum (UHV) and HREELS studies indicate that hydrogenation of ethylene on metal surfaces such as Ni(110), Pt(111) and Pd(111) occurs via *the bulk hydrogen existing as metal hydrides*.

Among mechanism types, Laidler and Townshend (Laidler and Townshend, 1961) in their work stated that the order of introduction of gases was found to be important for the ethylene hydrogenation mechanism, the relative rates being; Hydrogen first > Simultaneous > Ethylene first. According to their results, together with the analysis of the time course of the reaction under a variety of conditions, two mechanisms are involved: first one is the *Langmuir-Hinshelwood* reaction between *"adsorbed ethylene and hydrogen molecules",* this mechanism was being favoured by prior addition of ethylene or by excess of ethylene; and the second type is the *Rideal* reaction between *"adsorbed hydrogen" and "gaseous ethylene"*, and this mechanism was being favoured by prior addition of hydrogen or excess of hydrogen. It is pointed out that in spite of a considerable amount of experimental and theoretical investigations, certain important features of the mechanism of the ethylene and hydrogen reaction on surfaces, and of similar processes, still remain unsettled. Therefore, although much is now known about the molecular nature of the adsorption of the reactant gases on metal and other surfaces, some uncertainty about the overall nature of the reaction itself is claimed to be remained. Relatedly, Laidler and Townshend (Laidler and Townshend, 1961) in their work, concluded with proposing two main possibilities:

1. Reaction occurs between an *"adsorbed ethylene molecule"* and an *"adsorbed hydrogen molecule"* (or two absorbed atoms); this is the type of mechanism originally discussed by Langmuir and applied by Hinshelwood to a wide variety of reactions which is referred to as the **Langmuir-Hinshelwood (LH)** mechanism.

2. Reaction occurs between an *"adsorbed molecule"* and a *"molecule coming directly from the gas phase"*; such mechanisms were also considered by Langmuir and more recently advocated by Rideal, which are referred to as **Rideal (R) mechanisms.** There are two sub-cases stated:

I. Reaction occurs between an adsorbed ethylene molecule (or related species, such as an adsorbed ethyl radical) and a gaseous hydrogen molecule; thus, if adsorption of ethylene is of the associative type the mechanism may be written schematically as

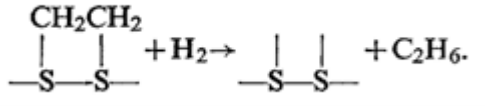

(2.1)

II. Reaction occurs between a pair of adsorbed hydrogen atoms and a gaseous ethylene molecule :

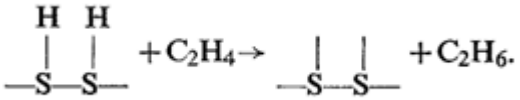

(2.2)

The evidence in favour of this mechanism, which is referred to as R-11, is stated to be adduced by Beeck and also by Jenkins and Rideal.

In Laidler and Townshend (Laidler and Townshend, 1961)'s study, it is stated possible to distinguish between the LH and R mechanisms by means of finding out how initial reaction rates are affected by changes of the reactant concentration; if the LH mechanism applies the rate will pass through a maximum as the pressure of either reactant is varied, while with either of the R mechanisms the rate will reach a limiting value. It is also explained that, the studies of the time course of the reactions, when interpreted from the same point of view, will also provide a means of distinguishing between the mechanisms. Ethylene is reported to be much more strongly adsorbed than hydrogen on most of the surfaces investigated, and so from the experimental view point, the best chance of

distinguishing between mechanisms is indicated as to work over a range of ethylene pressures. The results obtained in this investigation concluded that, on both nickel and iron films, *the hydrogenation of ethylene may occur either by a Langmuir-Hinshelwood or a Rideal mechanism, according to circumstances.*

In addition, according to the study of Harinipriya and Sangaranarayanan (Harinipriya and Sangaranarayanan, 2004), in terms of mechanistic sequences, hydrogenation of ethylene on metal surfaces can be mainly represented using the following sequential steps:

1. First one of these steps is the adsorption of ethylene forming a metal –π- ethylene complex:
   $CH2=CH2 + M \leftrightarrow M\text{-}CH2 = CH2$ (2.3)
2. Formation of a metal di-σ-ethylene complex:
   $$M\text{-}CH2 = CH2 \leftrightarrow \underset{\diagdown\quad\diagup}{CH_2 - CH_2}\ \text{M}$$ (2.4)
3. Dissociative adsorption of hydrogen on the metal surface:
   $2M + H2 \leftrightarrow 2M\text{-}Hads$ (2.5)
4. Displacement of adsorbed hydrogen atoms on the metal surface to metal di-σ-ethylene complex so as to form metal-ethyl complex:
   $$M\text{-}H + \underset{\text{M}}{\underset{\diagdown\quad\diagup}{CH_2 - CH_2}} \leftrightarrow M\text{-}CH2\text{-}CH3 + M$$ (2.6)
5. Displacement of neighboring adsorbed hydrogen atoms to the metal-ethyl complex leading to adsorbed ethane,
   $M\text{-}CH2\text{-}CH3 + M\text{-}H \leftrightarrow CH3\text{-}CH3\ ads + M$ (2.7)
6. Evolution of ethane gas from the metal surface:
   $(CH3\text{-}\ CH3)_{ads} \rightarrow (CH3\text{-}\ CH3)_{(g)} + M$ (2.8)

Stated by Filhol and co-workers, (Filhol et al., 2004), a detailed kinetic model was constructed to obtain a more detailed understanding of the compared hydrogenation reaction rates. The following mechanism resulted from the calculated pathways, where the adsorbed species are followed by a star:

$$C_2H_4(g) + H_2(g) + 2* \leftrightarrow C_2H_4* + 2H* \quad (2.9)$$

$$C_2H_4* + H* \leftrightarrow C_2H_5* + * \quad (2.10)$$

$$C_2H_5* + H* \rightarrow C_2H_6* + * \quad (2.11)$$

$$C_2H_6* \leftrightarrow C_2H_6(g) + * \quad (2.12)$$

The kinetics of the system was then simplified as follows:

- The adsorption reaction of ethylene and hydrogen is assumed to be very fast and corresponds to the global equilibrium (2.9).
- The first hydrogenation step (2.10) takes place from the most stable co-adsorption state, through Transition State 1 (TS1), toward the most stable ethyl state.
- The second hydrogenation step (2.11) relates this ethyl state to an adsorbed ethane molecule, through TS2, the backward reaction being neglected due to a much higher activation barrier.
- The surface coverage of ethane can be neglected, because it has a very small desorption energy, and the desorption step is expected to be a non-activated equilibrium (2.12).

Pirard (Pirard et al., 2008) similarly considered different ethylene hydrogenation reaction mechanisms in their work. According to their approach, at one hand, they considered *Langmuir–Hinshelwood mechanism* as one of the models with *non-competing* adsorption of hydrogen and ethylene and where the rate determining step is either the addition of "*molecularly adsorbed hydrogen"* or the addition of *"the second atom of hydrogen adsorbed dissociatively"*. In such a case, it is stated that, the hydrogen adsorption should be weak enough to be neglected. On the other hand, they also referred this model also corresponding to

an *Eley-Rideal mechanism* in which "*gaseous hydrogen would be directly added on adsorbed ethylene"*. As for another model, they considered the *competitive adsorption* of both reactants. Thus for this case, the rate-determining step is thought to be either the addition of "*molecularly adsorbed hydrogen"* or the addition of the "*second atom of hydrogen adsorbed dissociatively"*. In addition, for another model, a *non-competitive adsorption* of ethylene and hydrogen by an atomic mechanism is characterized, where its rate-determining step is assigned for the addition of the "*first hydrogen atom to adsorbed ethylene"*.

As stated in Haug's study (Haug et al., 2001) another straightforward mechanism for ethylene hydrogenation, known as the *Horiuti-Polanyi* mechanism, has long been considered the operable mechanism. The mechanism depicts "*the carbon-carbon bond of C_2H_4 to be parallel to the surface so that C_2H_4 forms two bonds to the surface through the two carbon atoms"*. Eventually, a co-adsorbed H atom migrates up to C_2H_4 and reacts, forming a "half-hydrogenated" species which then reacts with a second adsorbed H to form volatile ethane.

2.3.2 Ethylene Hydrogenation Mechanisms on Nickel (1 1 1), (1 0 0), (1 1 0) Surfaces

The catalytic hydrogenation of unsaturated hydrocarbons over transition metal catalysts, particularly nickel is known to be a commercial process in the production of fine chemicals and pharmaceuticals and in the hydrogenation of unsaturated fats and nitriles. Hence, the interactions of simplest unsaturated hydrocarbons are regarded as important, where especially ethylene and acetylene, with hydrogen on single-crystal transition metal surfaces have been studied for a long time (Haug et al., 2001).

Ni(1 1 1) experimental study takes place in the work of Daley's (Daley et al., 1994). It is reported in their study that, bulk H atoms, upon moving out from the bulk metal to the surface, readily hydrogenate C_2H_4 adsorbed on Ni (1 1 1) to form C_2H_6, while surface-bound H atoms have no hydrogenation activity under the conditions of these experiments. It is claimed that this result is the first observation of the role of bulk H specifically as a reactant in the hydrogenation of an unsaturated hydrocarbon on a transition metal and calls into question the generality of the *Horiuti-Polanyi* mechanism for catalytic hydrogenation reactions. It is further reported in this study that, high-resolution electron energy loss (HREEL) spectroscopy verifies the efficiency of the Xe beam in sweeping the surface clean of H, confirms the presence of both adsorbed C_2H_4 and bulk H, shows that the C-C bond lies parallel to the surface, and indicates that the C atom hybridization is between sp^2 and sp^3. The identicalness of the ethylene vibrational spectrum to that of C_2H_4 adsorbed on Ni (1 1 1) without bulk H demonstrates that the bulk H does not modify the C_2H_4-Ni interaction. The hydrogenation activity of bulk H is compared to that of surface-bound H. However, the surface-bound H experiment is stated as intriguing because although surface-bound H does not hydrogenate C_2H_4, it is very reactive toward exchange with ethylene. Moreover, it is explained that, the reaction coordinate for addition of an H atom to C_2H_4 in the gas phase involves a perpendicular approach to the plane of C_2H_4. To determine whether the direction of approach of the H atom is defined as the sole requirement for hydrogenation, 0.01 ML of C_2H_4 is adsorbed on top of a surface-bound H monolayer, formed by heating a crystal containing bulk H to just above the temperature for desorption of bulk H. After verification of this adsorption geometry by HREELS, the crystal temperature is ramped at 2 K/s and afterwards, it is reported in Daley's study that no ethane is detected. Additional experiments carried out with C_2H_4 adsorbed on top of lower coverage H layers where the ethylene has varying degrees of interaction with the surface also result in no hydrogenation. This reactivity difference between the bulk and surface H atoms, despite their identical perpendicular direction of approach, is expressed to be likely resulted from the different energies of the two atoms. Bulk H atoms are explained to be propelled out of the bulk with roughly 13 kcal/mol of energy

gained from descending the bulk/surface barrier whereas surface H atoms possess a thermal energy distribution characterized by the crystal temperature. The difference in reactivity is supposed also to arise from different barriers to hydrogenation for the two cases. In the bulk H experiment, it is reported that C_2H_4 is re-hybridized by its strong interaction with Ni whereas C_2H_4 adsorbed on top of the surface H layer retains its gas-phase structure, thus it is concluded that experiments are underway to delineate these possible origins for the reactivity difference.

It is also underlined in the work of Daley's (Daley et al., 1994) that if H_2 and then C_2H_4 are allowed to adsorb on the edges of the crystal, it is observed a small but detectable amount of hydrogenation. This hydrogenation activity from the crystal edges is presumed to arise from hydrogenation via bulk H whose production is facilitated by the rough surfaces of the crystal edges or it is likely to result from surface-bound H reacting with ethylene that has a very different structure on the crystal edges than on Ni (1 1 1). In addition, either possibility are considered to explain the small amount of C_2H_4 hydrogenation observed on Ni (1 0 0). Then afterwards, the result was the observation of ethylene hydrogenation on Ni (1 1 0) where the hydrogenation occurs only with the hydrogen that has been interpreted as forming a Ni hydride.

However, according to Haug's study (Haug et al., 2001), the universality of the hydrogenation mechanism has been called into question because a co-adsorbed layer of C_2H_4 and H on Ni (1 1 1), formed by exposure to 10^{-4} Torr of C_2H_4 and H_2 in an UHV environment, does not react to form ethane, even though C_2H_4 adsorbs with the geometry depicted by the *Horiuti-Polanyi* mechanism. Instead, hydrogen atoms that are initially beneath the surface, called bulk H, are observed to be the reactive species in hydrogenating C_2H_4 to C_2H_6. Bulk H reacts with the C_2H_4 as it emerges onto the surface, called surface-bound or surface□ H is unreactive for the hydrogenation of ethylene. Therefore, it is pointed out that the rapid reactivity of the bulk H is rationalized in terms of its direction of approach to C_2H_4. As the bulk H emerges, it approaches the adsorbed C_2H_4 from underneath and form a direction in which the rehybridized π orbitals of C_2H_4

oriented. This approach, in contrast to that of a surface-bound H atom, maximizes the overlap between the reacting hydrogen atom and the π orbitals and minimizes the Pauli repulsion between the reacting hydrogen atom and the hydrogen atoms of C_2H_4.

Moreover, Haug and co-workers (Haug et al., 2001) emphasized that the approach of an H atom from above and below the C_2H_4 molecular plane is the minimum energy path along the potential energy surface for hydrogen addition to C_2H_4 in the gas phase. But in addition, the lower barrier for hydrogenation that is encountered by a bulk H as compared to atom can be as much as 24 kcal/mol more energetic than a surface-bound H atom where its greater potential energy is defined as the result of its weaker binding to the Ni atoms in the bulk-surface interface. The fact that a bulk H atom can be 24 kcal/mol more energetic than a surface bound H atom means that there will be reaction channels open to bulk H that are closed to surface-bound H hence it is concluded more reasonable to expect reactivity with C_2H_4. Given that the energetics of the bulk H atom and the surface bound H atom are so different, it is also considered to expect the products of the reaction of surface-bound H to be distinct from the products of the reaction of bulk H.

As stated in Ceyer's work (Ceyer, 2001), hydrogenation mechanism depicts the carbon-carbon bond of C_2H_4 to be parallel to the surface. Eventually, a coadsorbed H atom migrates up to C_2H_4 and reacts, forming a "half-hydrogenated" species which then reacts with a second adsorbed H to form volatile ethane. However, in their work it is questioned that if this mechanism was correct, then it seems reasonable that a coadsorbed layer of C_2H_4 and H on Ni (1 1 1), formed by exposure to 10^{-4} Torr of C_2H_4 and H_2 in an UHV environment, should result in ethane formation, however, no ethane is observed according to the findings of previously stated studies (Daley et al., 1994; Lehwald and Ibach, 1979; Hasse et al., 1983). In contrast, it is also reported that C_2H_4 hydrogenation readily takes place on Ni (1 1 1) at high ethylene-H_2 pressures (Dalmai-Imelik and Massardier, 1977). Recently, it is emphasized that the absence of H absorbed in the bulk of Ni metal after exposure to low-pressure H_2 has been

shown to be at least one plausible molecular-level origin for the lack of hydrogenation activity under UHV conditions. This is affiliated with the reactive species in hydrogenating ethylene has been found to be a hydrogen atom emerging from the bulk onto the surface (Daley et al., 1994).

In addition, it is mentioned in Ceyer's study (Ceyer, 2001), that, the exact role of this "dissolved hydrogen", which is called "bulk H" remained unknown. The reason for the dearth of information about these practically important hydrogenation reactions is concluded as the inability to carry them out under single-collision conditions, such as afforded by UHV surface science techniques, where microscopic reaction steps are discernible. New capabilities of synthesis and characterization are stated to enable the chemistry of bulk H in hydrogenation reactions to be investigated under UHV conditions where the role of bulk H can be unambiguously determined. These investigations are reported to show that bulk H is not a modifier of the metal electronic structure or solely the supplier of surface-bound H. Rather, bulk H is the reactant in the hydrogenation of the ethylene (Daley et al., 1994) on Ni (1 1 1). It is stated that, the bulk H does not perturb the two-dimensional unit cell of Ni atoms, nor does it perturb the frequencies of the surface-bound H. The perturbation of the Ni surface electronic structure by bulk H is therefore explained minimal (Johnson et al., 1991) and these are concluded as important pieces of information in understanding the unique chemistry of bulk H.

In Paul's work (Paul et al., 1959), it was found that the activity of the catalytic surface was reduced by exposure to ethylene, or mixtures containing an excess of ethylene, owing to the formation of acetylene residues. Kinetic studies suggest a process in which hydrogen is adsorbed on the small fraction of the surface not occupied by acetylenic residues and the reaction takes place between this adsorbed hydrogen and ethylene in the gas phase. It is explained also that the hydrogenation of ethylene has served as a basis for numerous kinetic studies and as a reaction medium for studying surface catalysis as in the work of Beeck and co-workers (Beeck, 1950; Beeck et al., 1940). In addition, as for poisoning reactions, it is denoted by Paul's study (Paul et al., 1959), that the exposure of the

catalyst to ethylene reduces its activity for the hydrogenation reaction. These results are reported to fit the general model of ethylene poisoning of pure nickel films proposed by Jenkins and Rideal. It is postulated that ethylene is adsorbed and dissociates into an acetylenic residue plus two adsorbed hydrogen atoms. The hydrogen atoms are then available to react with ethylene, resulting in the so-called "self-hydrogenation reaction." The sites vacated by this reaction will adsorb more ethylene until all the groups of four sites capable of dissociatively adsorbing ethylene have been utilized. In Rideal's model the remaining sites are assumed to catalyze the hydrogenation of ethylene by adsorbing hydrogen, which then reacts with ethylene in the gas phase. In view of the catalyst activity studies and the considerable amount of kinetic data from other sources supporting the dissociation of ethylene on the catalyst, they concluded that, the Jenkins and Rideal approach is favored. Moreover it is reported that, Twigg's concept (Twigg, 1950), which requires that ethane be formed by the reaction between adsorbed ethyl radicals and adsorbed hydrogen atoms. There accordingly ethylene is explained to be adsorbed by the associative process where hydrogen is adsorbed only through the interaction of a gaseous hydrogen molecule and an adsorbed ethylene complex. However, Paul and co-workers (Paul et al., 1959) expressed that the arguments in favor of the Twigg concept are based not so much on the dependence of the rate on pressure and concentration as on the variation of first-order rate constants with temperature and on information for related reactions.

Regarding all these different studies and their conclusions, as also Neurock and van Santen (Neurock and van Santen, 2000) states that, despite the tremendous number of studies on ethylene hydrogenation, there are still a number of features about the reaction mechanism that are still unknown.

2.4 Binding energy relations among icosahedral nanoclusters; Ni_2, Ni_{13} and Ni_{55}

In terms of literature especially for the Ni_{55} nanocluster binding energies there are some values reported relatively. For Ni_{55} nanocluster, tight-binding molecular dynamics method used by Lathiotakis (Lathiotakis et al., 1996) and Luo (Luo, 2002) EAM method by Grigoryan and Springborg (Grigoryan and Springborg, 2003) and Montejano-Carrizales (Montejano-Carrizales et al., 1996), VASP-PBE function method by Wang (Wang et al., 2010), molecular dynamics study by Kar'kin (Karkin et al., 2008), GSA method by Xiang (Xiang et al., 2000) and DFT method by Singh and Kroll (Singh and Kroll, 2008) resulted in binding energies of 4.27eV/atom, 3.55eV/atom, 3.83eV/atom 3.87eV/atom, 3.92 eV/atom, 3.69eV/atom, 3.77eV/atom, 4.54eV/atom respectively. Bulk nickel binding energy was experimentally reported as 4.45eV/atom by Voter and Chen (Voter and Chen, 1987) where also the calculated average bond lengths are reported as 2.59 **Å**, 2.45 **Å,** 2.59 **Å, (**2.45, 2.52) **Å**, 2.36 **Å,** (2.35, 2.47, 2.41) **Å** by Lathiotakis (Lathiotakis et al., 1996), Luo (Luo, 2002) and Grigoryan and Springborg (Grigoryan and Springborg, 2003), Wang (Wang et al., 2010), Xiang (Xiang et al., 2000) and Singh and Kroll (Singh and Kroll, 2008) respectively.

CHAPTER 3

SURFACE MODELS AND CALCULATION METHODS

3.1 Ni_{13} and Ni_{55} Nanoclusters

Geometry optimization calculations for magic number cluster of Ni_{13} and Ni_{55} nanoclusters were carried out by using DFT method provided (Kohn and Sham, 1965) in Gaussian'03 (Frisch et al., 2004).

In all calculations, nickel clusters were neutral, their electrons were not kept frozen and nickel atoms were free in all directions. Different spin multiplicities were utilized in order to determine global minima. As mentioned by Lathiotakis (Lathiotakis et al., 1996) and Luo (Luo, 2002), it is found that Jahn-Teller distortions of electronically degenerate configurations play an important role in the full optimization of the nickel clusters. It is explicitly noted that a wrong structure for nickel clusters could be found by ignoring directional bonding in the d manifold in equilibrium geometry calculations. Hence, quantum mechanical calculations included Jahn–Teller distortions without using any symmetry constraint.

The first magic number cluster following the Nickel dimer is Ni_{13}. Magic number clusters are in general constructed by surrounding one single metal atom with metal atom layers by obeying the formula $y = 10\ n^2 + 2$ suggested by Schmid (Schmid, 1991) where y is the total number of atoms at the n^{th} layer. Ni_{13} cluster is developed by surrounding one single nickel atom with 12 nickel atoms conforming with Mackay icosahedral structure as suggested theoretically by Pellarin (Pellarin et al., 1994), Raghavan (Raghavan et al., 1989), Stave and DePristo (Stave and DePristo, 1991), Lathiotakis (Lathiotakis et al., 1996),

Northby (Northby, 1987) and experimentally by Nayak (Nayak et al., 1997). Similarly for construction of a Ni_{55} nanocluster, an input geometry is then set up from Ni_{13} nanocluster by adding a second layer according to the formula $y = 10\ n^2 + 2$. After forming the clusters, by performing Density Functional Theory calculations, different spin multiplicities are utilized in order to find the most stable geometry for the Ni_{13} and Ni_{55} nanocluster.

3.2Nickel Surface Clusters

Ni_{10} (1 1 1), Ni_{13} (1 0 0) and Ni_{10} (1 1 0) surface cluster geometries are obtained by using bulk nickel structure which has a face centered cubic lattice structure with lattice parameter a=3.5238 Å and space group number 225 (Wyckof, 1963).

In order to obtain specific model clusters, first of all, a large 3-dimension Ni cluster is constructed, then, some specific sections are taken out of that base-cluster which can define our adsorbent surface throughout our studies.

3.2.1 Ni_{10} (1 1 1), Ni_{13} (1 0 0) and Ni_{10} (1 1 0) Surface Clusters

A large section of (1 1 1), (1 0 0) and (1 1 0) surfaces are taken in a more specific way from the large-bare Nickel cluster, then, the model cluster is attained by diminishing the amount of atoms to the number of 10, 13 and 10 atoms respectively for the Ni (1 1 1), Ni (1 0 0) and Ni (1 1 0) surfaces according to the symmetry and adequacy of the cluster for our studies. Hydrogenating these specific bare model clusters, electronic activity is managed and prepared for the computations.

After obtaining these clusters, Single Point Energy Calculations (SPE) are performed to find the best spin multiplicity suitable for the geometry. In the pursuit of these SPE calculations giving the spin multiplicity value, clusters are optimized to find the best geometries of Ni_{10} (1 1 1), Ni_{13} (1 0 0) and Ni_{10} (1 1 0) surface clusters.

3.3Ethylene Molecule

Prior to the adsorption calculations equilibrium geometry (EG) of C_2H_4 as a reactant molecule is obtained by calculating spin multiplicity values and therefore with optimization.

3.4 Calculation Methods

3.4.1 Methods related with Cluster Constructions and Ethylene Adsorption Studies

All calculations in this study were based on DFT (Kohn and Sham, 1965) as implemented in Gaussian'03 suit of programs (Frisch et al., 2004). In order to take into account the exchange and correlation, Becke's (Becke, 1988; Becke and Roussel, 1989) three-parameter hybrid method involving the Lee, Yang, and Parr (Lee et al., 1988) correlation functional (B3LYP) formalism was used in this study. It has already been demonstrated by Baker and co-workers (Baker et al., 1996) that hybrid B3LYP method is a high-quality density functional method certainly for organic chemistry. For Ni_{10} (1 1 1), Ni_{13} (1 0 0) and Ni_{10} (1 1 0) surface clusters and Ni_{13} nanocluster, 6-31G(d,p) basis set is used for all atoms including nickel atoms. However, for the greater icosahedral structure; the Ni_{55} nanocluster; 86-411(41d) G basis set is used for the Ni atoms in order to make calculations possible to be solved. Still, in both computations of ethylene adsorption reactions, for the ethylene molecule, 6-31G (d,p) basis set is also used since it contains C and H atoms, and since it is known that 6-31G (d,p) basis set is a suitable and favored basis set for these atoms.

During the calculations all atoms of the Ni_{13} nanocluster were kept relaxed, where Ni_{10} (1 1 1), Ni_{13} (1 0 0) and Ni_{10} (1 1 0) surface clusters were kept fixed. The dangling bonds of the terminal nickel atoms of surface clusters were terminated with H atoms to obtain a neutral cluster. All nickel atoms and terminating H atoms of surface clusters were kept fixed during all calculations. All of the reactant and product molecules were kept relaxed. Equilibrium geometry (EG) calculations were in general performed for determination of

adsorption energies. Computed <S2> values confirmed that the spin contamination was very small (after annihilation). Convergence criteria which are gradients of maximum force, rms force, and maximum displacement and rms displacement in Gaussian'03 software are 0.000450, 0.000300, 0.001800 and 0.001200, respectively.

The computational strategy employed in this study is as follows: Initially, the correct spin multiplicity of the nanocluster, surface clusters and adsorbing molecule is determined by Single Point Energy (SPE) calculations. SPE's are calculated with different spin multiplicity numbers for each cluster system and the spin multiplicity number which corresponds to the lowest SPE is accepted as the correct spin multiplicity. The cluster and the adsorbing molecule, ethylene, are then fully optimized geometrically by means of equilibrium geometry (EG) calculations. The relative adsorption energy is defined as the following formula:

$$\Delta E = E_{System} - (E_{Cluster} + E_{Adsorbate}) \quad (3.1)$$

where E_{System} is the calculated equilibrium energy of the given geometry containing the cluster and the adsorbing molecule, $E_{Cluster}$ is the energy of the cluster, and $E_{Adsorbate}$ is that of the adsorbing molecule, e.g. ethylene in this case.

3.4.2 Methods for Hydrogenation Reactions for Ethylene on Ni_{13} Nanocluster

As given in the previous sections, there are different mechanisms favored among researchers for the ethylene hydrogenation reaction. These differences are usually stated to be related with the cluster size of the adsorbent or experimental conditions such as pressure or rates, or even the sequence of introducing materials and likewise. Therefore, in a generalized point of view, in this study, we tried to compute each possibility that is mentioned among the reaction mechanisms in terms of theoretical calculations as much as the computational tools facilitated the progress.

In this sense, the reaction paths that are taken into consideration are as follows:

I. Investigation of Rideal Reaction Mechanisms
    a. Rideal-I Type Mechanism; Reaction occurs between an adsorbed ethylene molecule and a gaseous hydrogen molecule
    b. Rideal-II Type Mechanism; Reaction occurs between an adsorbed hydrogen molecule and a gaseous ethylene molecule

II. Langmuir-Hinshelwood (LH) Reaction Mechanisms; Reaction occurs between an adsorbed ethylene molecule and adsorbed hydrogen molecule
    a. Mechanism-I
    b. Mechanism-II
    c. Mechanism-III

In order to progress through, first of all Ni_{13} nanocluster as the adsorbent, ethylene and hydrogen molecule as the adsorbates all optimized and their lowest spin multiplicities were calculated separately before they are allowed to interact with each other. Taking a reaction mechanism into consideration, mainly there are three steps that take place in each mechanism; which are; the formation of C_2H_5, formation of C_2H_6, and desorption of C_2H_6. The reaction mechanisms usually differ from each other during the formation of C_2H_5 and C_2H_6 in terms of their relative energies, activation barriers and geometries. Thus, while investigating, for a mechanism type, first the formation of C_2H_5 is fulfilled and it is implemented with obtaining reaction coordinate calculations. From these calculations, activation energies, equilibrium geometries and transition states are determined. Then, with the next reaction coordinate driving calculations, similar procedure is applied to the formation of C_2H_6 and then and also desorption of C_2H_6 is calculated as the final reaction mechanism step. The relevant data from these three main stages are expected to enable us to have an insight about the probability of a suggested mechanisms which also takes place in the literature and hence this study is also to be a contribution to the theoretical literature among quantum mechanical calculations.

3.4.3 Methods of Correlations for Binding Energy Relations

Quantum mechanical investigations are consisted of structural information and total system energy for the optimum geometry of the considered cluster. In order to convert calculated total energy of the cluster to atomic binding energy, the following formula is used:

$$\text{Binding Energy}\left(\frac{\text{eV}}{\text{atom}}\right) = \frac{\{\text{Total energy of Ni}_\text{n}\text{ cluster}\} - n*\{\text{Single Ni atom energy}\}}{N} \qquad (3.2)$$

where, n is the number of atoms in the cluster. It should be noted that the quantum mechanical calculation method was kept the same for both the single atom and the cluster.

The parameter of $n^{-1/3}$, where n is the number of atoms in the cluster, in general provides a linear relationship with binding energy of clusters. The intercept of the resulting line with the binding energy axis provides a theoretical estimate for probable binding energy of bulk nickel at an infinite number of atoms. In this study, the computed binding energy of Ni_{55} nanocluster is used together with the previous literature data including the binding energies of Ni_2 (dimer) and Ni_{13} nanoclusters for investigating the above correlation. These findings are compared with experimental and theoretical data given in the previous literature sections.

CHAPTER 4

RESULTS and DISCUSSION

4.1. Ethylene Adsorption Studies on Ni_{13} Nanocluster, Ni(111), Ni(100) and Ni(110) Surface Model Clusters

4.1.1. Optimization of the Adsorbate; Ethylene Molecule

EG for C_2H_4 as reactant molecule is obtained by taking the total charge to be neutral and with a singlet spin multiplicity. Figure 4.1 gives the optimized ethylene molecule where C–C and C–H distances are computed as 1.330 **Å** and 1.087 **Å**, respectively where the experimental values are stated as 1.337 **Å** (Kuchitsu, K., 1992) and 1.34 **Å** (Kirk-Othmer, 2007) for C–C distance where it is reported as 1.103 **Å** (Kuchitsu, K., 1992) and 1.10 **Å** (Kirk-Othmer, 2007) for the C–H distance .

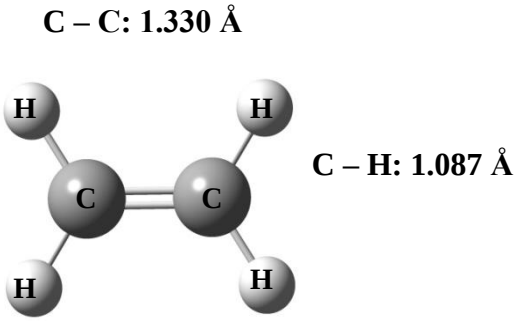

Figure 4.1 Optimized Ethylene Molecule.

4.1.2. Formation and Optimization of the Adsorbent

4.1.2.1. Ni_{13} Nanocluster

EG for Ni_{13} nanocluster is obtained by taking the total charge as neutral and the spin multiplicity as 7 corresponding to the lowest SPE. Figure 4.2 shows the optimized geometry of Ni_{13} nanocluster. Average Ni–Ni (Vertex–Vertex) and average Ni–Ni (Center–Vertex) distances are calculated to be 2.389 **Å** and 2.274 **Å**, respectively.

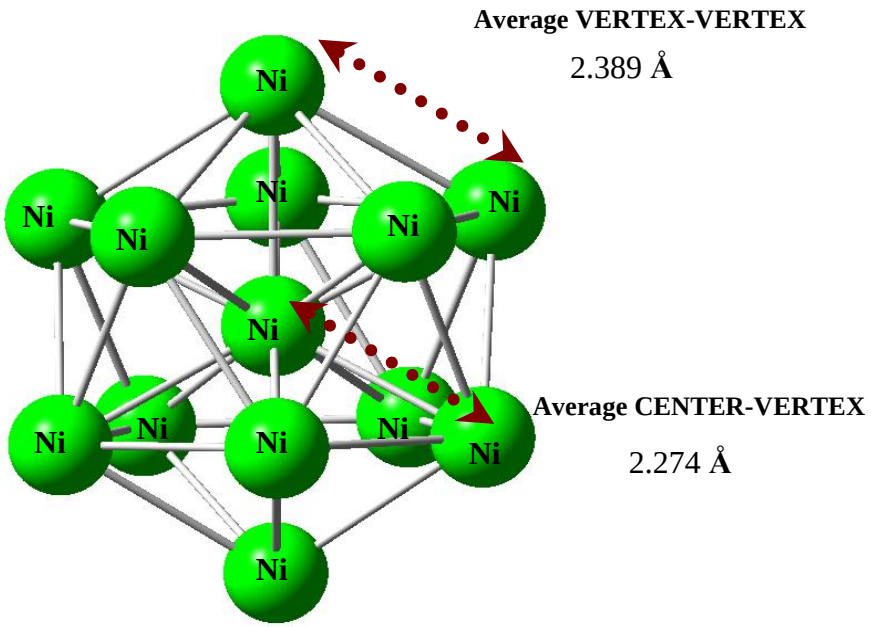

Figure 4.2 Optimized icosahedral structure of Ni_{13} Nanocluster.

4.1.2.2. Ni(1 1 1), Ni(1 0 0) and Ni(1 1 0) Surface Clusters

Spin multiplicity corresponding to the lowest spin multiplicity numbers for Ni_{10} (1 1 1), Ni_{13} (1 0 0) and Ni_{10} (1 1 0) surface clusters are determined as 4, 5 and 2 respectively, where Ni atoms in these surfaces are kept fixed during calculations. The optimized Ni_{10} (1 1 1), Ni_{13} (1 0 0) and Ni_{10} (1 1 0) surface clusters are shown in Figure 4.3, Figure 4.4 and Figure 4.5 respectively, where the Ni-Ni distance for bulk nickel structure is 2.492 **Å** for these geometries.

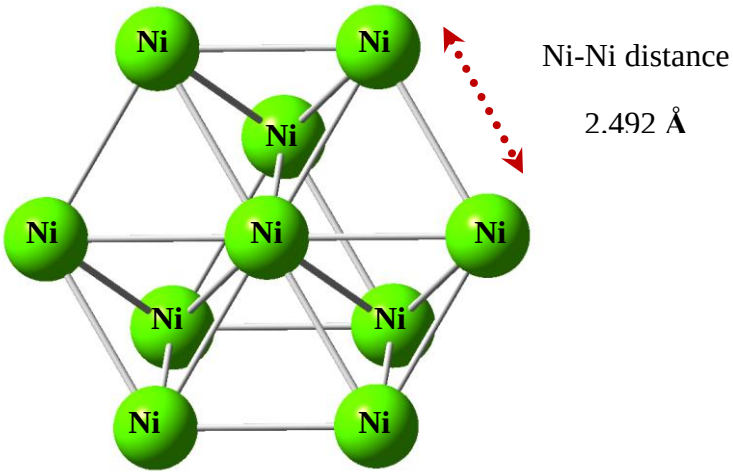

Figure 4.3 Optimized Ni_{10} (1 1 1) surface cluster.

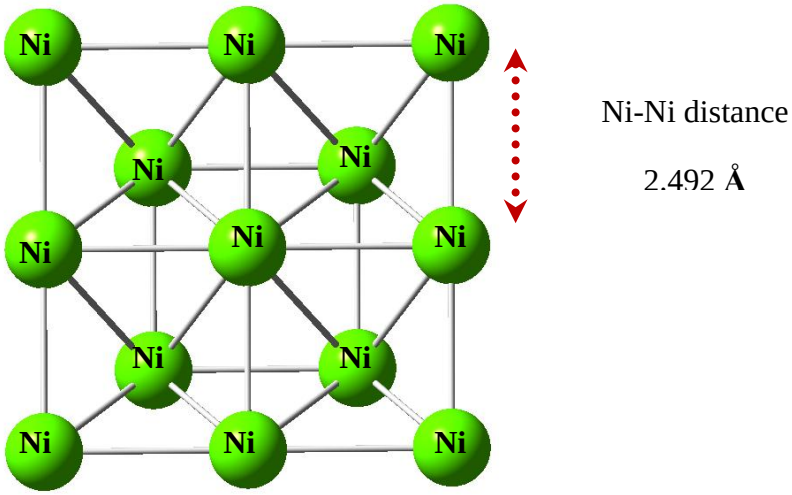

Figure 4.4 Optimized Ni_{13} (1 0 0) surface cluster.

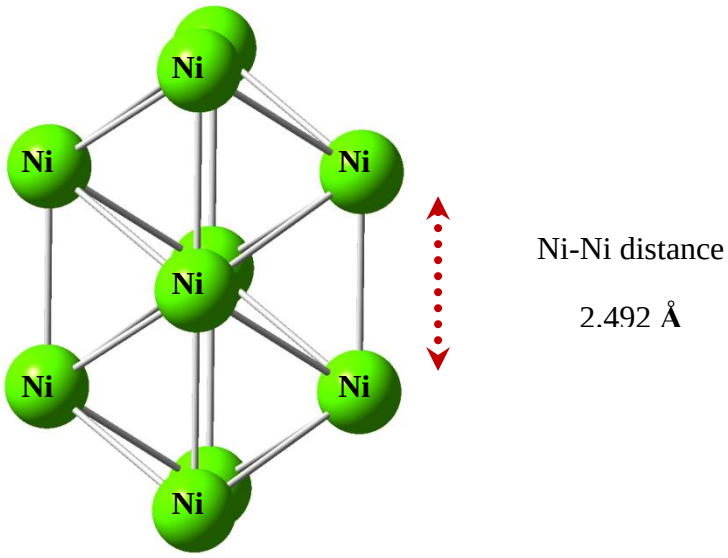

Figure 4.5 Optimized Ni_{10} (1 1 0) surface cluster.

4.1.3. Ethylene Adsorption Energies and Geometries

4.1.3.1. Adsorption of Ethylene on Ni_{13} nanocluster

Ethylene adsorption on the Ni_{13} nanocluster is studied by using EG calculations. It is found that ethylene is adsorbed molecularly with adsorption mode of π on Ni_{13} nanocluster, as shown in Figure 4.6.

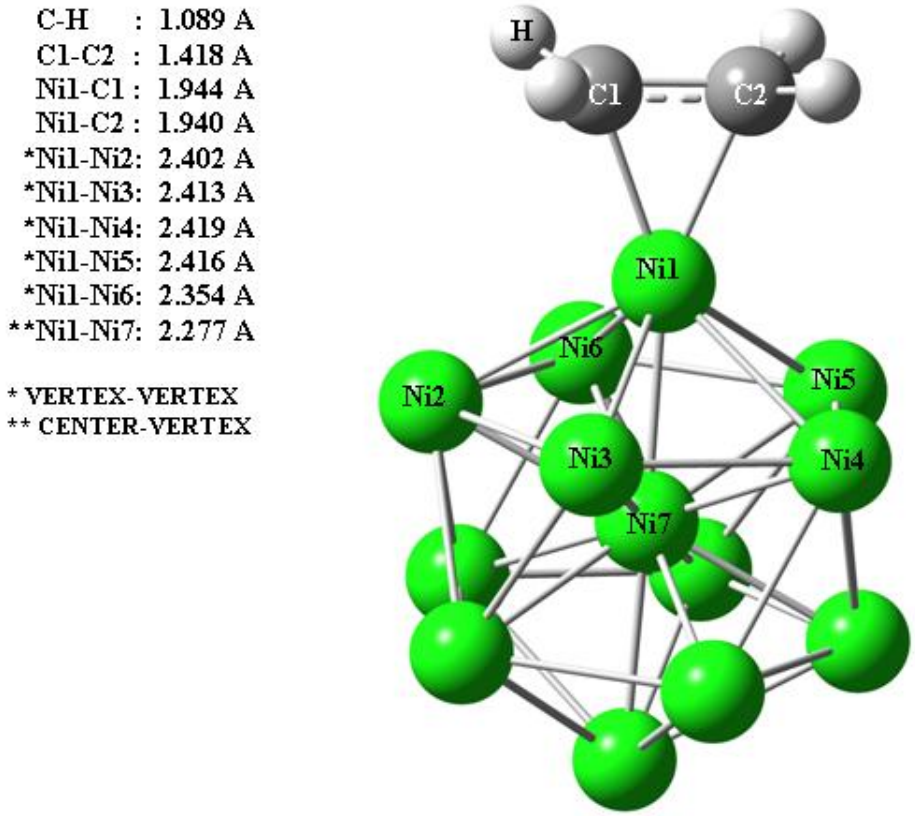

Figure 4.6 Equilibrium geometry of adsorbed ethylene on Ni_{13} nanocluster with adsorption mode of π.

Average Ni–Ni (Vertex–Vertex) and average Ni–Ni (Center–Vertex) distances for the ethylene adsorbed nanocluster are changed very little as compared to the bare cluster (2.390 **Å** and 2.274 **Å**, respectively), where distance between the ethylene and surface of the nanocluster (the height of the C–C axis from the surface in **Å**) is obtained to be 1.808 **Å**. Ethylene adsorption energy of the nanocluster is found as -50.86 kcal/mol.

4.1.3.2. Adsorption of Ethylene on Ni_{10} (1 1 1) Surface Cluster

Ethylene adsorption is studied molecularly on Ni_{10} (1 1 1) surface cluster by π adsorption mode, as shown in Figure 4.7.

(a)

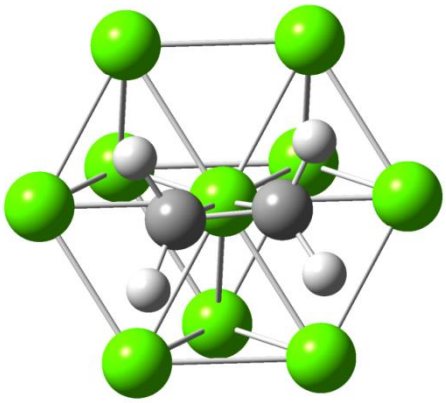

(b)

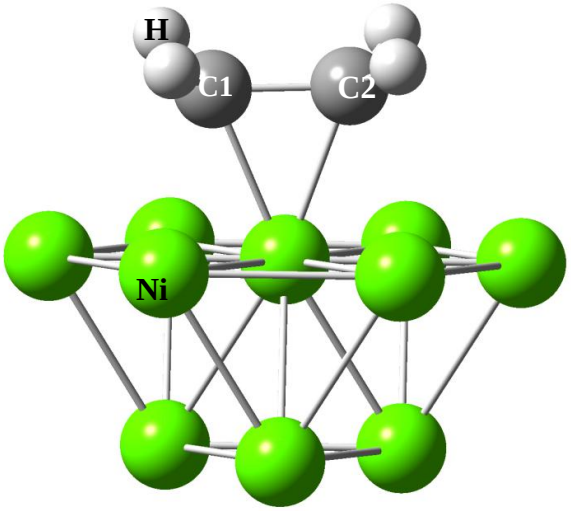

C1-Ni: 2.030 Å

C2-Ni: 2.017 Å

C1-C2: 1.449 Å

C-H: 1.091 Å

Figure 4.7 Equilibrium geometry of adsorbed ethylene on Ni_{10} (1 1 1) surface cluster model with adsorption mode of π a) Top view b) Side view.

Here, distance between the ethylene and surface of the cluster is obtained to be 1.887 **Å**. Ethylene adsorption energy of the Ni_{10} (1 1 1) surface cluster is found as -20.48 kcal/mol.

4.1.3.3. Adsorption of Ethylene on Ni_{13} (1 0 0) Surface Cluster

Ethylene adsorption by π adsorption mode on the Ni_{13} (1 0 0) surface cluster is studied also by EG calculations, as represented in Figure 4.8.

(a)

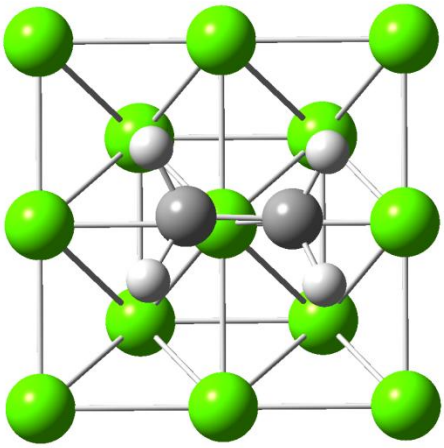

(b)

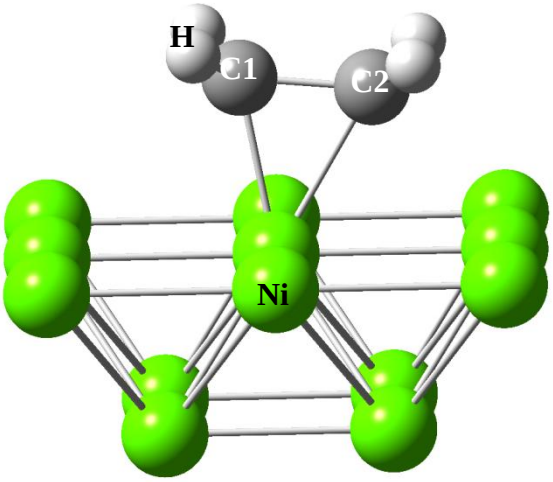

Figure 4.8 Equilibrium geometry of adsorbed ethylene on Ni_{13} (1 0 0) surface cluster model with adsorption mode of π a) Top view b) Side view.

Distance between the ethylene and surface is obtained to be 1.907 **Å**, where adsorption energy of the Ni_{13} (1 0 0) surface cluster is computed to be -32.44 kcal/mole.

4.1.3.4. Adsorption of Ethylene on Ni_{10} (1 1 0) Surface Cluster

Ethylene is adsorbed by π adsorption mode molecularly on Ni_{10} (1 1 0) surface cluster as indicated in Figure 4.9.

a)

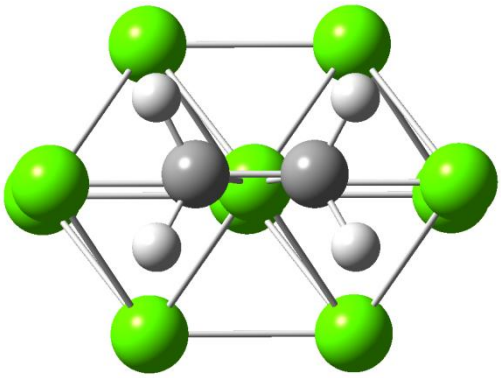

(b)

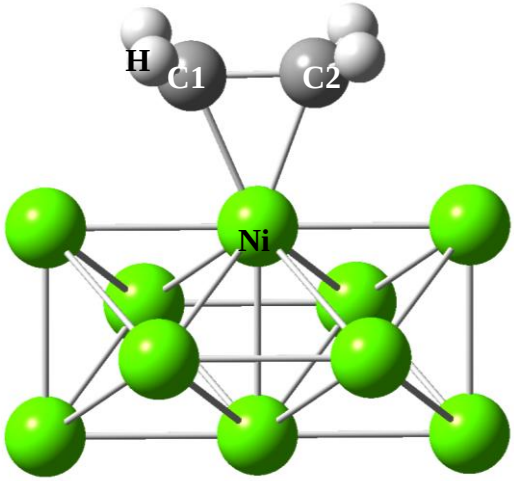

C1-Ni: 1.967 Å

C2-Ni: 1.948 Å

C1-C2: 1.451 Å

C-H: 1.091 Å

Figure 4.9 Equilibrium geometry of adsorbed ethylene on Ni_{10} (1 1 0) surface cluster model with adsorption mode of π a) Top view b) Side view.

The distance between ethylene and surface is calculated to be 1.818 **Å**. Ethylene adsorption energy of the Ni_{10} (1 1 0) surface cluster is computed as -39.27 kcal/mol.

4.1.4. Discussion

It is known that decreasing the particle size to very small atomic ensembles can sometimes affect activity. Metal atoms in the cluster which have very low coordination numbers form very strong bonds with the adsorbate to compensate for the smaller number of metal–metal bonds (van Santen and Neurock, 2006). This increases binding energy between the metal and the adsorbate.

A comparison of ethylene adsorption energies on Ni (1 1 1), Ni (1 0 0) and Ni (1 1 0) surface models and Ni_{13} nanocluster with available theoretical and experimental literature data is given in Table 4.1. Table 4.1 also gives the relevant distances between ethylene molecule and Ni surface as well as C–C, C–H and C–Ni bond lengths. Ethylene adsorption energy on Ni_{10} (1 1 1) surface cluster was calculated to be -20.48 kcal/mol with π adsorption mode. It is considerably higher than the value of -3.68 kcal/mol with π adsorption mode reported on Ni (1 1 1) by a (3×2) slab geometry by Vang (Vang et al., 2006). Although there is a significant difference between the adsorption energies, a comparison between these studies can not be made since the related bond distances of ethylene adsorption geometry are not reported in the above reference. In terms of experimental literature for ethylene adsorption on Ni (1 1 1) surface, the C–C bond distance is reported as 1.47 **Å** in a HREELS study done by Ibach and Lehwald (Ibach and Lehwald, 1981). It is similar to our computed C–C bond length of 1.45 **Å**. In addition, according to the study of Bao (Bao et al., 1994) where the values are determined using scanned-energy mode photoelectron diffraction, the C–C bond distance is obtained as 1.60 **Å**. It is considerably higher than our calculated value of 1.45 **Å** as well. However, their reported distance of C–C axis from surface is 1.90 **Å**. This is well-matched with the C–C-surface distance value of 1.89 **Å** obtained in our study.

As also given in Table 4.1, ethylene adsorption energy was computed as -32.44 kcal/mol with π-adsorption mode on Ni_{13} (1 0 0) surface cluster model. This value is higher than other theoretical values of -18.88 kcal/mol (Bernardo and Gomes, 2001b) and -15 kcal/mol (Crispin et al., 1999) reported on Ni_{16} (1 0 0)

cluster where their bond distances are not reported. In our study the C–C bond distance and the C–Ni distances were calculated to be 1.449 **Å** and 2.117 **Å** and 1.978 **Å**, respectively. The corresponding distances for π-adsorption mode were reported as 1.434 **Å** and 1.9075 **Å** in a theoretical study by Bernardo and Gomes (Bernardo and Gomes, 2001a). However, in terms of experimental literature, there is no experimental work reported for ethylene adsorption on Ni (1 0 0) cluster. It is reported that ethylene adsorption on Ni (1 1 0) gives an energy value of −45.65 kcal/mol in the experimental study by Brown (Brown et al., 1999). Here the presence of CH and CH_2 species were assumed on the Ni (1 1 0) surface. In the present study ethylene adsorption energy value was calculated to be −39.27 kcal/mol on Ni (1 1 0) with π-adsorption mode and without any assumption of the presence of CH and CH_2 species. Presently, there is no theoretical or experimental literature concerning ethylene adsorption on Ni_{13} nanocluster. The coordination numbers of Ni are 9, 8, and 7 for Ni (1 1 1), Ni (1 0 0) and Ni (1 1 0) surface models, respectively. On the other hand, the coordination number of Ni on Ni_{13} nanocluster is 6. It is also reported by Bernardo and Gomes (Bernardo and Gomes, 2001a) that for most metals two general types of low temperature spectra have been reliably identified and have been assigned to two distinct non-dissociative adsorption modes of ethylene. These are the di-σ adsorption and π adsorption modes. In the di-σ adsorption mode ethylene molecule interacts directly with two metal atoms while it interacts with a single metal atom in the π-adsorption mode. It is claimed that in some cases both types of species coexist, in others one type occurs on one crystal surface of a given metal and the other on a different one. Ni (1 1 1), Ni (1 0 0) and Ni (1 1 0) surface cluster models mentioned previously have also different adsorption energies with respect to particular adsorption modes such as di-σ and the π-adsorption modes. In the present study π-adsorption mode of ethylene is observed on all clusters. Ethylene was observed to have only π adsorption mode on Ni_{13} nanocluster. Therefore, in order to obtain a relevant correlation for adsorption energies with respect to coordination numbers, ethylene adsorption on Ni_{10} (1 1 1), Ni_{13} (1 0 0) and Ni_{10} (1 1 0) surface cluster models are studied only with π adsorption mode.

TABLE 4.1 Comparison of ethylene adsorption energies on Ni surface cluster models and Ni_{13} nanocluster.

Coordination Number	Surface	Studies	Energy of Adsorption (kcal/mole)	Mode of adsorption	Distance (A)			
					C_2H_4 – Surface	C-C	C-H	C-Ni
9	Ni(111)	Theoretical This Study	-20.48 [a]	π [a]	1.89 [a]	1.45 [a]	1.091 [a]	2.014 [a] 2.029 [a]
		Theoretical Other	-12.98 [b]	di-σ [b]	-	-	-	-
			-3.68 [c]	π [c]	-	-	-	-
			-4.0 [d]	di-σ [d]	1.89 [d]	1.49 [d]	-	-
			-13.0 [d]	di-σ [d]				
		Experimental	-	-	-	1.47 [e]	-	-
			-	-	1.90 [f]	1.60 [f]	-	-

TABLE 4.1 Cont'. Comparison of ethylene adsorption energies on Ni surface cluster models and Ni_{13} nanocluster.

Coordination Number	Surface	Studies	Energy of Adsorption (kcal/mole)	Mode of adsorption	Distance (A)			
8	Ni(100)	Theoretical This Study	-32.44 [a]	π [a]	1.9065 [a]	1.449 [a]	1.0869 [a]	2.11 [a] 1.98 [a]
		Theoretical Other	-	π [b]	1.9075 [b]	1.434 [b]	1.0876 [b]	-
			-	di-σ [b]	1.8689 [b]	1.462 [b]	1.0954 [b]	-
			-40.68 [g]	di-σ [g]	-	-	-	-
			-18.88 [g]	π [g]	-	-	-	-
			-27 [h]	di-σ [h]	-	1.438 [h]	-	2.05 [h]
			-15 [h]	π [h]	-	1.420 [h]	-	2.07 [h]
		Experimental	-	-	-	-	-	-

TABLE 4.1 Cont'. Comparison of ethylene adsorption energies on Ni surface cluster models and Ni_{13} nanocluster.

Coordination Number	Surface	Studies	Energy of Adsorption (kcal/mole)	Mode of adsorption	Distance (A)			
7	Ni(110)	Theoretical This Study	-39.27 [a]	π [a]	1.8178 [a]	1.451 [a]	1.0905 [a]	1.948 [a] 1.967 [a]
		Theoretical Other	-	-	-	-	-	-
		Experimental	-45.65 [i]	(large π contribution) [i]	-	-	-	-
6	Ni_{13}	Nanocluster This Study	-50.86 [a]	π [a]	1.808 [a]	1.418 [a]	1.0890 [a]	1.942 [a]

[a] Yilmazer et al., 2010.
[b] Bernardo and Gomes, 2001a.
[c] Vang et al., 2006.
[d] Fahmi and van Santen, 1997.
[e] Ibach and Lehwald, 1981.
[f] Bao et al., 1994.
[g] Bernardo and Gomes, 2001b.
[h] Crispin et al., 1999.
[i] Brown et al., 1999.

When adsorption energy is plotted against Ni coordination number as shown in Figure 4.10, a correlation exists if the adsorption modes are similar. In other words, when a trend line is added to the data of π-adsorbed mode for Ni_{10} (1 1 1), Ni_{13} (1 0 0) and Ni_{10} (1 1 0) surface cluster models and Ni_{13} nanocluster, it can be clearly stated that ethylene adsorption energy increases with decreasing Ni coordination number from 9 to 6.

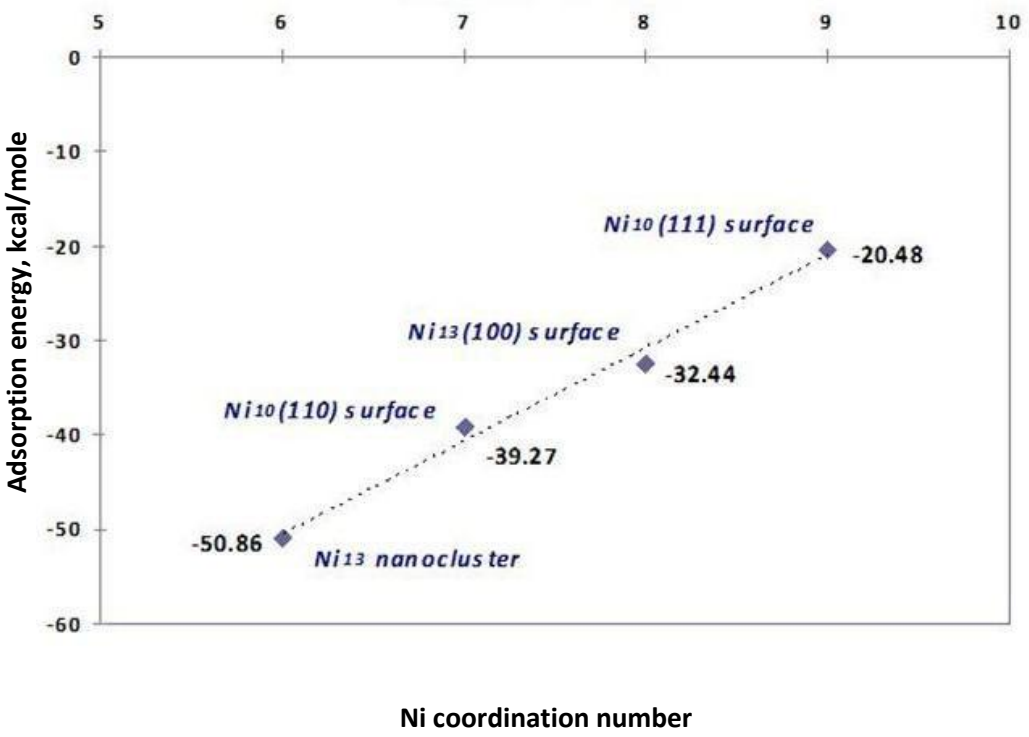

Figure 4.10 The inverse correlation between relative ethylene adsorption energies and the coordination number of Ni atoms in a series of different nickel surface cluster models and Ni_{13} nanocluster.

4.2. Ethylene Adsorption Study on Ni_{55} Nanocluster

4.2.1. Formation and Optimization of the Adsorbent; Ni_{55} Nanocluster

Geometry optimization calculations for magic number cluster of Ni_{55} are carrried out by using DFT method provided in Gaussian'03 (Frisch et al., 2004). In all our calculations, nickel clusters were neutral, their electrons were kept relaxed and nickel atoms were free in all directions. Different spin multiplicities are utilized in order to determine global minima.

Lathiotakis (Lathiotakis et al., 1996) and Luo (Luo, 2002) found that Jahn-Teller distortions of electronically degenerate configurations play an important role in the full optimization of the nickel clusters. It was explicitly noted that a wrong structure for nickel clusters could be found by ignoring directional bonding in the d manifold in equilibrium geometry calculations. Hence, quantum mechanical calculations included Jahn–Teller distortions without using any symmetry constraint.

Equilibrium geometry calculation of Ni_{55} nanocluster; since without using any symmetry constraint; by allowing Jahn-Teller deformation, resulted in a distorted IC geometry structure as shown in Figure 4.11 a and b and with more details in Figure 4.12 as also suggested experimentally by Parks (Parks et al., 1991), and Pellarin (Pellarin et al., 1994), and theoretically by Lathiotakis (Lathiotakis, 1996) and Luo (Luo, 2002).

(a)

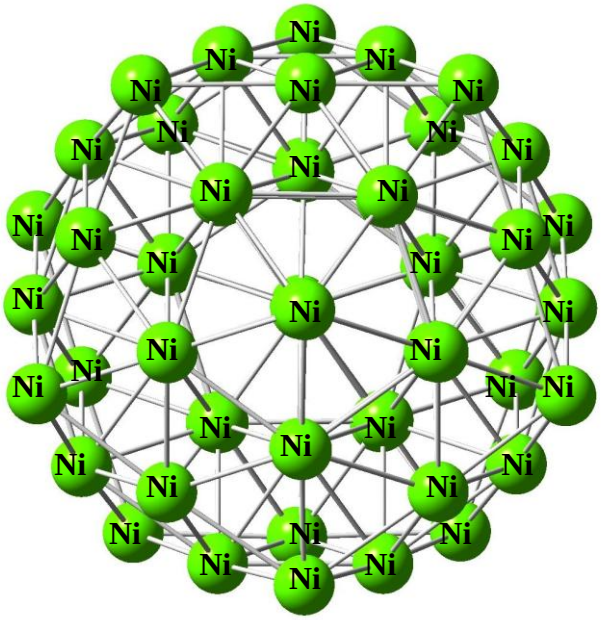

(b)

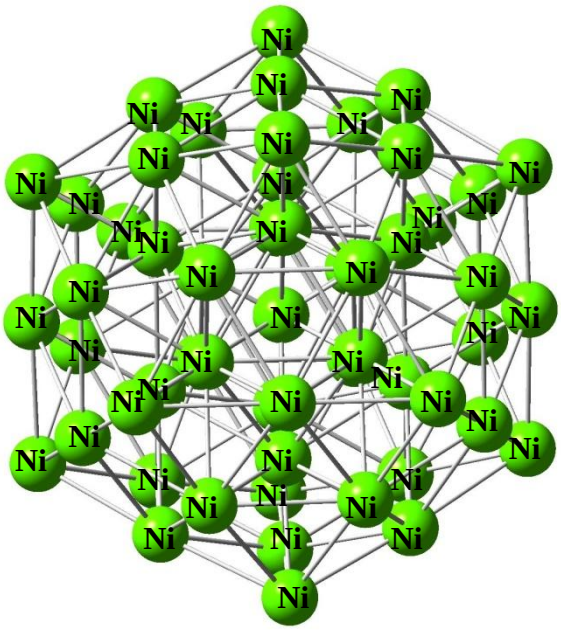

Figure 4.11 Optimized Ni_{55} surface cluster-ball and bond type model illustration a) top view, b) side view.

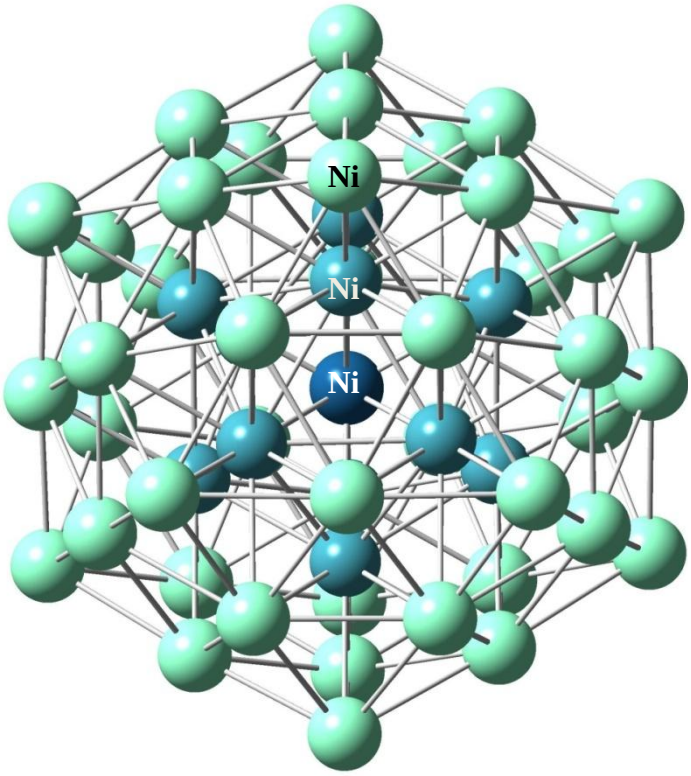

Average bond distance between the first shell and the center atom:

2.42946 A

Average bond distance between the atoms in the first shell and the other atoms neighboring them (including center atom and the second shell atoms):

2.49176 A

Average bond distance considering only vertex atoms in the outer (second shell) and the atoms neighboring them:

2.56034 A

Figure 4.12 Optimized Ni_{55} surface cluster- ball and bond type model illustration detailed side view- darkest atom is the core- centre Ni atom; medium-dark colored Ni atoms are the first layer of the cluster; and lightest colored surrounding Ni atoms are the second layer atoms.

Calculations were performed at various spin multiplicity values for Ni_{55} cluster in order to determine the lowest-energy configuration. Lowest spin result is obtained as 11.

After optimizing the geometry with respect to the lowest spin value attained, binding energy; average bond distance between the first shell and the center atom; average bond distance between the atoms in the first shell and the other atoms neighboring them (including center atom and the second shell atoms); and average bond distance considering only vertex atoms in the outer (second shell) and the atoms neighboring them are given in Table 4.2.

Table 4.2 Calculated Bond Lengths of the Ni_{55} distorted IC nanocluster.

Spin Multiplicity	**Binding energy per atom (eV/atom)**	**Bond Length (Å)**		
		Average bond distance between the first shell and the center atom	Average bond distance between the atoms in the first shell and the other atoms neighboring them (including center atom and the second shell atoms)	Average bond distance considering only vertex atoms in the outer (second shell) and the atoms neighboring them
11	-3.508	2.429 ± 0.020	2.492 ± 0.009	2.560 ± 0.028

As indicated in the Table 4.2, for Ni_{55} nanocluster; average bond distance between the first shell and the center atom is resulted as 2.429 ± 0.020 **Å**, where it is calculated as 2.492 ± 0.009 **Å** for the average bond distance between the atoms in the first shell and the other atoms neighboring them (including center atom and the second shell atoms) and finally for the average bond distance considering only vertex atoms in the outer (second shell) and the atoms neighboring them, it is obtained as 2.560 ± 0.028 **Å.** These values can be favorably compared to the theoretical literature values summarized in Table 4.3.

Table 4.3 Values of binding energy and bond length of IC Ni_{55} cluster.

References	**Method**	**B.E (eV)/atom**	**Mean Distance (Å)**
Lathiotakis et al., 1996	TB-MD	4.27	2.59
Luo, 2002	TB-MD	3.55	2.45
Grigoryan and Springborg, 2003	EAM	3.83	2.59
Montejano-Carrizales et al., 1996	EAM	3.87	-
Wang et al., 2010	DFT	3.92	2,45 2,52
Kar'kin et al., 2008	MD	3.694*	-
Xiang et al., 2000	GSA	3.77	2.36
Singh and Kroll, 2008	DFT	4.54	2.35 (interatomic) 2.47 (1^{st} shell) 2.41 (2^{nd} shell)
This Study	DFT	3.508	2.49

*Read from graph

In terms of distances (all in **Å)**, our findings (2.49 mean cluster bond length) compared well with the calculated average bond lengths of 2.59, 2.45**,** 2.59**, (**2.45, 2.52), 2.36**,** (2.35, 2.47, 2.41) by Lathiotakis (Lathiotakis, 1996), Luo (Luo,2002) and Grigoryan and Springborg (Grigoryan and Springborg , 2003), Wang (Wang et al., 2010), Xiang (Xiang et al., 2000) and Singh (Singh and Kroll, 2008), respectively.

4.2.2. Ethylene Adsorption Energies and Geometries on Ni_{55} Nanocluster

Ni_{55} nanocluster has two alternative adsorption sites having coordination numbers (CN) as 6 and 8 that can be considered for the cluster surface geometry.Therefore, in order to observe the coordination number relation with respect to the adsorption energies, ethylene adsorption is studied for these two different coordination numbers of Ni_{55} nanocluster.

4.2.2.1. Adsorption of Ethylene on Ni_{55} Nanocluster with coordination number 6

Ethylene adsorption is studied with π-adsorption mode having CN 6 on Ni_{55} nanocluster by using DFT/B3LYP and basis set of 86-411(41d)G in Gaussian'03. The adsorption energy is approximately found as -22.07 kcal/mole and the relevant adsorption geometry distances are shown in Figure 4.13.

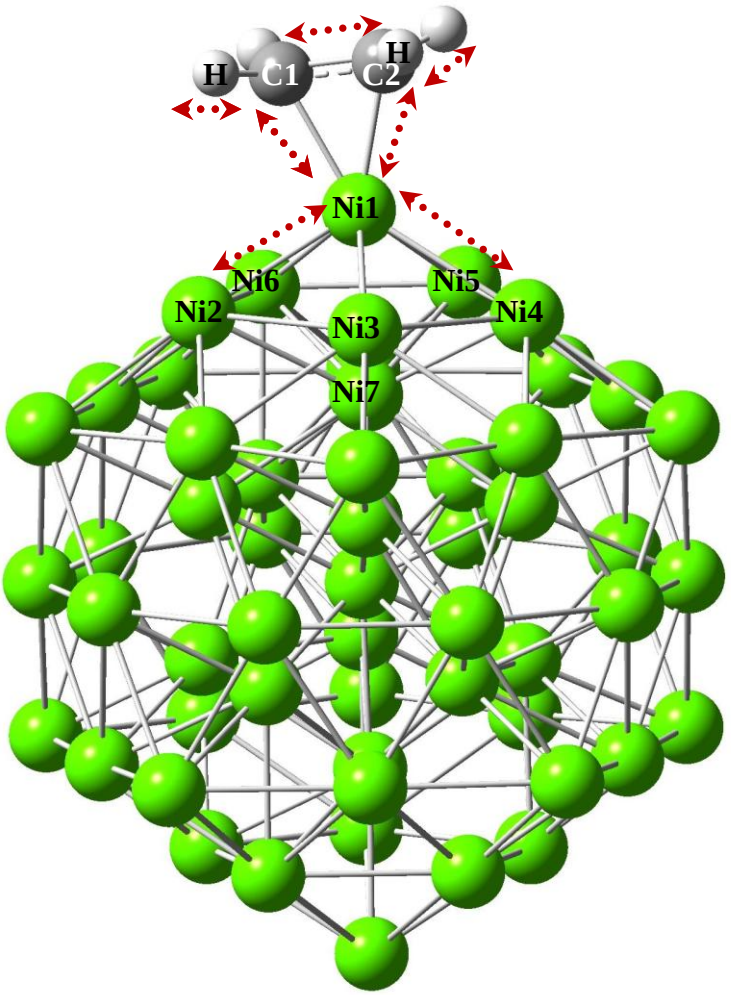

Figure 4.13 Equilibrium geometry of adsorbed ethylene on Ni_{55} nanocluster with CN 6 by π- adsorption mode.

4.2.2.2. Adsorption of Ethylene on Ni_{55} Nanocluster with coordination number 8

Similarly for CN 8 with π-adsorption mode on Ni_{55} nanocluster ethylene adsorption is studied by using DFT/B3LYP and basis set of 86-411(41d)G in Gaussian'03. The adsorption energy is found as -14.82 kcal/mole approximately and the adsorption geometry distances are similarly shown in Figure 4.14

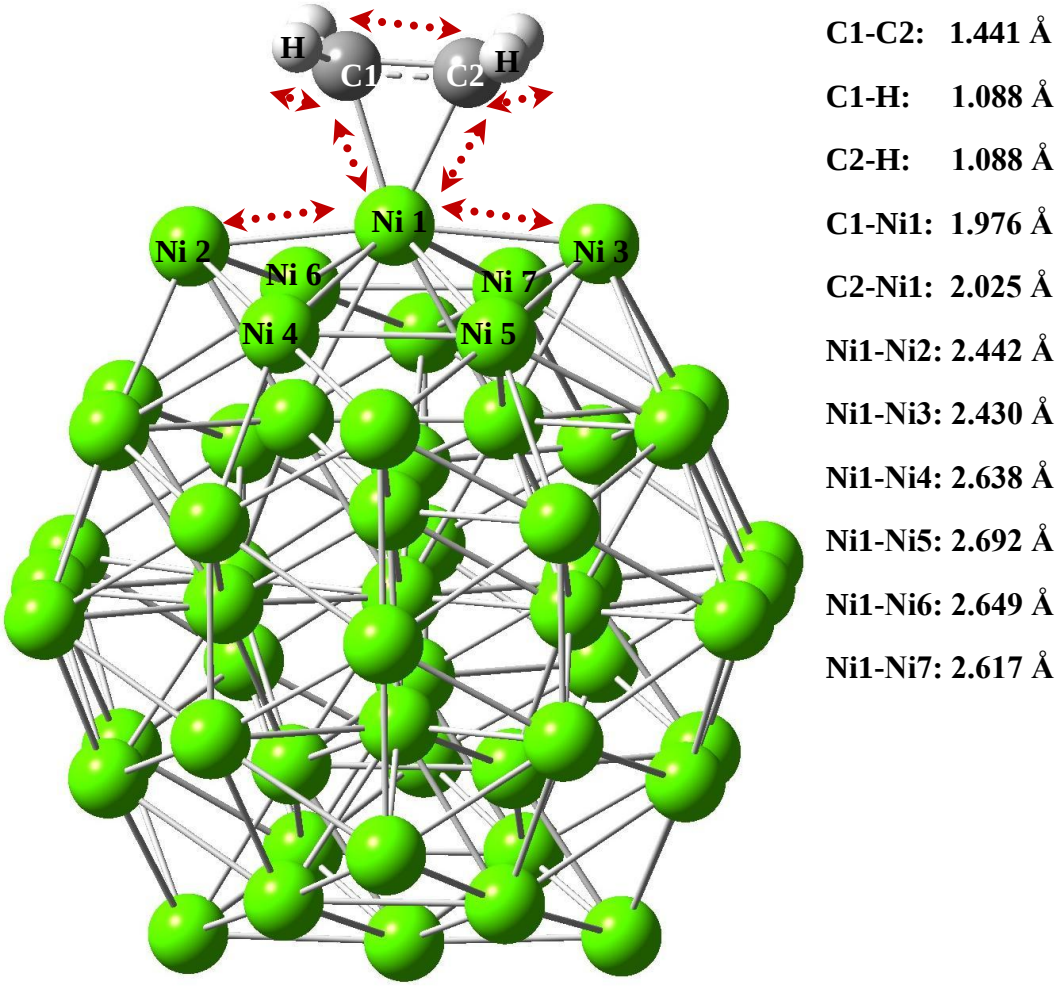

Figure 4.14 Equilibrium geometry of adsorbed ethylene on Ni_{55} nanocluster with CN 8 by π- adsorption mode.

4.2.3. Discussion

So far from our calculations different adsorption energy results are obtained from ethylene adsorption on Ni_{55} nanocluster approximately as -22.07 and -14.82 kcal/mole for different coordination numbers of CN 6 and 8 respectively where geometry distances are given in Figures 4.13 and Figure 4.14.

4.3. Binding Energy Correlations for Ni_2(dimer), Ni_{13} and Ni_{55} nanoclusters

For binding energy considerations, a correlation line is drawn and the intercept of binding energies is obtained against the value of "$n^{-1/3}$" for the cluster. The parameter of "$n^{-1/3}$", where n is the number of atoms in the cluster, in general provides a linear relationship with binding energy of clusters.

The intercept of the resulting line with the binding energy axis provides a theoretical estimate for probable binding energy of bulk nickel at an infinite number of atoms.

The result of interception as plotted in Figure 4.15 gives a good estimation for bulk nickel binding energy at infinite "n". This interception result is found as 4.58 eV/atom where the experimental value is reported as 4.45 eV/atom in the literature by Voter and Chen (Voter and Chen, 1987).

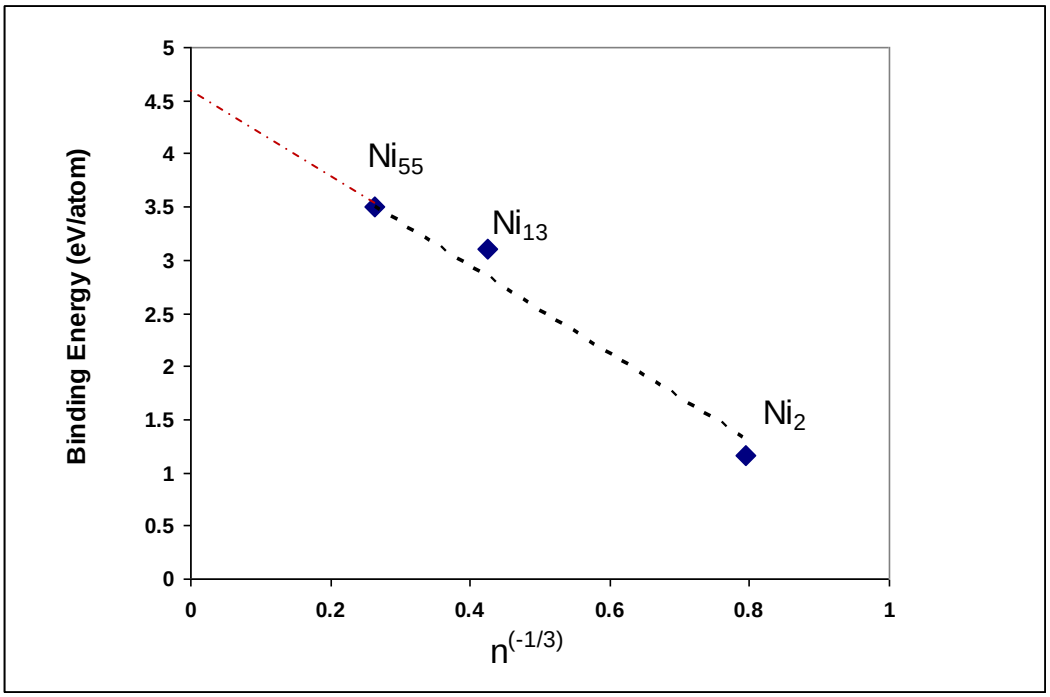

Figure 4.15 Binding energy relation as a function of $n^{(-1/3)}$ for the magic number clusters Ni_2, Ni_{13} and Ni_{55} nanocluster, where n is the atom number in the cluster.

In this work, the computed binding energy data of Ni_2 dimer and Ni_{13} nanocluster from literature are used together with the energy results of Ni_{55} nanocluster obtained in this study, for the investigation of the above correlation. The findings of theoretical binding energies of 2-atom, 13-atom and 55-atom nickel nanoclusters and their intercepts which are reported in the literature, are summarized in Table 4.4 together with our results stated as 3.508eV/atom for Ni_{55} binding energy; which the table also importantly includes experimental binding energy of bulk nickel as 4.45 eV/atom determined by Voter and Chen (Voter and Chen, 1987) as mentioned previously.

Table 4.4 Binding energy values for Ni_2, Ni_{13} and Ni_{55} nanoclusters

The authors	**Method**	**Ni_2**	**Ni_{13}**	**Ni_{55}**	**Intercept**
		B.E (eV/atom)			
Calleja et al., 1999	DFT/ double-ζ bases	1.199	2.757		4.56
Lathiotakis et al., 1996	TB-MD (minimal parameter)	0.93	3.16	4.10	5.69
Luo, 2002	TB-MD (simulated annealing)	-	2.99	3.55	4.45
Grigoryan and Springborg, 2003	EAM	1.81	3.38	3.83	4.93
Reuse and Khanna, 1995	DFT/LSD	1.61	4.26		7.32
Wang et al., 2010	DFT/PBE	2.23	3.33	3.92	4.08
Xiang et al., 2000	GSA	2.11[a]	3.38[a]	3.77	
Singh and Kroll, 2008	DFT/FS potential	-	3.84	4.51	
Yao et al., 2007	DFT/GGA	-	3.87[a]	4.57[a]	
Onal et al., 2009	DFT / B3LYP / m6-31 G*	1.078	2.700	-	4.57
	DFT / B3LYP / 6-31 G**	0.657	2.856	-	5.39
	DFT/ B3LYP/ 86-411(41d)G	1,158	3,109	3,508[b]	4.58
Voter and Chen, 1987	Experimental				4.45

[a] Read from graph

[b] This study

It is noticed that the techniques used during the calculations affected the accuracy of the results reported in the previous literature. For instance, Lathiotakis (Lathiotakis et al., 1996), found an over-estimated bulk value of 5.69 eV/atom by using minimal parameter tight binding molecular dynamics method whereas Luo (Luo, 2002) preferred tight binding molecular dynamics with the simulated annealing technique achieving a value of 4.45 eV/atom. It is also possible that the inclusion of Ni_{55} result may have improved the correlation that can only be made with Ni_2 dimer and Ni_{13} nanocluster.

4.3.1. Discussion

Selection of spin multiplicity of Ni_{55} cluster as 11 resulted in the lowest binding energy of 3.508 eV/atom which leads to the intercept of value 4.58 eV/atom together with the correlation considering Ni_2 and Ni_{13} nanoclusters. This intercept result, which actually refers to theoretical bulk value, is in reasonable agreement with the experimental bulk value of 4.45 eV/atom (Voter and Chen, 1987).

4.4. Investigation of Ethylene Hydrogenation Mechanisms on Ni_{13} Nanocluster

4.4.1. Investigation of Rideal Reaction Mechanisms

4.4.1.1. Rideal – I Type Mechanism; Reaction occurs between an adsorbed ethylene molecule and a gaseous hydrogen molecule

In this part, a reaction coordinate mechanism is performed between a previously adsorbed ethylene molecule C_2H_4(ads) on Ni_{13} nanocluster and a hydrogen molecule H_2(g) coming through the surface of the cluster. The reaction coordinate is chosen as the distance between Carbon atom of the ethylene molecule and one H atom of the hydrogen molecule. The related steps are given as follows:

Step 1, $C_2H_4(g) \rightarrow C_2H_4(ads)$ (4.1)

Step 2, $H_2(g) + C_2H_4(ads) \rightarrow C_2H_5(ads) + H(ads)$ (4.2)

Step 3, $C_2H_5(ads) + H(ads) \rightarrow C_2H_6(ads)$ (4.3)

Step 4, $C_2H_6(ads) \rightarrow C_2H_6(g)$ (4.4)

Step 1, illustrates the ethylene adsorption on the bare Ni_{13} nanocluster, as can be shown in Figure 4.16. The ethylene adsorption energy is calculated as -50.86 kcal/mole.

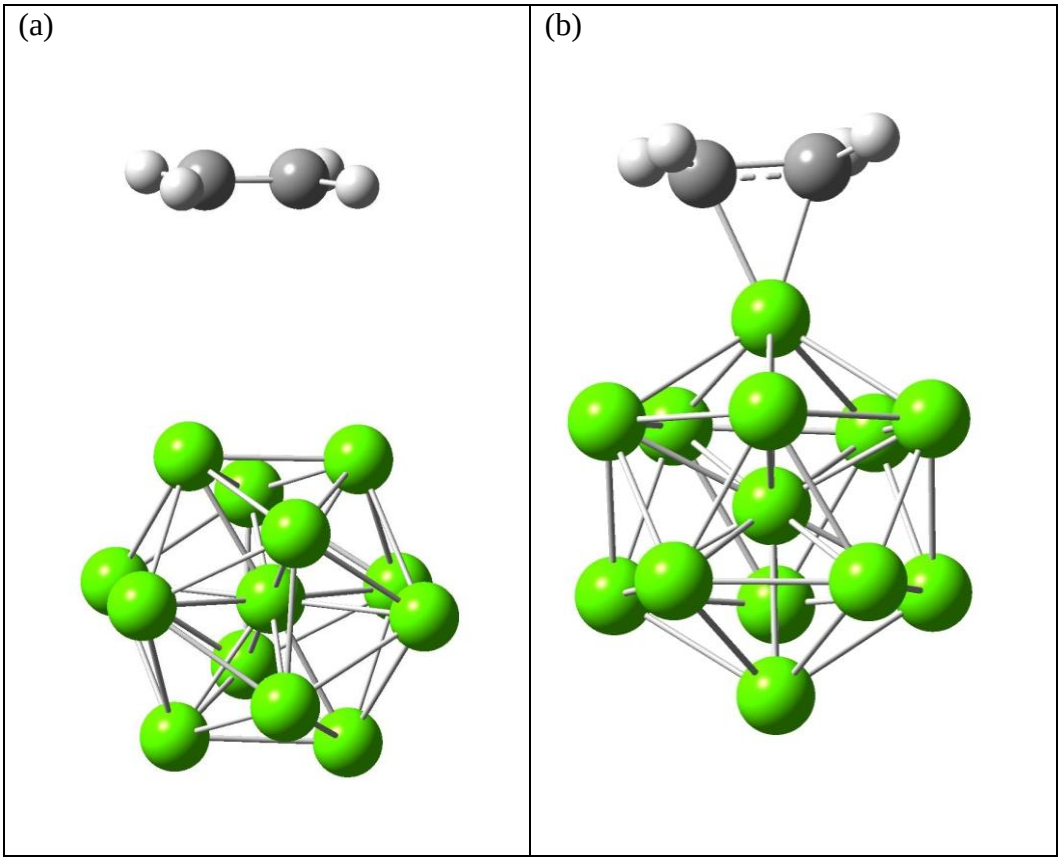

Figure 4.16 Ethylene adsorption on Ni_{13} nanocluster a) input geometry; before the adsorption; b) C_2H_4(ads) after the adsorption.

Step 2, describes the formation of C_2H_5 through the reaction between H_2(g) and the C_2H_4(ads) shown in Figure 4.17 where the activation barrier is computed as 38.20 kcal/mole.

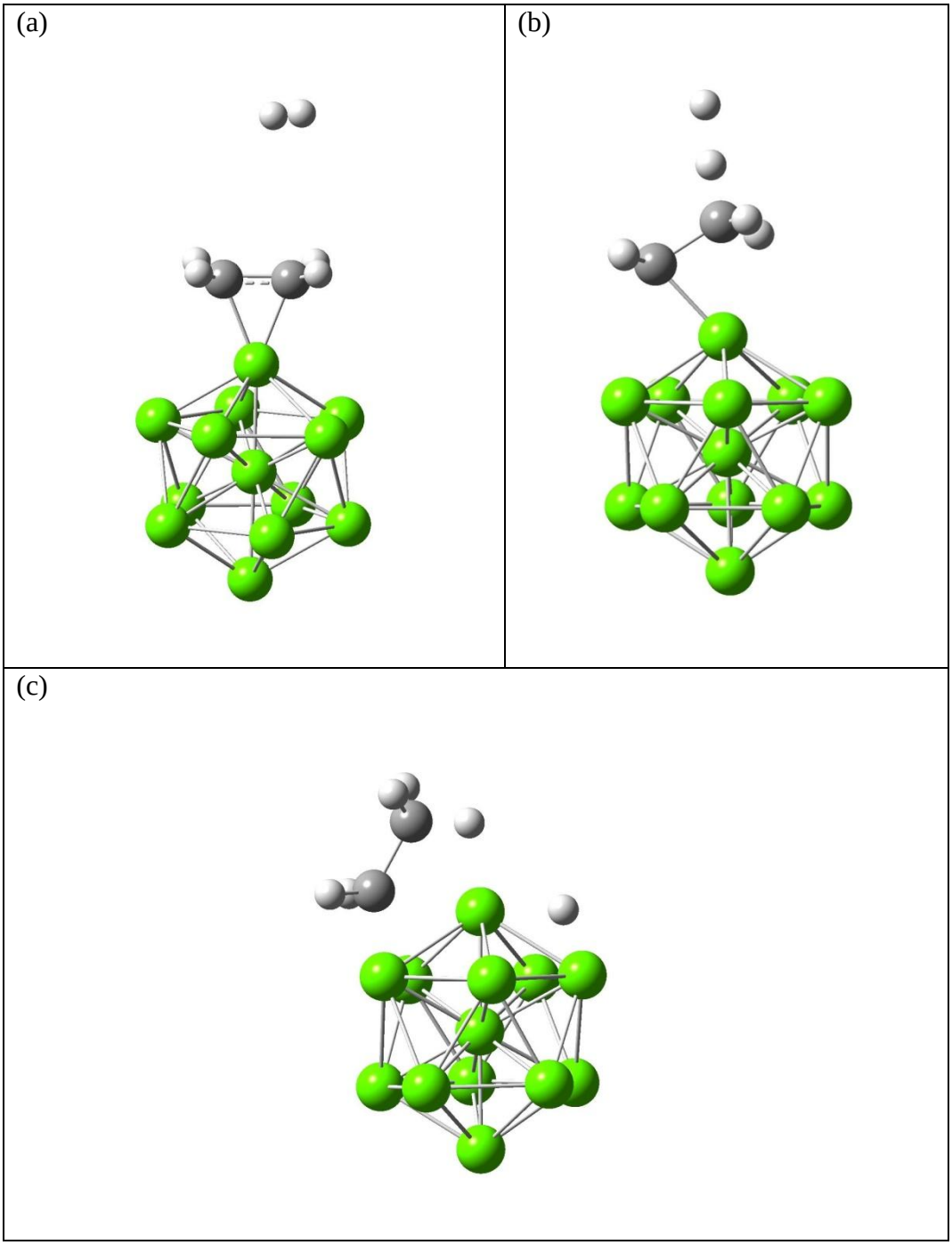

Figure 4.17 Reaction between C_2H_4(ads) and H_2(g); formation of C_2H_5(ads) a) input geometry before the reaction; b) TS geometry of the reaction c) EG geometry of formed C_2H_5

Step 3, is the formation of C_2H_6(ads) by the reaction between C_2H_5(ads) and H(ads) as given in Figure 4.18, where the activation barrier is computed as 34.23 kcal/mole.

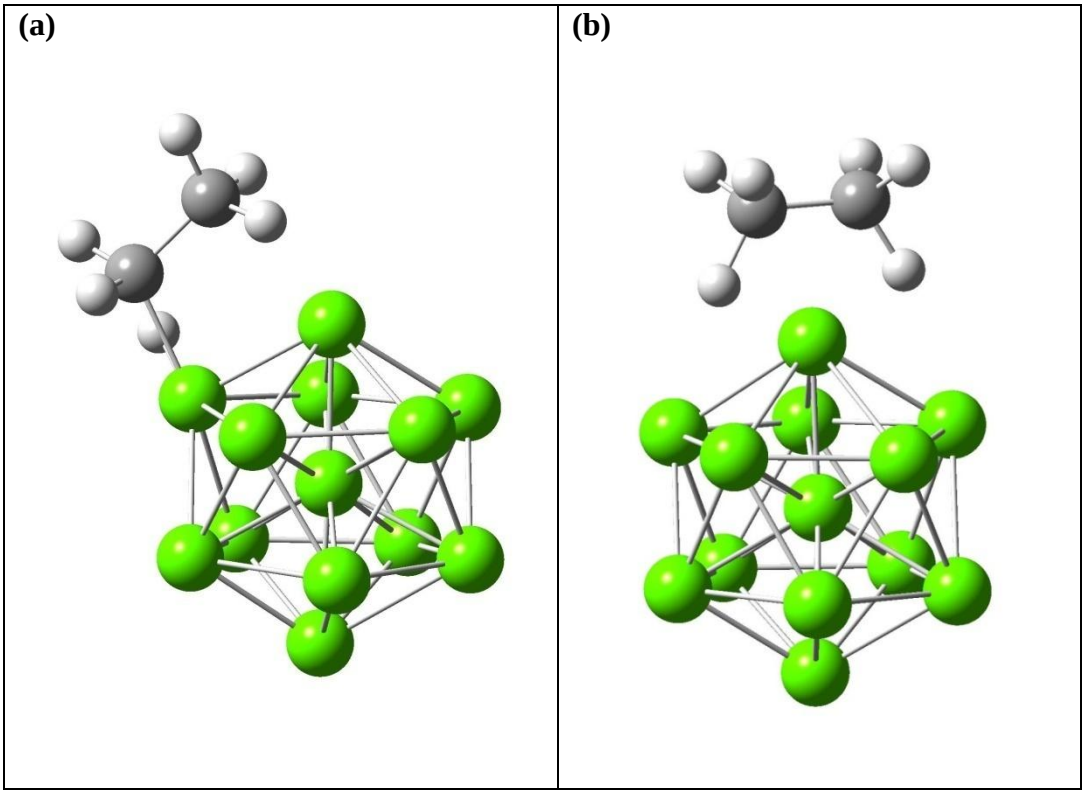

Figure 4.18 a) TS geometry of formation of C_2H_6(ads) b) EG geometry of the C_2H_6(ads)

Step 4 is the desorption of C_2H_6(ads) from the Ni nanocluster surface, which is computed as 10.52 kcal/mole as the energy.

4.4.1.2. Rideal – II Type Mechanism; Reaction occurs between an adsorbed hydrogen molecule and a gaseous ethylene molecule

In this case, similar to the Rideal-I, but this time H_2 (ads) molecule being adsorbed on to the surface at first and then C_2H_4 (g) gaseous molecule is coming to the surface of Ni_{13} nanocluster is the sequence that is considered as the mechanism. Mechanism steps are stated as follows:

Step 1, $H_2(g) \rightarrow H_2(ads)$ (4.5)

Step 2, $H_2(ads) + C_2H_4(g) \rightarrow C_2H_5(ads) + H(ads)$ (4.6)

Step 3, $C_2H_5(ads) + H(ads) \rightarrow C_2H_6(ads)$ (4.7)

Step 4, $C_2H_6(ads) \rightarrow C_2H_6(g)$ (4.8)

For Step 1, H_2(g) molecule is adsorbed molecularly on the Ni_{13} nanocluster surface. The adsorption energy calculated is -19.39 kcal/mole for this step where the geometries are shown in Figure 4.19.

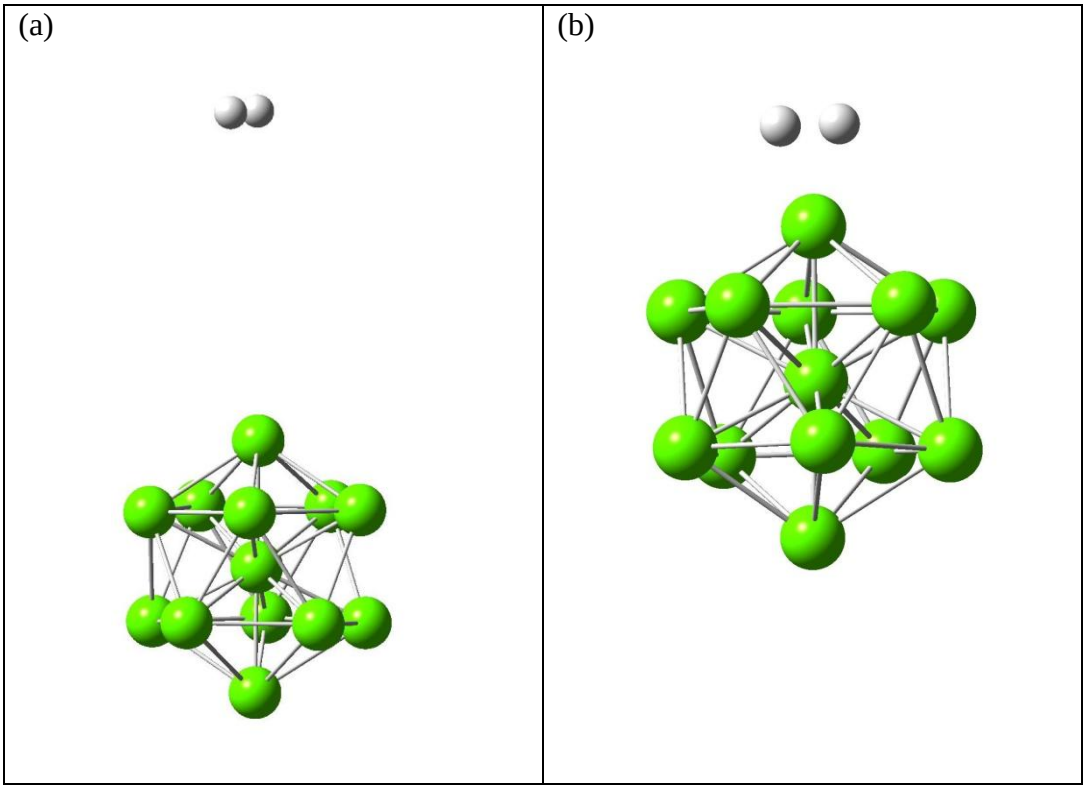

Figure 4.19 a) Input geometry before H_2(g) adsorps on Ni_{13} nanocluster b) EG geometry of the H_2(ads)

Step 2, $H_2(ads) + C_2H_4(g) \rightarrow C_2H_5(ads) + H(ads)$ (4.6)

Step 3, $C_2H_5(ads) + H(ads) \rightarrow C_2H_6(ads)$ (4.7)

Step 4, $C_2H_6(ads) \rightarrow C_2H_6(g)$ (4.8)

Steps from 2-4 are still being calculated.

4.4.2. Langmuir-Hinshelwood (LH) Reaction Mechanisms; Reaction occurs between an adsorbed ethylene molecule and adsorbed hydrogen molecule

This mechanism type suggests reaction occurring between the previously adsorbed reactants on the surface of the adsorbent. Some different consequences are considered for this part also, related with one of the the adsorbate taking in place as "H_2 molecule", "dissociated H_2 molecule" or "H atom" which will react together with the C_2H_4.

4.4.2.1. Mechanism-I

Here Hydrogen molecule is previously "*dissociated"* on the surface of the cluster before C_2H_4 (g) is introduced, adsorbed and reacts. Reaction steps can be shown as follows:

Step 1, $H_2(g) \rightarrow H_2(ads)$ (4.9)

Step 2, $H_2(ads) \rightarrow H(ads) + H(ads)$ (4.10)

Step 3, $2\ H(ads) + C_2H_4(g) \rightarrow C_2H_4(ads) + 2\ H(ads)$ (4.11)

Step 4, $2H(ads) + C_2H_4(ads) \rightarrow C_2H_5(ads) + H(ads)$ (4.12)

Step 5, $C_2H_5(ads) + H(ads) \rightarrow C_2H_6(ads)$ (4.13)

Step 6, $C_2H_6(ads) \rightarrow C_2H_6(g)$ (4.14)

Step 1, is the adsorption of H_2(g) o the cluster surface. Adsorption energy is computed as -19.39 kcal/mole where related schemes are given in Figure 4.20.

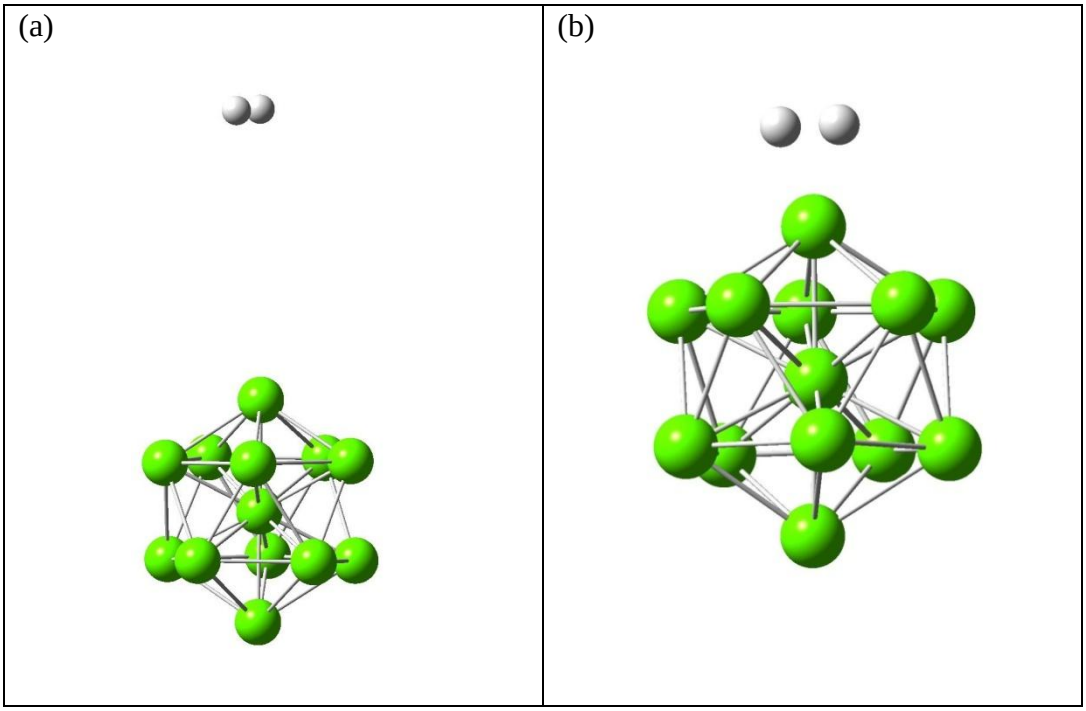

Figure 4.20 a) Input geometry before H_2(g) adsorption on Ni_{13} nanocluster surface b) H_2(ads) formation

Step 2, is the dissociation of H_2(ads) into 2H(ads) which is illustrated in Figure 4.21. Dissociation energy is computed as -22.77 kcal/mole.

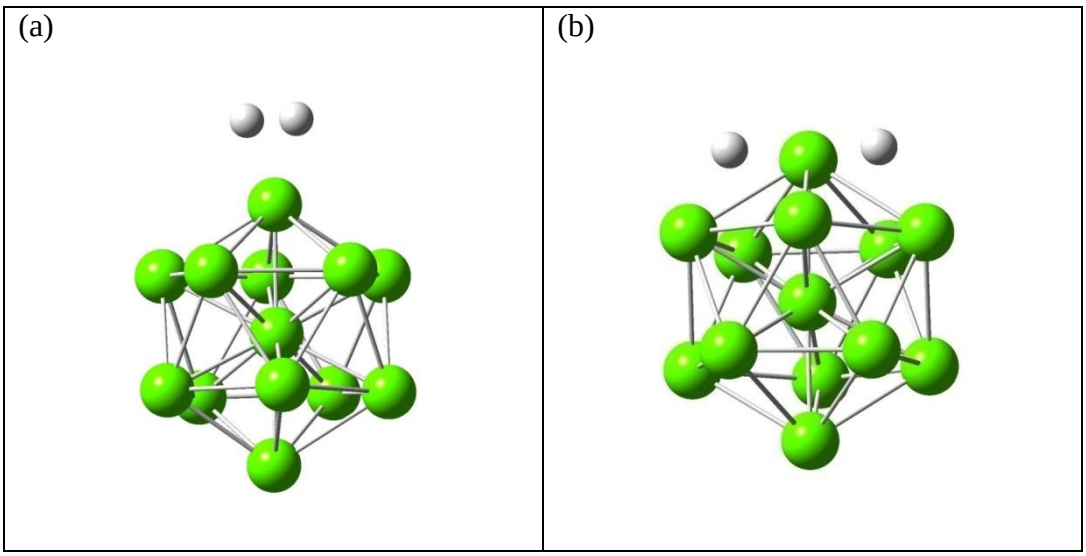

Figure 4.21 Input geometry a) before and b) after dissociation of H_2(ads)

Step 3, is the adsorption of ethylene molecule on to the Ni_{13} nanocluster surface where hydrogens are dissociatively adsorbed previously which is shown in Figure 4.22, where adsorption energy is calculated as -55.35 kcal/mole.

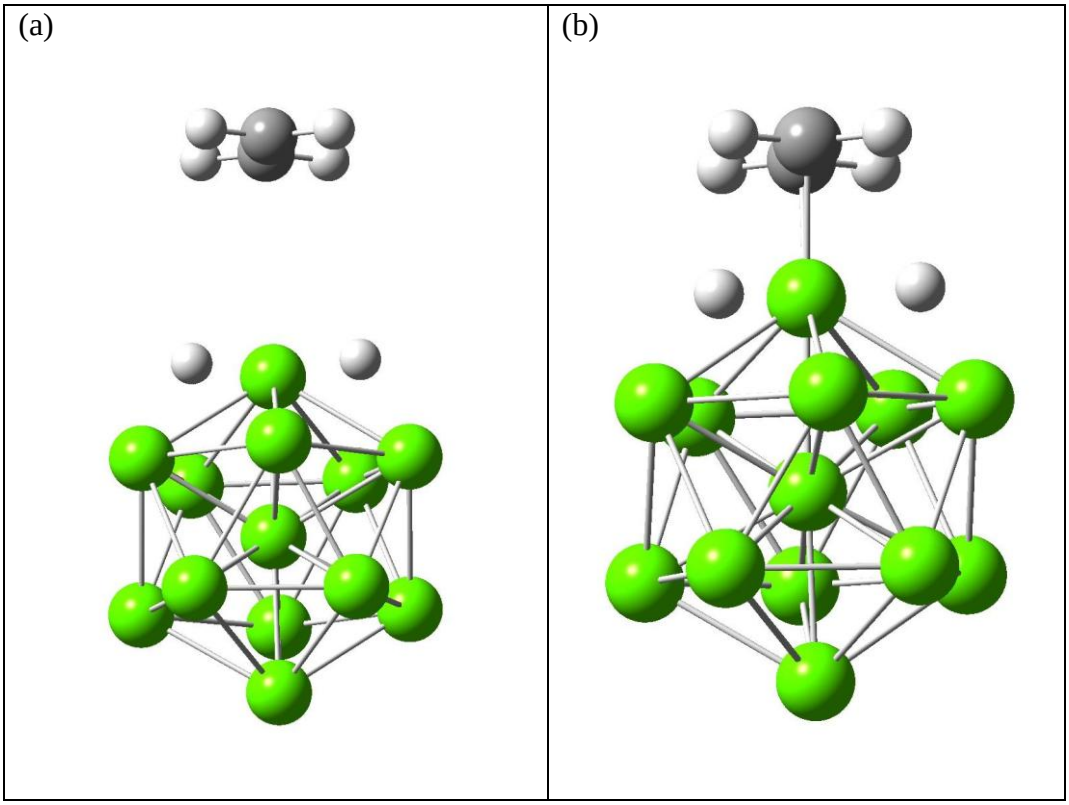

Figure 4.22 Adsorption of C_2H_4 on to the cluster surface a) input geometry b) adsorbed geometry.

Step 4, is the reaction between adsorbed H atoms and the C_2H_4(ads), where C_2H_5(ads) forms with activation barrier 6.65 kcal/mole and with geometries shown in Figure 4.23.

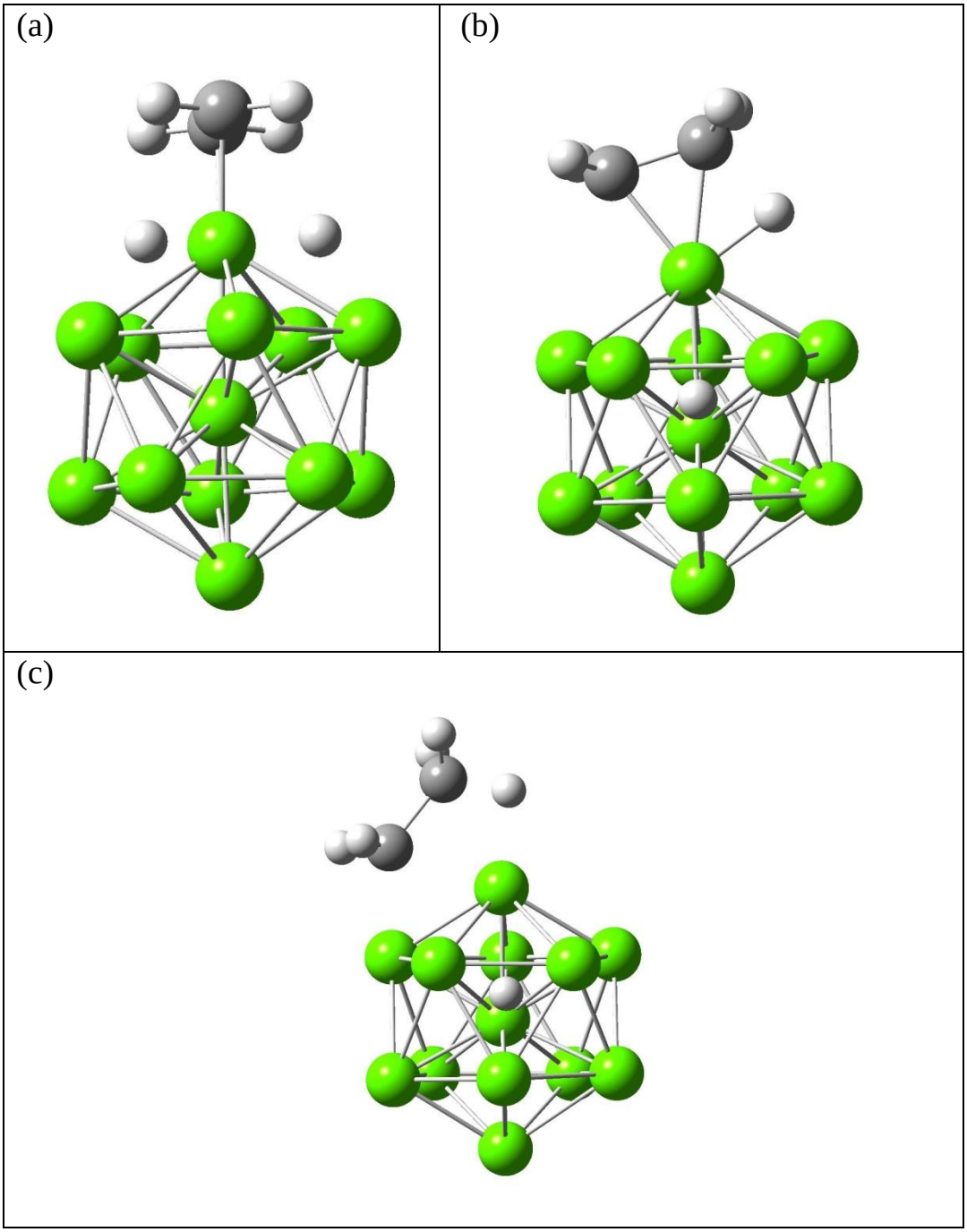

Figure 4.23 C_2H_5(ads) formation a) input geometry b) TS geometry b) EG geometry.

Step 5, is the formation of C_2H_6(ads) molecule, which has an activation barrier of 38.28 kcal/mole shown in Figure 4.24.

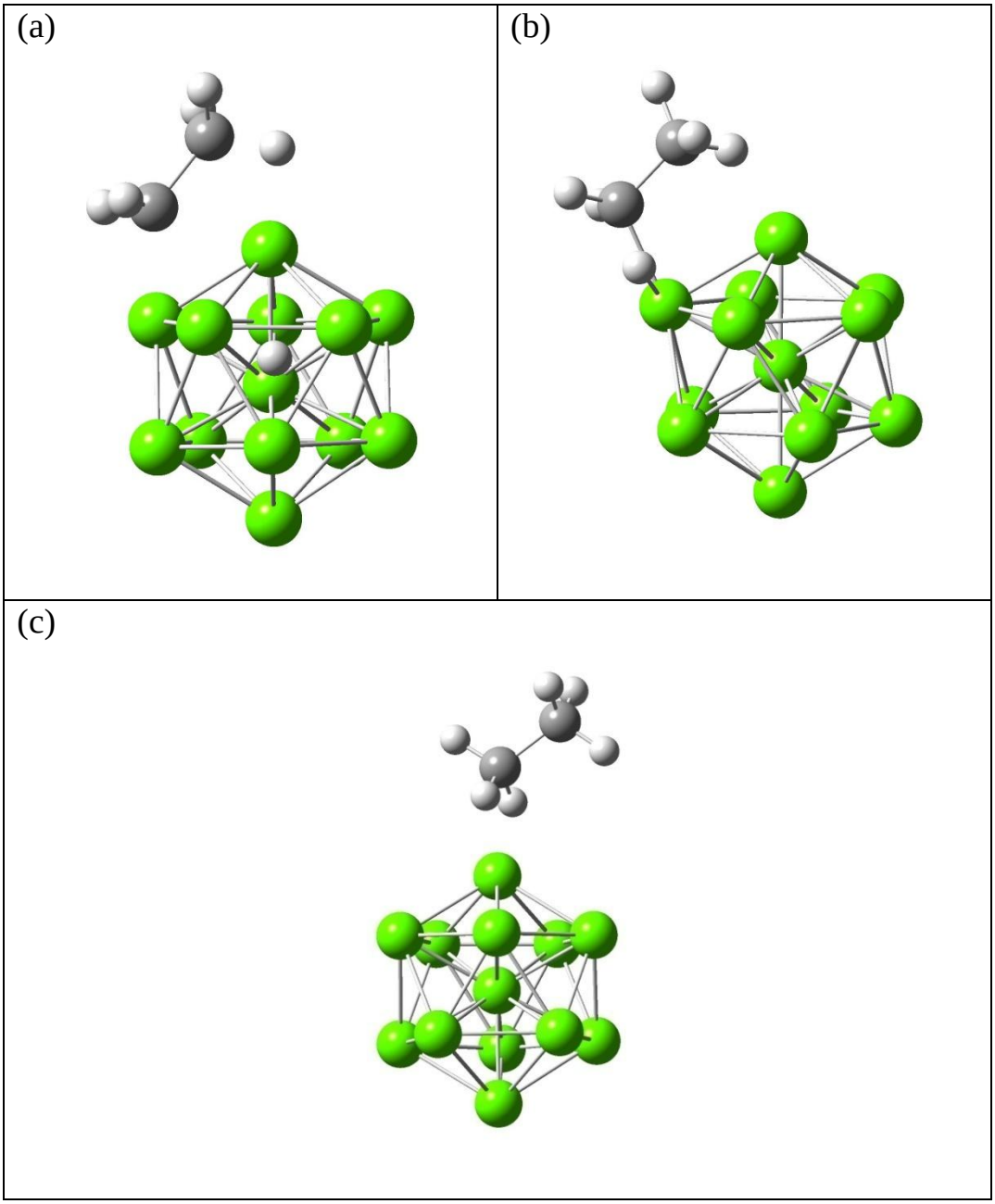

Figure 4.24 C_2H_6(ads) formation a) input geometry b) TS geometry b) EG geometry.

Step 6, is the desorption of C_2H_6(ads) molecule from the cluster surface with the energy 19.09 kcal/mole.

4.4.2.2. Mechanism-II

For this case, after H_2 molecule and ethylene molecule is adsorbed on the surface, hydrogenation reaction is proceded where the steps can be indicated as follows.

Step 1, $H_2(g) \rightarrow H_2(ads)$ (4.15)

Step 2, $H_2(ads) + C_2H_4(g) \rightarrow C_2H_4(ads) + H_2(ads)$ (4.16)

Step 3, $H_2(ads) + C_2H_4(ads) \rightarrow C_2H_5(ads) + H(ads)$ (4.17)

Step 4, $C_2H_5(ads) + H(ads) \rightarrow C_2H_6(ads)$ (4.18)

Step 5, $C_2H_6(ads) \rightarrow C_2H_6(g)$ (4.19)

Step 1, is the adsorption of H_2(g) molecule on the surface cluster, which has an energy of -19.39 kcal/mole and its geometry is shown in Figure 4.25.

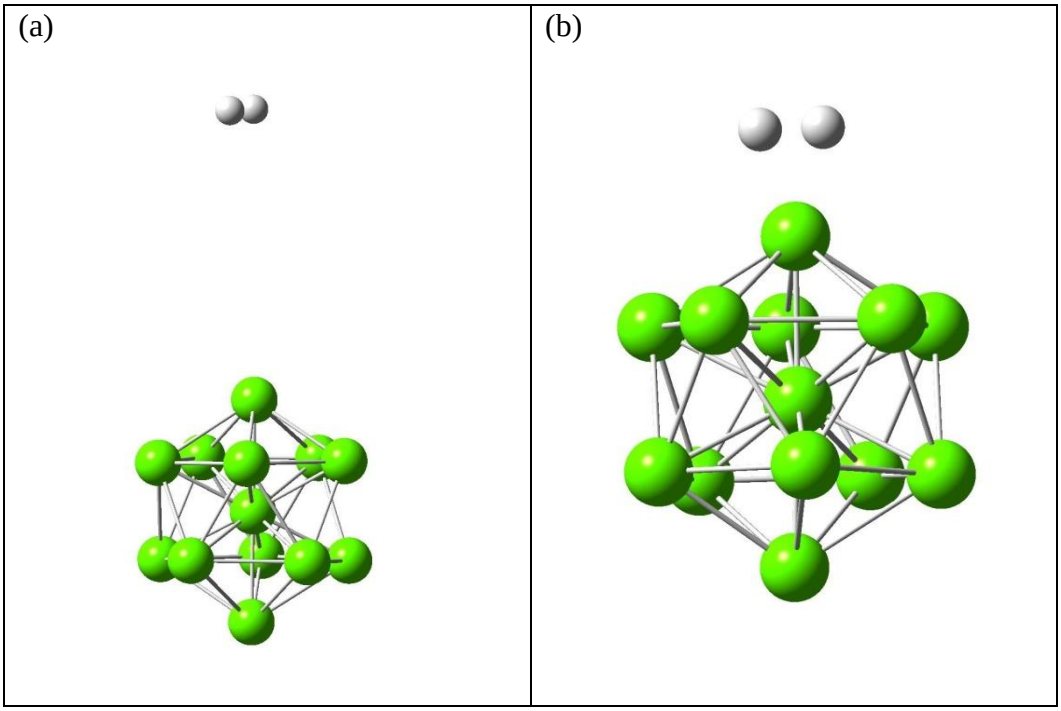

Figure 4.25 a) Input geometry before H_2(g) adsorption on Ni_{13} nanocluster surface b)H_2(ads) formation

Step 2, is the adsorption of C_2H_4(g) on to the cluster surface, near to the site of adsorbed hydrogen molecule H_2(ads) where the energy is calculated as -51.23 kcal/mole and the related geometries are given in Figure 4.26.

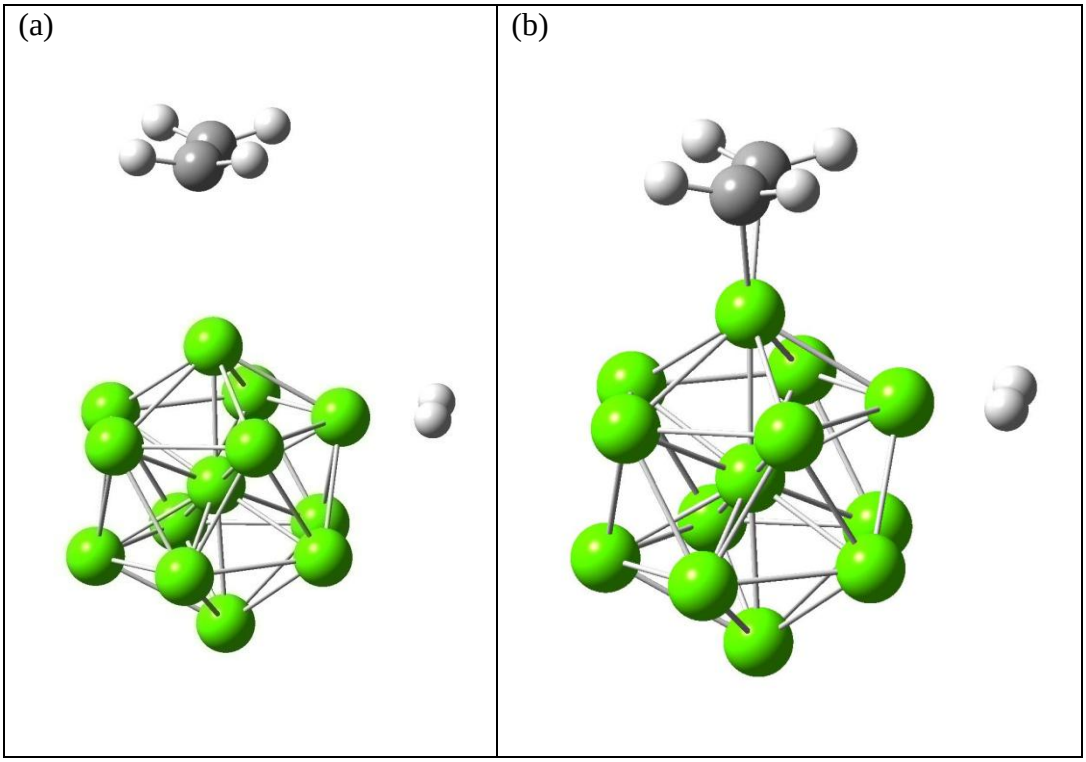

Figure 4.26 a) Input geometry before C_2H_4(g) adsorption on Ni_{13} nanocluster surface b) C_2H_4(ads) formation

Step 3, $H_2(ads) + C_2H_4(ads) \rightarrow C_2H_5(ads) + H(ads)$ (4.17)

Step 4, $C_2H_5(ads) + H(ads) \rightarrow C_2H_6(ads)$ (4.18)

Step 5, $C_2H_6(ads) \rightarrow C_2H_6(g)$ (4.19)

Steps 3-5 are still on progress.

4.4.2.3. Mechanism-III

For this case, after H_2 molecule and ethylene molecule is adsorbed on the surface, hydrogenation reaction is proceded where the steps can be indicated as follows.

Step 1, $C_2H_4(g) \rightarrow C_2H_4(ads)$ (4.20)

Step 2, $H_2(g) + C_2H_4(ads) \rightarrow C_2H_4(ads) + H_2(ads)$ (4.21)

Step 3, $H_2(ads) + C_2H_4(ads) \rightarrow C_2H_5(ads) + H(ads)$ (4.22)

Step 4, $C_2H_5(ads) + H(ads) \rightarrow C_2H_6(ads)$ (4.23)

Step 5, $C_2H_6(ads) \rightarrow C_2H_6(g)$ (4.24)

This time, Step 1 is the adsorption of $C_2H_4(g)$ on to the surface of the cluster which is with the energy of -50.86 kcal/mole and shown in Figure 4.27

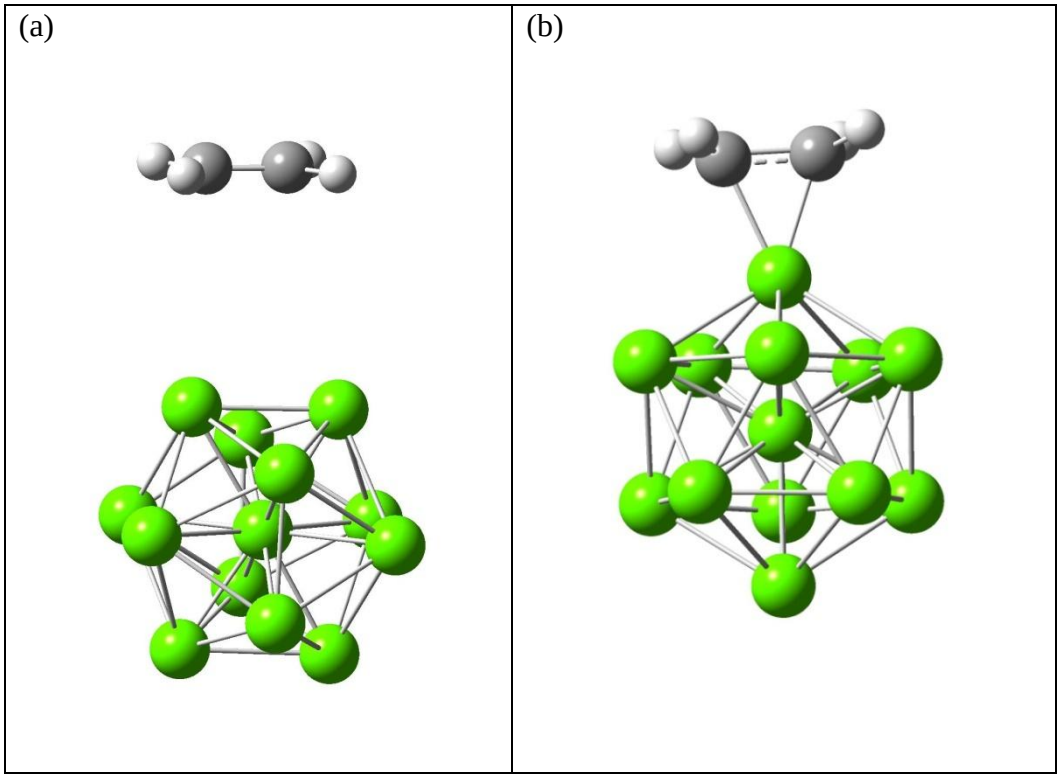

Figure 4.27 Adsorption of $C_2H_4(g)$ on to the cluster a) input geometry b) adsorbed geometry.

Step 2 is the adsorption of H_2(g) on to the surface molecularly while C_2H_4(ads) is on the surface, where its energy is -19.75 kcal/mole with the shown geometries in Figure 4.28.

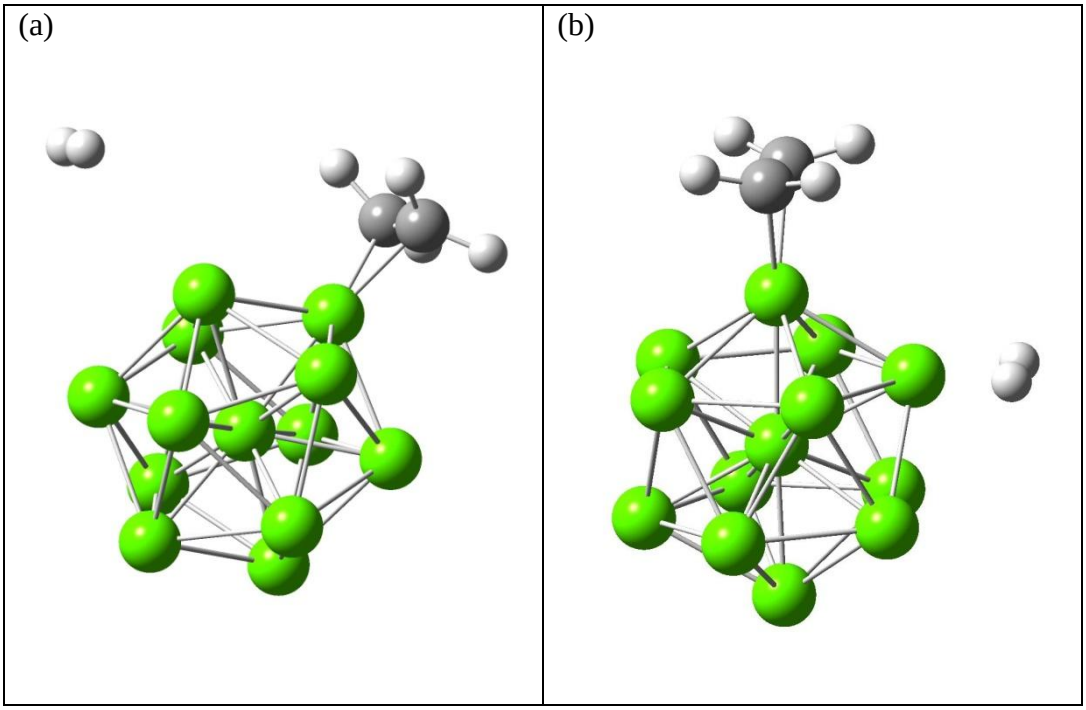

Figure 4.28 Adsorption of H_2(g) on to the cluster a) input geometry b) adsorbed geometry.

Step 3, $H_2(ads) + C_2H_4(ads) \rightarrow C_2H_5(ads) + H(ads)$ (4.22)

Step 4, $C_2H_5(ads) + H(ads) \rightarrow C_2H_6(ads)$ (4.23)

Step 5, $C_2H_6(ads) \rightarrow C_2H_6(g)$ (4.24)

Steps indicated above are being computed.

4.4.3. Discussion

Considering completed mechanisms Rideal-I and L-H Mechanism-I, their Potential Energy Diagrams are plotted. For Rideal-I the related potential energy diagram is given in Figure 4.29 and similarly for the L-H Mechanism-I related potential energy diagram is given in Figure 4.30. In comparison of plots, both suggested mechanisms seem to enable hydrogenation reaction with similar energies and total barriers.

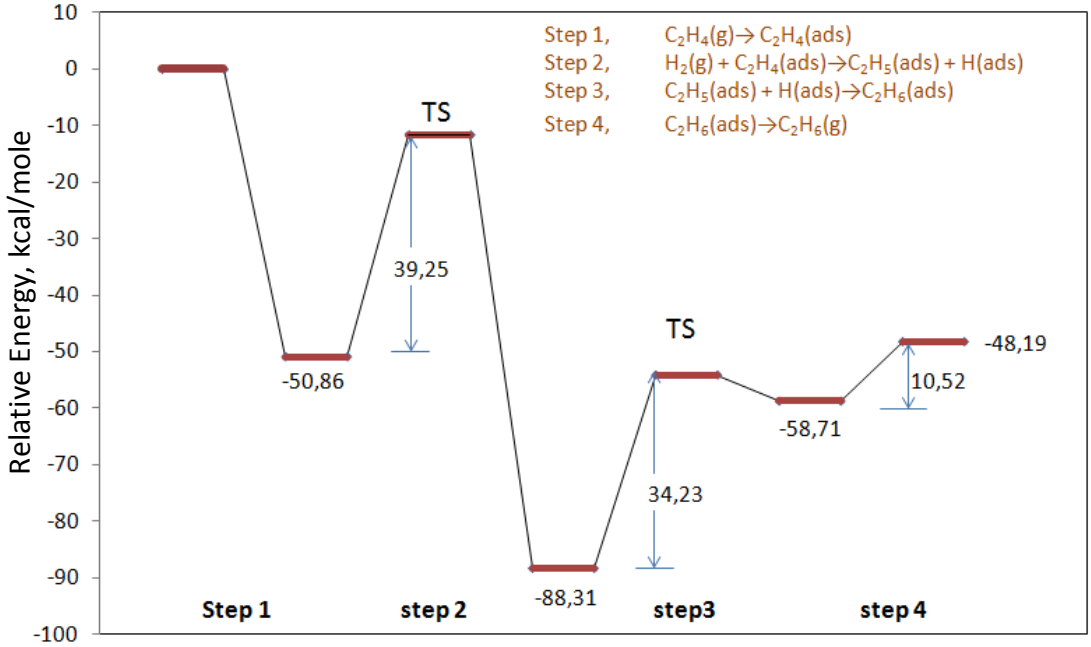

Figure 4.29 PE diagram for the Rideal-I mechanism

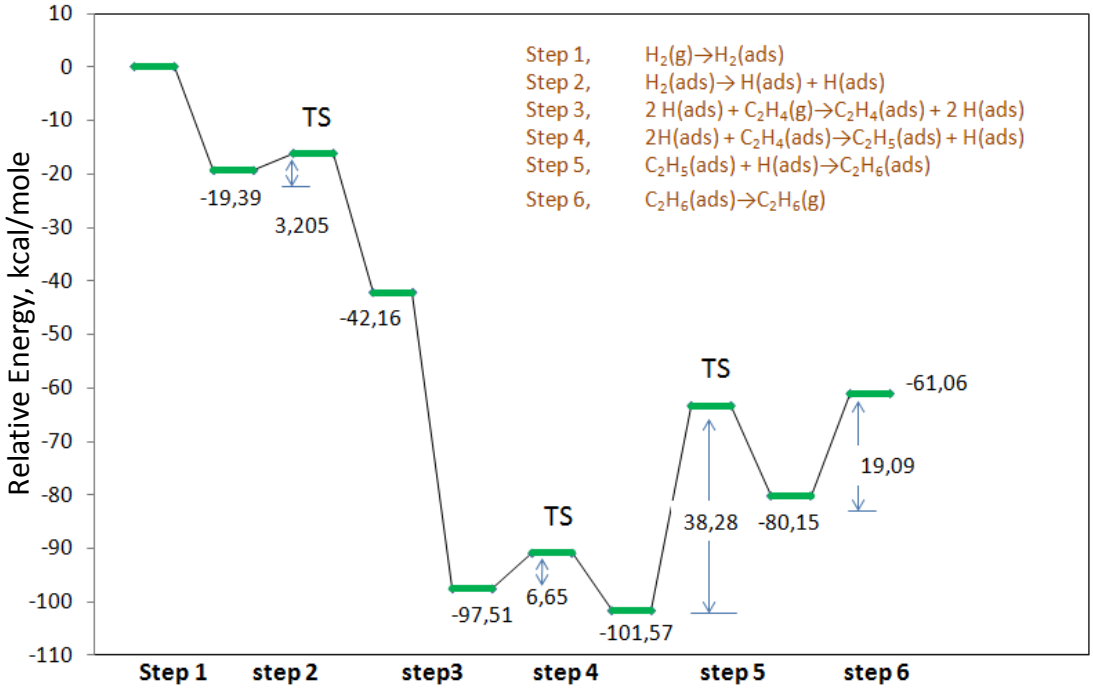

Figure 4.30 PE diagram for the L-H Mechanism-I

CHAPTER 5

CONCLUSIONS

Ethylene adsorption was studied by use of DFT with B3LYP formalism and basis sets of 6-31G(d,p) in Gaussian 03. When the surface activities of Ni with respect to ethylene adsorption energies on Ni(111), Ni(100) and Ni(110) surface clusters and Ni_{13} nanocluster are compared with each other, it can be clearly stated that ethylene adsorption energy increases with Ni coordination number decreasing from 9 to 6. It was found that ethylene on Ni_{13} nanocluster has adsorbed molecularly with a relative energy value of -50.86 kcal/mol where the energy value was obtained as -20.48 kcal/mole, -32.44 kcal/mole and -39.27 kcal/mole for Ni_{10}(111), Ni_{13}(100) and Ni_{10}(110) surface clusters with π adsorption mode, respectively.

Performing the calculations with DFT/B3LYP and basis set of 86-411(41d)G in Gaussian'03, ethylene adsorption is studied on Ni_{55} nanocluster for its two coordination numbers as 6 and 8. Adsorption energies obtained from ethylene adsorption computations on Ni_{55} nanocluster are obtained approximately as -22.07 and -14.82 kcal/mole for the coordination numbers 6 and 8 respectively.

Ni_{55} cluster is investigated by DFT/B3LYP and with the basis set of 86-411(41d)G in Gaussian'03 in order to obtain its binding energy. Its resulting distorted icosahedral (IC) geometry, is computed to have the average bond length of the cluster as 2.49 Å. This bond distance is in good agreement with the experimental and theoretical literature such as the following literature data: 2.59 **Å**, 2.45 **Å,** 2.59 **Å, (**2.45, 2.52) **Å**, 2.36 **Å,** (2.35, 2.47, 2.41) **Å** reported by Lathiotakis et al. (Lathiotakis et al., 1996), Luo (Luo, 2002), Grigoryan and

Springborg (Grigoryan and Springborg, 2003), Wang et al., (Wang et al., 2010), Xiang et al., (Xiang et al., 2000) and Singh and Kroll (Singh and Kroll, 2008) respectively.

Binding energy for the Ni_{55} cluster is found as 3.508 eV/atom with the lowest spin multiplicity value as 11. Regarding the binding energy correlations together with Ni_2 and Ni_{13} nanoclusters, the intercept is calculated as 4.58 eV/atom for the bulk value. This intercept 4.58 eV/atom; is in good agreement with the experimental bulk value of 4.45 eV/atom as reported by Voter and Chen (Voter and Chen, 1987).

REFERENCES

Baker, J.; Muir, M.; Andzelm, J.; Scheiner, A. ACS Symposium Series 1996, 629, 342-367.

Bao, S., Hofmann, Ph., Schindler, K.M., Fritzsche, V., Bradshaw, A.M., Woodruff, D.P., Casado, C., Asensio, M.C., 1994, "Following the changes in local geometry associated with a surface reaction: the dehydrogenation of adsorbed ethylene", J. Phys. Condens. Matter 6: L93–L98

Becke, A.D., 1988, "Density- Functional Exchange Energy Approximation with Correct Asympthotic Behavior", Phys. Rev. B, 38: 3098-3100

Becke, A.D., Roussel, M.R., 1989, "Exchange Holes in Inhomogeneous Systems- A Coordinate Space Model" , Phys. Rev. A., 39: 3761-3767

Beeck, O., 1950, "Hydrogenation Catalysis", Discussions Faraday Soc., 8, 118-128

Beeck, O., Smith, A.E., Wheeler, A., 1940, Proc. Roy. SOC. (London), 177, 63

Bernardo, G.P.M., Gomes, J.A.N.F., 2001, "Theoretical Aspects of Heterogeneous Catalysis", Kluwer Academic Publishers, Netherlands

Bernardo, C.G.P.M. , Gomes, J.A.N.F., 2001, "The adsorption of ethylene on the (100) surfaces of platinum, palladium and nickel: a DFT study" , J. Mol. Struct., (Theochem) 542: 263–271

Bond, G.C., 1962, "Catalysis by Metals", Academic Press, New York

Brown, W.A., Kose, R., King, D.A., 1999, “The role of adsorption heats and bond energies in the assignment of surface reaction products: ethyne and ethene on Ni(110)”, J. Mol. Catal. A: Chem. 141: 21–29

Calleja, M., Rey, C., Alemany, M.M.G., Gallego, L.J., Ordejon, P., Sanchez-Portal, D., Artacho, E., Soler, J.M., 1999, “Self-consistent density-functional calculations of the geometries, electronic structures, and magnetic moments of Ni-Al clusters”, Phys.Rev.B, 60: 2020-2024

Ceyer, S.T., 2001, “The Unique Chemistry of Hydrogen beneath the Surface: Catalytic Hydrogenation of Hydrocarbons”, Acc. Chem. Res., 34, 737-744

Cremer, P., Stanners, C., Niemantserdriet, J. W., Shen, Y. R., Somorjai, G. A., 1995, “The conversion of di-σ bonded ethylene to ethylidyne on Pt(111) monitored with sum frequency generation: evidence for an ethylidene (or ethyl) intermediate”, Surf. Sci., 328, 111-118

Christensen, A., Stoltze, P., Norskov, J.K., 1995, “Size dependence of phase separation in small bimetallic clusters”, J. Phys. Condens. Matter, 7: 1047-1057

Cleveland, C.L., Landman,U., 1991, “The energetics and structure of nickel clusters: Size dependence”,J. Chem. Phys., 94: 7376-7396

Crispin, X., Lazzaroni, R., Geskin, V., Baute, N., Dubois, P., Jrme, R., Brdas, J.L.,1999, “Controlling the Electrografting of Polymers onto Transition Metal Surfaces through Solvent vs Monomer Adsorption” J. Am. Chem. Soc. 121(1): 176–187

Daley, S.P., Utz, A.L., Trautman, T.R., Ceyer, S.T., 1994, “Ethylene Hydrogenation on Ni(11 1) by Bulk Hydrogen”, J. Am. Chem. Soc., 116: 6001-6002

Dalmai-Imelik, G., Massardier, J., 1977, “Catalytic Activity of Single-Crystal Faces: Ethylene and Benzene Hydrogenation on (111), (110) and (100) Faces of Ni.”, In Proceedings of the Sixth International Congress on Catalysis, Chemical Society: London, 90-100.

Daw, M.S., Foiles, S.M., Baskes, M. I., 1993, “The embedded-atom method: a review of theory and applications”, Mater. Sci. Rep. 9: 251-310

Doye, J. P. K., Wales, D. J., 1998, “Global minima for transition metal clusters described by Sutton.Chen potentials”, New J. Chem. 22: 733-744

Dumesic, J.A., Rudd, D.F., Aparicio, L.M., Rekoske, J.E., Trevino, A.A., 1993, “The Microkinetics of Heterogeneous Catalysis”, American Chemical Society, Washington, DC

Egawa, C., Iwai, H., Oki, S., 2000, “Ethylene hydrogenation on fcc Co and Fe thin films grown on Ni(100)”, 454–456 : 347–351

Fahmi, A., van Santen, R.A., 1997, “Density functional study of acetylene and ethylene adsorption on Ni(111)”, Surf. Sci. 371: 53–62

Filhol, J.S., Simon, D., Sautet, P., 2004, “Understanding the High Activity of a Nanostructured Catalyst Obtained by a Deposit of Pd on Ni: First Principle Calculations”, J. AM. CHEM. SOC. , 126, 3228-3233

Frisch, M.J., Trucks, G.W., Schlegel, H.B., Scuseria, G.E., Robb, M.A., Cheeseman, J.R., Montgomery Jr., J.A., Vreven, T., Kudin, K.N., Burant, J.C., Millam, J.M., Iyengar, S.S., Tomasi, J., Barone, V., Mennucci, B., Cossi, M., Scalmani, G., Rega, N., Petersson, G.A., Nakatsuji, H., Hada, M., Ehara, M., Toyota, K., Fukuda, R., Hasegawa, J., Ishida, M., Nakajima, T., Honda, Y., Kitao, O., Nakai, H., Klene, M., Li, X., Knox, J.E., Hratchian, H.P., Cross, J.B., Bakken, V., Adamo, C., Jaramillo, J., Gomperts, R., Stratmann, R.E., Yazyev, O., Austin,

A.J., Cammi, R., Pomelli, C., Ochterski, J.W., Ayala, P.Y., Morokuma, K., Voth, G.A., Salvador, P., Dannenberg, J.J., Zakrzewski, V.G., Dapprich, S., Daniels, A.D., Strain, M.C., Farkas, O., Malick, D.K., Rabuck, A.D., Raghavachari, K., Foresman, J.B., Ortiz, J.V., Cui, Q., Baboul, A.G., Clifford, S., Cioslowski, J., Stefanov, B.B., Liu, G., Liashenko, A., Piskorz, P., Komaromi, I., Martin, R.L., Fox, D.J., Keith, T., Al-Laham, M.A., Peng, C.Y., Nanayakkara, A., Challacombe, M., Gill, P.M.W., Johnson, B., Chen, W., Wong, M.W., Gonzalez, C., Pople, J.A., ,2004, "Gaussian 03, Revision D.01, Gaussian, Inc., Wallingford, CT,

Fulton, J.W., Crosser, O.K., 1965, "Influence of Catalyst Particle Size on Reaction Kinetics: Hydrogenation of Ethylene on Nickel", 11(3): 513-520

Ghiotti, G., Boccuzzi, F., Chiorino, A., 1989, Stud. Surf. Sci. Catal. 48: 415–423

Grigoryan,V.G., Springborg, M., 2001, "A theoretical study of the structure of Ni clusters (Ni_N)", Phys. Chem. Chem. Phys, 3: 5135-5139

Grigoryan, V.G., Springborg, M., 2003, "Structure and energetics of Ni clusters with up to 150 atoms" Chem. Phys. Lett. 375: 219-226

Hasse, W., Günter, H.; Henzler, M., 1983, "Study of Self-Hydrogenation of Ethene on Clean Ni(111).", Surf. Sci., 126: 479-486.

Harinipriya, S., Sangaranarayanan, M.V., 2004, "Estimation of the activation energies for heterogeneous catalytic processes from thermodynamic and structural considerations", Journal of Molecular Catalysis A: Chemical, 207: 107-116

Haug, K.L., Bürgi, T., Gostein, M., Trautman, T.R., Ceyer, S.T., 2001, "Catalytic Hydrogenation of Acetylene on Ni(111) by Surface-Bound H and Bulk H", J. Phys. Chem. B, 105: 11480-11492

Heinrichs, B., Schoebrechts, J.-P., Pirard, J.-P., 2001, "Palladium–Silver Sol–Gel Catalysts for Selective Hydrodechlorination of 1,2-Dichloroethane into Ethylene: III. Kinetics and Reaction Mechanism", J. Catal. 200: 309–320.

Horiuti, I., Polanyi, M., 1934, "Exchange reactions of hydrogen on metallic surfaces", Trans. Faraday Sci. 30: 1164–1172

Huang, W., McCormick, J.R., Lobo, R. F., Chen, J.G., 2007, "Selective hydrogenation of acetylene in the presence of ethylene on zeolite-supported bimetallic catalysts", Journal of Catalysis, 246: 40–51

Ibach, H., Lehwald, S., 1981, "Angular Profiles in EELS and the assignment of vibrational modes", J. Vac. Sci. Technol. 18: 625–628

Janssens, T. V. W., Stone, D., Hemminger, J. C., Zaera, F., 1998, "Kinetics and mechanism for the H/D exchange between ethylene and deuterium over Pt(111)", J. Catal., 177: 284-295

Johnson, A., Maynard, K., Daley, S., Yang, Q., Ceyer, S. T., 1991, "Hydrogen Embedded in Ni: Production by Incident Atomic Hydrogen and Detection by High-Resolution Electron Energy Loss", Phys. Rev. Lett., 67: 927-930

Kar'kin, I.N., Kar'kina, L.E., Gornostyrev, Yu. N., 2008, "Effect of Chemical Interaction on the Stability of Metal Clusters in FCC Metals", The Physics of Metals and Metallography, 106: 260-265.

Kirk-Othmer Encyclopedia of Chemical Technology, "Ethylene," John Wiley & Sons, Inc. 10: 593–632

Klots, T. D., Winter, B. J., Parks, E. K., Riley, S. J., 1991, "Icosahedral Structure in Hydrogenated Cobalt and Nickel Clusters", Journal of Chemical Physics, 95: 8919-8930

Kohn, W., Sham, L.J., 1965, “Self Consistent Equations Including Exchange and Correlation Effects”, Phys. Rev., 140: A1133–A1138
Kuchitsu, K. In *Structure Data of Polyatomic Molecules*; Kuchitsu, K., Ed.; Springer-Verlag: Berlin, 1992

Laidler, K.J., Townshend, R.E., 1961, “Kinetics of the Ethylene Hydrogenation on Evaporated Nickel and Iron Films”, Transactions of the Faraday Society, volume 57, issue 9

Land, T. A., Michely, T., Behm, R., Hemminger, J. C., Comsa, G., 1992, “Direct observation of surface reactions by scanning tunneling microscopy: Ethylene→ethylidyne→carbon particles→graphite on Pt(111) ”, J. Chem. Phys., 97: 6774- 6783

Lathiotakis, N.N., Andriotis, A. N., Menon, M., Connolly, J., 1996, “Tight binding molecular dynamics study of Ni clusters”, J. Chem. Phys. 104: 992-1003

Lee, C., Yang, W., Parr, R.G., 1988, “Development of the Colle-Salvetti Correlation- Energy Formula into a Functional of the Electron”, Phys. Rev. B, 37: 785-789

Lehwald, S., Ibach, H., 1979, “Decomposition of Hydrocarbons on Flat and Stepped Ni(111).”, Surf. Sci., 89, 425-445

Lopez, N., Janssens, T.V.W., Clausen, B.S., Xu, Y., Mavrikakis, M., Bligaard, T., Norskov, J.K., 2004, “On the origin of the catalytic activity of gold nanoparticles for low-temperature CO oxidation”, J. Catal. 223: 232–235

Luo, C., 2002, “Energies and structural properties of nickel clusters determined by tight-binding simulations: Ni_4–Ni_{55}”, Modelling Simul. Mater. Sci. Eng., 10: 13-20

Montejano-Carrizales, J. M., Iñiguez, M.P., Alonso, J.A., J.Cluster Sci., 1994, 5, 287

Montejano-Carrizales, J.M., Iñiguez, M.P., Alonso, J.A., Lopez, M.J., 1996, "Theoretical study of icosahedral Ni clusters within the embedded-atom method", Phys. Rev. B 54: 5961-5969

Moors, M., Bocarme´, T.V., Kruse, N., 2007, "Surface reaction kinetics studied with nanoscale lateral resolution", Catalysis Today, 124: 61-70

Nayak, S.J., Khanna, S.N., Rao, B.K., Jena, P., 1997, "Physics of nickel clusters: Energetics and equilibrium geometries", J. Phys. Chem., 101: 1072-1080

Neurock, M., Hansen, E.W., 1998, "First-Principles-Based Molecular Simulation of Heterogeneous Catalytic Surface Chemistry", Compurers them. Engng., 22: 1045-l060.

Neurock, M., van Santen, R.A., 2000, "A First Principles Analysis of C−H Bond Formation in Ethylene Hydrogenation", J. Phys. Chem. B, 104 (47): 11127-11145

Norskov, J.K., 1991, "Electronic factors in catalysis", Prog. Surf. Sci., 38: 103-144.

Northby, J.A., 1987, "Structure and binding of Lennard-Jones clusters: 13≤N≤147", J. Chem. Phys. 87: 6166-6177

Onal, I., Sayar, A., Uzun, A., Ozkar, S., 2009, "A Density Functional Study of Ni_2 and Ni_{13} Nanoclusters", J. Comput. Theor. Nanosci. 6: 867–872

Park, C., Keane, M.A., 2004, "Catalyst support effects in the growth of structured carbon from the decomposition of ethylene over nickel", 221: 386–399

Parks, E.K., Riley, S.J., 1995, “Nickel cluster structure determined from the adsorption of molecular nitrogen: Ni_{49}-Ni_{71}”, Z. Phys. D, 33: 59-70

Parks, E. K., Winter, B. J., Klots, T. D., Riley, S. J., 1991, “The Structure of Nickel Clusters”, Journal of Chemical Physics 94: 1882-1902

Parks, E.K., Zhu, L., Ho, J., Riley, S.J., 1994, “The structure of small nickel clusters. I. Ni_3–Ni_{15}”,J. Chem. Phys. 100: 7206-7222

Parks, E.K., Zhu, L., Ho, J., Riley, S.J., 1995, “The structure of small nickel clusters. II. Ni_{16}–Ni_{28} ”, J. Chem. Phys. 102: 7377-7389

Pauls, A.C., Comings, E.W., Smith, J.M., 1959, “Kinetics of the Hydrogenation of Ethylene”, AICHE JOURNAL, Volume: 5 Issue: 4 Pages: 453-457

Pellarin, M., Baguenard, B., Vialle, J.L., Lerme, J., Broyer, M., Miller J., Perez, A., 1994, “Evidence for icosahedral atomic shell structure in nickel and cobalt clusters.Comparison with iron clusters”, Chem. Phys. Lett. 217: 349-356.

Pirard, S.L., Heinrichs, B., Heyen, G., Pirard, J.P., 2008, “Optimization of experimental procedure and statistical data treatment for kinetics of ethylene hydrogenation on a copper-magnesia catalyst”, Chemical Engineering Journal, 138: 367–378

Qi, Y., Çağin, T., Johnson,W.L., Goddard W.A., 2001, “Melting and crystallization in Ni nanoclusters: The mesoscale regime”, J. Chem. Phys., 115: 385-394

Raghavan, K., Stave, M.S., DePristo, A.E., 1989, “Ni Clusters- Structures and Reactivity with D2”, J. Chem. Phys., 91: 1904-1917

Reuse, F.A., Khanna, S.N., 1995, " Geometry, electronic structure, and magnetism of small Ni_n (n = 2–6, 8, 13) clusters", Chem. Phys. Lett. 234: 77-81

Rosei, F., 2004, "Nanostructured surfaces: challenges and frontiers in Nanotechnology", J. Phys. Condens. Matter., 16: 1373–1436

Schmid, G., 1991, "Large metal clusters and colloids — Metals in the embryonic state" Chem. Rev. 92: 1709-1727

Schmid, G., Maihack, V., Lantermann, F., Peschel, S., 1996, "Ligand-stabilized metal clusters and colloids: properties and applications", J. Chem. Soc., Dalton Trans., 589–595

Singh, R., Kroll, P., 2008, "Structural, electronic, and magnetic properties of 13-, 55-, and 147-atom clusters of Fe, Co, and Ni: A spin-polarized density functional study", Physical Review B, Issue: 24 Article Number: 245404

Stave, M.S., DePristo, A.E., 1992, "The structure of Ni_N and Pd_N clusters: $4 \leq N \leq 23$", J. Chem. Phys. 97: 3386-3389

Stoltze, P., 1994, "Simulation of surface defects", J. Phys. Condens. Matter 6: 9495-9517

Twigg, G.H., 1950, "The Mechanism of Catalytic Hydrogenation of Ethylene", Discussions Faraday Soc., 8, 152-159

Van Santen, R.A., Neurock, M., 2006, "Molecular Heterogeneous Catalysis", Wiley-VCH, Weinheim

Van Santen, R.A., Niemantsverdriet, J.W., 1995, "Chemical Kinetics and Catalysis", Plenum Press, New York

Vang, R.T., Honkala, F.K., Dahl, S., Vestergaard, E.K., Schnadt, J., Lagsgaard, E., Clausen, B.S., Norskov, J.K., Besenbacher, F., 2006, "Ethylene dissociation on flat and stepped Ni(111): A combined STM and DFT study" Surf. Sci. 600: 66–77

Vlachos, D.G., Schmidt, D., Aris, R., 1992, "Structures of small metal clusters. I. Low temperature behavior", J. Chem. Phys. 96: 6880-6890

Voter A.F., Chen, S.P., 1987, "Accurate interatomic potentials for Ni, Al and Ni3Al", Mater. Res. Soc. Symp. Proc. 82: 175-180

Wang, Q., Lim, K.H., Yang, S.W., Yang, Y., Chen, Y., 2010, "Atomic carbon adsorption on Ni nanoclusters: a DFT study",Theor Chem Acc., accepted

Wetzel, T.L., DePristo, A.E., 1996, "Structures and energetics of Ni_{24}-Ni_{55} clusters" J. Chem. Phys. 105: 572-580

Winter, B. J., Klots, T. D., Parks, E. K., Riley, S. J., 1991, "Chemical-Identification of Icosahedral Structure for Cobalt and Nickel Clusters", Zeitschrift für Physik D-Atoms, Molecules and Clusters, 19: 375-380

Wyckof, R.W.G., "Crystal Structures", 2nd Edition, Volume 1, John Wiley & Sons, New York (1963)

Xiang, Y., Sun, D.Y., Gong, X.G., 2000, "Generalized Simulated Annealing Studies on Structures and Properties of Nin (n = 2-55) Clusters", J. Phys. Chem. A, 104: 2746-2751

Yagasaki, E., Masel, R. I., 1994, "Variation in the Mechanism of Catalytic Reactions with Crystal Face. In Catalysis; Spivey, J. L., S. K. A., Ed.; Royal Society of Chemistry: Cambridge, 1994; Vol. 11, p 163.

Yao, Y.H., Gu, X., Ji, M., Gong, X.G., Wang, D., 2007, "Structures and magnetic moments of Nin (n = 10 ~ 60) clusters", Physics Letters A, 360: 629–631

Yata, M., Madix, R.J., 1995, "Kinetic isotope effects and tunneling in C-H bond activation of ethylene and ethylidyne on Pt(111)", Surf. Sci., 328: 171-180

Yilmazer, N.D., Fellah M.F., Onal, I., 2010, "A density functional theory study of ethylene adsorption on Ni_{10}(1 1 1), Ni_{13}(1 0 0) and Ni_{10}(1 1 0) surface cluster models and Ni_{13} nanocluster", Applied Surface Science, 226: 5088-5093

Zaera, F., 1996, "On the mechanism for the hydrogenation of olefins on transition-metal surfaces: The chemistry of ethylene on Pt(111)" Langmuir: 12, 88-94

Zaera, F., Janssens, T. V. W., Ofner, H., 1996, "Reflection absorption infrared spectroscopy and kinetic studies of the reactivity of ethylene on Pt(111) surfaces" Surf. Sci., 368, 371-376

APPENDIX A

General Overview of Quantum Chemistry

"The goal of quantum mechanical methods is to predict the structure, energy and properties for an N-particle system, where N refers to both the electrons and the nuclei. The energy of the system is a direct function of the exact position of all of the atoms and the forces that act upon the electrons and the nuclei of each atom. In order to calculate the electronic states of the system and their energy levels, quantum mechanical methods attempt to solve Schrödinger's equation. While most of the work that is relevant to catalysis deals with the solution of the time-independent Schrödinger equation, more recent advances are in the development of time-dependent density functional. The time-independent Schrödinger equation is:

$$\hat{H}\Psi = E\Psi \tag{A1}$$

where Ψ is the wavefunction and E is the energy of the N-particle system. $\hat{H}$ is the Hamiltonian operator, which is comprised of the kinetic and potential energy operators which act on the overall system wavefunction Ψ. The wavefunction can extend between $+\infty$ and $-\infty$ and depends upon the positions of the atoms in the system along with the spin of each electron. The square of the wavefunction (Ψ^2) describes the probability distribution for the N-particle system. The Schrödinger equation is actually nothing more than a force balance on the electrons and the nuclei of the system. The Hamiltonian is comprised of two essential terms, the kinetic energy operator, $\hat{T}$, and the potential energy operator, $\hat{V}$. For an N-particle system, these operators can be written as

$$\hat{T} = -\sum_{i=1}^{N} T_i = -\sum_{i=1}^{N} \frac{\hbar}{2m_1} \bigtriangledown_i^2 = -\sum_{i=1}^{N} \frac{\hbar}{2m_i} \left(\frac{\partial^2}{\partial x^2} + \frac{\partial^2}{\partial y^2} + \frac{\partial^2}{\partial z^2} \right) \tag{A2}$$

$$\hat{V} = \sum_{i=1}^{N} \sum_{j>i}^{N} V_{ij} \tag{A3}$$

where T_i is the kinetic energy of particle i and V_i and V_j refer to the potential energy terms for electronic interactions between electron–electron, electron–nuclei and, nuclei–nuclei interactions.

A number of simplifying approximations are required to solve this N-particle system, as will be discussed later. The first is the Born–Oppenheimer approximation, which indicates that since the mass of an electron is nearly 2000 times smaller than the mass of a proton, the electrons move many orders of magnitude faster than nuclear motion. Therefore, the electronic motion can be strictly decoupled from the nuclear motion. The electronic wavefunction can then be solved separately for a fixed set of nuclear positions (R). The hamiltonian for the electronic system now becomes

$$\hat{H} = -\sum_{i}^{n} \frac{\hbar}{2m_i} \bigtriangledown_i^2 - \sum_{i}^{n} \sum_{a}^{N} \frac{Z_a}{|r_i - R_a|} e^2 + \sum_{i}^{n} \sum_{j>i}^{n} \frac{1}{|r_i - r_j|} e^2$$

$$Kinetic \quad Nuclear–Electron\ Attraction \quad Electron–Electron\ Repulsion$$

$$+ \sum_{a}^{n} \sum_{b>a}^{n} \frac{Z_a Z_b}{|R_a - R_b|} e^2$$

$$Nuclear–Nuclear\ Repulsion \tag{A4}$$

The first term of the hamiltonian describes the kinetic energy of the electron. The second term describes the attractive interaction between the electron and the nuclei where r_i and R_a refer to the positions of electron i and atom a. The number of electrons is defined as n and the number of nuclei as N. The third term describes electron–electron repulsion. The final term refers to the nuclear–nuclear

repulsive interactions. Since the nuclear charges are decoupled from the electronic wavefunction, this summation can be computed in a straight forward manner and does not change upon the solution to the electronic structure.

The Born–Oppenheimer approximation is usually a very good approximation since the nuclear mass is so much greater than the electronmass. Uncoupling the electronic motion from the nuclear motion enables one to solve for the electronic structure for a fixed set of nuclei. The final term, which describes electron–electron repulsion, prevents the direct solution to the electronic structure. The solution requires convergence of the electronic structure via an iterative scheme. This is known as the self-consistent field approximation, which is discussed later.

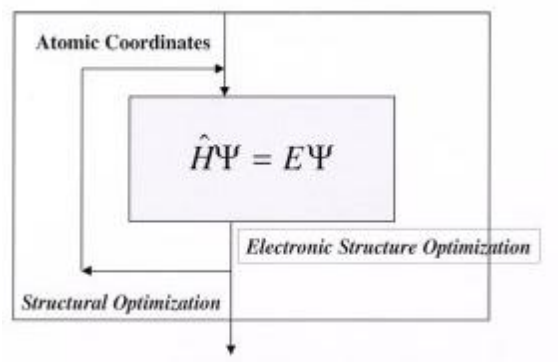

Figure A1. The lowest level hierarchical structure for most quantum mechanical computational algorithms. The inner loop is used to converge the self-consistent field in order to establish the electronic structure to within a user-defined tolerance. The outer loop is used to optimize the structure to within a defined geometric tolerance.

Nearly all quantum mechanical codes are comprised of the basic structure shown in Figure A1, where there are two primary nested loops. The inner loop requires the convergence of the electronic structure for a fixed set of atomic positions. The outer loop moves the atoms in order minimize the forces upon each atom and to converge upon the lowest energy of geometric structure for the system. The initial atomic positions are necessary to describe the starting

structure. The structure studied can be that of a simple molecule, a macromolecule, a bulk metal or metal oxide, the unit cell of a zeolite, a complex system comprised of catalytic surface along with adsorbates, solution molecules and ions, etc. Structures can be described in terms of Cartesian coordinates, direct coordinates, or z-coordinates. The electronic structure can be mathematically represented by an infinite number of basis functions. More practically, these functions are truncated and described by a finite number of basis sets. A wide range of different basis sets currently exist and depend on the solution method used, the type of problem considered and the degree of accuracy required for solution. These functions can take on one of several forms, including Slater-type functions, Gaussian functions, and plane waves. An infinite number of basis functions would be required for true accuracy and the complete electronic structure. This can be relaxed to a finite number of basis functions with some potential loss in accuracy. The number of basis functions used is then based on the relative degree of accuracy that one desires along with the CPU expenditures required to calculate. The structural positions of the atoms and their basis functions are the only chemically specific input. Of course, there are typically a number of additional variables which describe the state of the system (the number of electrons, orbital occupations and the charge of the system), the type of calculation performed (a single point calculation, geometry optimization, a transition-state search, a molecular dynamics simulation), instructions on how the calculation is performed (the electronic and geometric convergence criterion, the density mixing scheme), the relative accuracy of the calculation (expanded basis sets, increased energy cutoffs, etc.), and the specifications on output that are requested (orbitals, population analyses, density of states, frequencies, thermodynamic properties, etc.) that are all required (Van Santen and Neurock, 2006).

The Potential Energy Surface

The output from the simulation of an optimized molecular structure includes the optimized atomic coordinates, which define the optimal structure, the optimized electronic structure for these specific coordinates and the total energy for this system. A schematic of the optimization of the O_2 in the gas phase is shown in Figure A2.

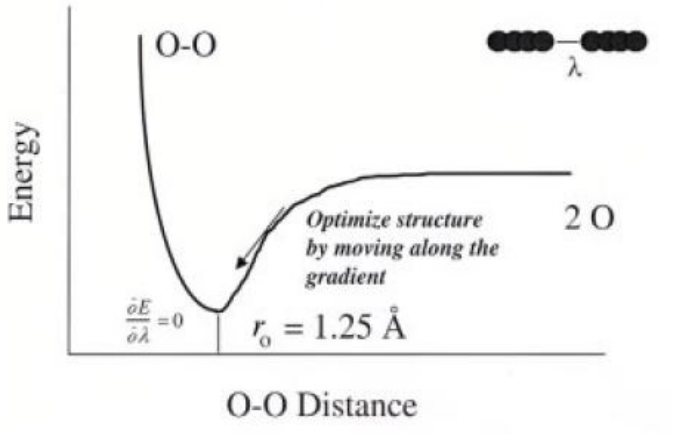

Figure A2. A schematic which shows the one-dimensional potential energy surface for O_2. The single defining internal coordinate, λ_i, is the distance between oxygen atoms. The energy is minimized when its derivative, with respect to changes in its Cartesian or its internal atomic coordinates, is zero ($dE/d\lambda_i = 0$) and the second derivative of energy, with respect to changes in its Cartesian or internal atomic coordinates, is greater than 0 ($d^2E/d\lambda^2_i > 0$).

The energy for the O_2 molecule is plotted at its initial starting geometry (i.e. λ= O–O distance = $2\dot{A}$) The electronic structure is calculated and subsequently used to determine the forces on each atom for the particular state that is being probed. These forces are then used to determine the new positions of the atoms in the system. This process is repeated in order to converge upon the energy for the optimized geometric structure. The results can be used to determine

a host of different molecular properties, including electron density, electron affinity, ionization potential, relative energies for reaction processes, vibrational spectroscopy and a wide range of other chemical properties.

As we move from the one-dimensional O_2 example shown in Figure A2, the potential energy surface becomes much more complicated.

Figure A3, depicts the presence of local and global minima as well as local and global maxima. The local, and a global minima ocur when the derivative of the energy with respect to the structural degree of freedom λ_i is zero for all degrees of freedom $\lambda_i(dE/d\lambda_i = 0)$. Transition states occur at saddle points along the potential energy surface. The derivative of the energy with respect to the degree of freedom λ_i is zero for all degrees of freedom for transition-state structures. In addition, the second derivative of the energy with respect to the degree of freedom λ_i is equal to zero for all degrees of freedom λ_i except for the mode which corresponds to the reaction coordinate.

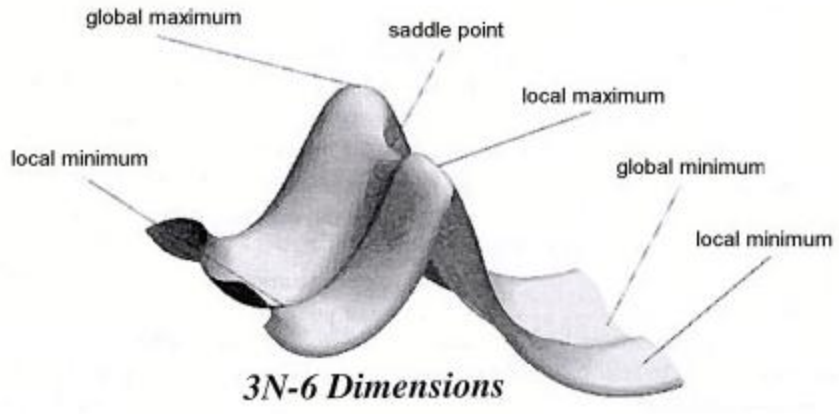

Figure A3. A more complex three-dimensional potential energy surface. The surface displays a global maximum and minimum ($dE/d\lambda_i = 0$) and transition (or saddle) points $d^2E/d\lambda_i{}^2 > 0$ for all modes, λ_i, except the reaction trajectory, which instead is defined as $d^2E/d\lambda i^2 < 0$."

(Van Santen and Neurock, 2006)

“General Electronic Structure Methods

Electronic structure methods can be categorized as ab initio wavefunction-based, ab initio density functional theoretical, or semiempirical methods. Wavefunction methods start with the Hartree–Fock (HF) solution and have a well-prescribed methods that can be used to increase its accuracy. One of the deficiencies of HF theory is that it does not treat electron correlation. Electron correlation is defined as the difference in the energy between the HF solution and the lowest possible energy for the particular basis set that is used. Electron correlation refers to the fact that the electrons in a system correlate their motion so as to avoid one another. This physical picture then points out the deficiency of describing electrons in fixed orbital states. The electrons in reality should be further apart than predicted by HF theory. An exact solution of the Schrödinger equation requires the full treatment of electron correlation along with complete basis sets. Although this is unachievable, the breakdown of the inaccuracies into correlation and basis set expansion provides for a well-prescribed way in which to improve continually the accuracy and approach the exact wavefunction for the N-particle system.

Density functional theory is also derived from first principles but is fundamentally different in that it is not based on the wavefunction but instead on the electron density of the N-particle system. Hohenberg and Kohn showed that the energy for a system is a unique functional of its electron density. The true exchange-correlation functional necessary to provide the exact DFT solution, however, is unknown. The accuracy of density functional theory (DFT) is then limited to quality of the exchange-correlation functional that is used.

Semi-empirical methods avoid the solution of multicenter integrals that describe electron–electron interactions and instead fit these interactions to match experimental data. We will only discuss ab initio wavefunction and DFT methods here as they are more reliable for calculations concerning heterogeneous catalytic surfaces.

A series of general approximations are necessary in order to solve the Schrödinger equation. Born–Oppenheimer and the time-independence approximations are introduced, which indicate that the energy of the system can be determined by solving for the electronic wavefunction." (Van Santen and Neurock, 2006)

Hartree–Fock Self Consistent Field Approximation

"The self-consistent field approximation is used to reduce the N-electron problem into the solution of n-single-electron systems. It reduces a 3n variable problem into n single electron functions that depend on three variables each. The individual electron–electron repulsive interactions shown in Eq. (A4) are replaced by the the repulsive interactions between individual electrons and an electronic field described by the spatially dependent electron density, $\rho(r)$. This avoids trying to solve the difficult multicenter integrals that describe electron–electron interactions. The only trouble is that the electron density depends upon how each electron interacts with it. At the same time, the electron interaction with the field depends upon the density. A solution to this dilemma is to iterate upon the density until it convergences. The electron density that is used as the input to calculate the electron-field interactions must be equivalent, to within some tolerance, to that which results from the convergence of the electronic structure calculation. This is termed the self-consistent field (SCF). This approach used in solving for n molecular orbitals within a self-consistent field is known as the Hartree–Fock solution. The molecular orbitals are the individual electronic states that describe the spatial part of the molecular spin orbital.

Electrons are fermions and have non-integral spin. The wavefunction must therefore be antisymmetric with respect to the exchange of spin, that is, $\Psi = -\Psi$. The Slater determinant shown in Eq. (A5) provides the simplest wave function with the correct antisymmetry.

$$\Psi(x_1, x_2, ...x_n) = \frac{1}{\sqrt{N!}} \begin{vmatrix} \psi_1(x_1) & \psi_2(x_1) & \dots & \psi_n(x_1) \\ \psi_1(x_2) & \psi_2(x_2) & \dots & \psi_n(x_2) \\ \dots & \dots & \dots & \dots \\ \psi_1(x_n) & \psi_2(x_n) & \dots & \psi_n(x_n) \end{vmatrix} \tag{A5}$$

The N-electron Schrödinger equation is now reduced to n single-electron problems that take the following form:

$$\hat{h}_i \psi_i = \varepsilon_i \psi_i \tag{A6}$$

$$\left[-\frac{1}{2} \bigtriangledown^2 + V_C(r) + \mu_x^i \right] \psi = \varepsilon_i \psi_i \tag{A7}$$

where ψ_i refer to the individual molecular orbitals. The single-electron Hamiltonian, which is shown here in brackets, depends upon the electronic distribution within the molecular orbitals Ψ_i. This is what leads to the SCF solution scheme where the electrons simply interact with an average potential. In this solution scheme, electron correlation which describes the interactions between electrons is not included. This results in much of the errors associated with the Hartree–Fock solution." (Van Santen and Neurock, 2006)

Basis Set Approximation

"The molecular orbitals can be described by a linear combination of atomic orbitals (X_i) as follows

$$\varphi_i(r) = \sum_{j=1}^{N_{basis}} C_{ij}\chi_j(r) \tag{A8}$$

where C_{ij} is a coefficient which relates the atomic orbital j to molecular orbital i. This is known as the basis set approximation. More generally, the basis functions presented in Eq. (A8) do not have to be atomic orbitals but can simply be a series of basis functions used to describe the molecular orbitals. Atomic orbitals tend to be the most natural choice of basis functions for molecular-based systems. Gaussian- or Slater-type basis functions are often used because they are easier to solve for computationally. Solid-state systems described by periodic methods, on the other hand, are more naturally represented by using periodic plane wave basis functions. In theory, the most accurate solution would require an infinite number of basis functions. Instead, the number of basis functions is truncated to a smaller set which is still able to capture the essential features of the wavefunction.

The accuracy can improve by increasing the number and extent of the basis orbitals. In the atomic basis scheme, for example, one can increase the number of basis functions on each atom to increase the size and spatial extent. In addition, polarization and diffuse functions can also be added to improve the displacement of electron density away from an atom in a particular environment as well as its spatial extent. In periodic systems, the number of plane waves must be expanded. Full ab initio treatments for complex transition metal systems are difficult owing to the expense of accurately simulating all of the electronic states of the metal. Much of the chemistry that we are interested in, however, is localized around the valence band. The basis functions used to describe the core electronic states can thus be reduced in order to save on CPU time. The two

approximations that are typically used to simplify the basis functions are the frozen core and the pseudopotential approximations. In the frozen core approximations, the electrons which reside in the core states are combined with the nuclei and frozen in the SCF. Only the valence states are optimized. The assumption here is that the chemistry predominantly takes place through interactions with the valence states. The pseudopotential approach is similar.

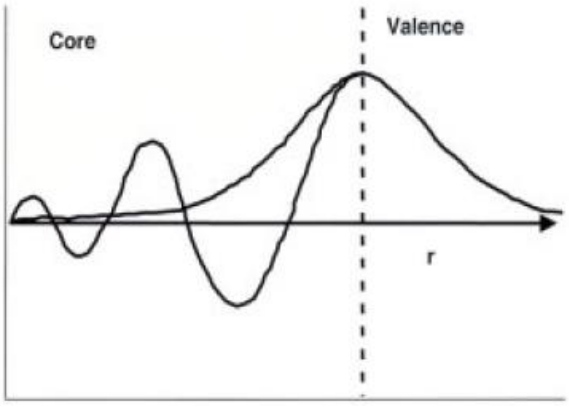

Figure A4. A schematic showing the comparison of the full electron wavefunction and the pseudopotential-derived wave function. The strongly bound core electrons are replaced by a smoother analytical function.

The valence electrons oscillate in the core region as is shown in Figure A4, which is difficult to treat using plane wave basis functions. Since the core electrons are typically insensitive to the environment, they are replaced by a simpler smooth analytical function inside the core region. This core can also now include possible scalar relativistic effects. Both the frozen core and pseudopotential approximations can lead to significant reductions in the CPU requirements but one should always test the accuracy of such approximations." (Van Santen and Neurock, 2006)

Hartree–Fock Solution Strategy

"The single-electron wave equations from Eq. (A6) can be written in a more compact matrix form as the following equation:

$$F^t C^t = S C^t \varepsilon \tag{A9}$$

where F^t, C^t and S refer to the Fock, orbital coefficient and orbital overall intergral matrices, respectively. ε is a diagonal matrix which is comprised of the molecular orbital energies. Hall and Roothaan, simultaneously, proposed a solution strategy to solve the Hartree–Fock system based on the following secular equations:

$$\sum_{\nu=1}^{N} \left(F_{\mu\nu} - \varepsilon_i S_{\mu\nu} \right) c_{\nu i} = 0 \tag{A10}$$

where $F_{\mu\nu}$ refers to the Fock operator elements, $H_{\mu\nu}$ are the Hamiltonian elements, $S_{\mu\nu}$ are the overlap integrals for electrons in orbitals μ and ν, and $C_{\nu i}$ are the molecular orbital coefficients. These matrix elements are defined by the following equations:

$$F_{\mu\nu} = H_{\mu\nu}^{core} + \sum_{i}^{N/2} \sum_{\lambda}^{N_{basis}} \sum_{\sigma}^{N_{basis}} C_{\nu i} C_{\sigma i} \Big[2(\mu\nu|\lambda\sigma) - (\mu\sigma|\lambda\nu) \Big] \tag{A11}$$

$$H_{\mu\nu}^{core} = \int \mathrm{d}\overline{r}_1 \chi_\mu(\overline{r}_1) h(\overline{r}_1) \chi_\nu^*(\overline{r}_2) \tag{A12}$$

$$S_{\mu\nu} = \int \mathrm{d}\overline{r}_1 \chi_\mu(\overline{r}_1) \chi_\nu^*(\overline{r}_1) \tag{A13}$$

The terms (μν|λσ) and (μσ|λν) are electron repulsion integrals:

$$J_{ij} = (\mu\nu|\lambda\sigma) = \int\int \mathrm{d}\overline{r}_1\,\mathrm{d}\overline{r}_2\,\chi_\mu(\overline{r}_1)\chi^*_\nu(\overline{r}_1)\frac{1}{r_{12}}\chi_\lambda(\overline{r}_2)\chi^*_\sigma(\overline{r}_2) \tag{A14}$$

$$K_{ij} = (\mu\sigma|\lambda\nu) = \int\int \mathrm{d}\overline{r}_1\,\mathrm{d}\overline{r}_2\,\chi_\mu(\overline{r}_1)\chi^*_\sigma(\overline{r}_1)\frac{1}{r_{12}}\chi_\lambda(\overline{r}_2)\chi^*_\nu(\overline{r}_2) \tag{A15}$$

which more specifically refer to the Coulomb (J_{ij}) and exchange (K_{ij}) interaction between an electron and other electrons in the system. The specific orbital energy levels can be written in terms of core Hamiltonian elements along with the Coulomb and exchange energies as follows:

$$\varepsilon_i = H^{core}_{ij} + \sum_{j=1}^{N/2}(2J_{ij} - K_{ij}) \tag{A16}$$

The total energy of the ground-state system can then be written as:

$$E_{HF} = \frac{1}{2}\sum_{\mu=1}^{N}\sum_{\nu=1}^{N} P_{\mu\nu}\left(F_{\mu\nu} + H^{core}_{\mu\nu}\right) + \sum_{a\neq b}^{nucl}\frac{q_a q_b}{|R_a - R_b|} \tag{A17}$$

where P is the charge density matrix which is made up of the elements, $P_{\lambda\sigma}$, which are comprised of the orbital coefficients $C_{\lambda i}$ and σi evaluated over all occupied orbitals:

$$P_{\lambda\sigma} = 2\sum_{i=1}^{occupied} C_{\lambda i}C^*_{\sigma i} \tag{A18}$$

The spatial electron density ρ(r) is defined by the density matrix elements as follows:

$$\rho(r) = \sum_{\mu=1}\sum_{\nu=1} P_{\mu\nu}\,\phi_\mu(r)\phi_\upsilon(r) \tag{A19}$$

The solution strategy for solving for the self-consistent field and the final energy in the basic Hartree–Fock theory is shown in Figure A5. The user starts with a simple guess for the initial ρ(r) density or the orbital coefficient matrix, C. The coefficient matrix can then be used to calculate the Fock elements. The Hamiltonian and overlap elements are also computed and used to solve the Roothan–Hall equations. This results in a new set of orbital coefficients along with the overall energy for the system. The new orbital coefficients are used to calculate new density and Fock matrix elements along with a new system energy. The procedure continues until the calculated density (orbital coefficients) is the same as that which was used in the input to the problem. The results ultimately provide the electron density, orbital overlap and the final energy state levels of the system." (Van Santen and Neurock, 2006)

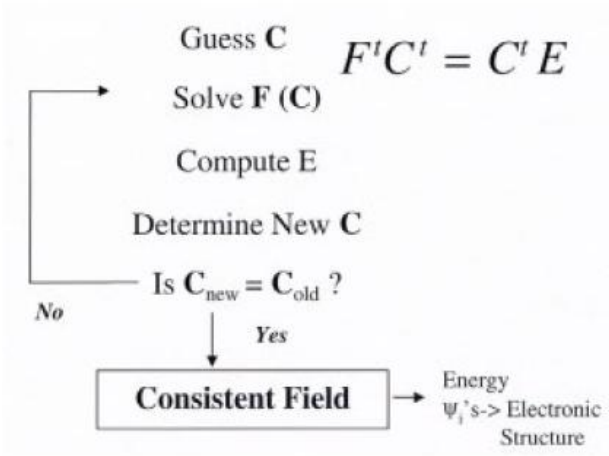

Figure A5. Schematic illustration of the basic solution strategy for solving for the self–consistent field and the final energy in Hartree–Fock methods.

Density Functional Theory

"The development of density functional theory (DFT) has had a tremendous impact on modeling heterogeneous catalytic systems. There are now a number of reviews which describe the application and impact of DFT on catalysis. The relative accuracy of DFT, along with the size of the systems that it can handle, makes it attractive for modeling heterogeneous catalytic systems. Density functional theory is derived from first-principles and does not require adjustable parameters. DFT methods formally scale as N3 and thus permit more realistic models of the intrinsic reaction than can be afforded by higherlevel wavefunction-based methods. Density functional theory can be traced to the developments by Thomas, Fermi and Dirac in which electron correlation was treated as a functional of the electron gas. The practical application of DFT theory, however, is attributed to work of Hohenberg and Kohn, who formally proved that the ground-state energy for a system is a unique functional of its electron density. Kohn and Sham extended the theory to practice by showing how the energy could be partitioned into kinetic energy for the motion of the electrons, potential energy for the nuclear–electron attraction, electron–electron repulsion which involves with Coulomb as well as self interactions and exchange correlation which covers all other electron–electron interaction. The energy of an *N*-particle system can then be written as

$$E[\rho] = T[\rho] + U[\rho] + E_{XC}[\rho] \tag{A20}$$

Kohn and Sham demonstrated that the *N*-particle system could be rewritten as a set of *n*-electron problems (similar to the molecular orbitals in wavefunction methods) that could be solved self-consistently in a manner which was similar to the SCF wavefunction methods. Namely,

$$\hat{H}\psi_i = \varepsilon_i \psi_i \tag{A21}$$

or more specifically

$$\left[-\frac{\hbar^2}{2m} \bigtriangledown^2 + V_{ion}(r) + \frac{e^2}{2} \int \frac{\rho(r)\rho(r')}{|r-r'|} \mathrm{d}^3 r + V_{XC}(r) \right] \psi_i(r) = \varepsilon_i \psi_i(r) \tag{A22}$$

The first three terms are similar to HF theory, thus corresponding to the kinetic energy of the electron, the potential for nuclear–electron attractive interactions and the Hartree repulsive interactions between electrons. The final term, $V_{XC}(r)$, corresponds to the Exchange correlation potential which is the derivative of the exchange correlation energy with respect to the density. This is more formally recognized as the chemical potential and written as

$$\mu_{XC}(r) = \frac{\delta E_{XC}[\rho(r)]}{\delta \rho[r]} \tag{A23}$$

The total energy of the system is then defined as

$$E[\{\psi\}] = 2 \sum_i \psi_i \left[-\frac{\hbar^2}{2m} \right] \bigtriangledown^2 \psi \mathrm{d}^3 r + \int V_{ion}(r)\rho(r)\mathrm{d}^3 r + \frac{e^2}{2} \int \frac{\rho(r)\rho(r'}{|r-r'|} \mathrm{d}^3 r \mathrm{d}^3 r' + E_{XC}\left[\rho(r)\right] + E_{ion}(\{R_i\}) \tag{A24}$$

The energy is formally a function of the density. The density of the system is still written as the sum of squares of the Kohn–Sham orbitals:

$$\rho(r) = \sum_{OCC} |\psi_i(r)|^2 \tag{A25}$$

The Kohn–Sham equations are solved in a very similar manner to that used to solve the Hartree–Fock system in that one iterates on the correct spatial distribution of the electron density. In the theory presented thus far, DFT can be considered as an exact approach. Unfortunately, the exchange correlation energy is not known. It is at this point where approximations must be introduced in order to solve the electronic structure problem. The most basic solution to Eq. (A22) is to invoke the local density approximation which assumes that exchange-correlation per electron is equivalent to the exchange correlation per electron in a *homogeneous electron gas* which has the same electron density at a specific point *r*. This is typically written as:

$$E_{XC}(r) = \int \rho(r)\varepsilon_{XC}\Big[\rho(r)\Big]\,\mathrm{d}r \tag{A26}$$

The local density approximation (LDA) is valid only in the region of slowly varying electron density. The LDA approximation is obviously an oversimplification of the actual density distribution and is well-known to lead to calculated bond and binding energies that are over-predicted. One of the primary shortcomings of the local density approximation is that the Exchange correlation charge distribution is not spherically homogeneous. Non-local gradient corrections are introduced to allow for non-spherical electron density distributions. As such, the correlation and exchange energies are functionals of both the density and the gradient with respect to the density. These gradient corrections take on various different functional forms which include the BP86 (Becke and Perdew corrections), PW91 (Perdew–Wang exchange functional), PBE (Perdew–Burke–Ernzerhof) or RPBE (Revised PBE functional). By way of example, the widely used Becke (B88) correction to the Local Spin Density Approximation to the exchange is given by

$$E_x^g = b\sum_\sigma \frac{\rho_\sigma x_\sigma^2}{|1 + 6bx_\sigma \sin h^{-1}x_\sigma}\,\mathrm{d}r \tag{A28}$$

where

$$x_\sigma \equiv \frac{\bigtriangledown \rho}{\rho_\sigma^{4/3}} \tag{A29}$$

The functional takes on the correct r^{-1} asymptote behavior. x_σ is the dimensionless density gradient shown in Eq. (A29) and ρ_σ is the density. The term *b* is simply a fitting parameter for the energy that is regressed against atomic data. Despite the importance of the exchange correlation functional, there is no formal path toward the development of more accurate functionals. The accuracy of DFT is therefore typically less than what can be expected from higher level ab initio methods such as coupled-cluster theory. More recent developments in functionals attempt to couple an exchange component derived from Hartree–Fock theory which provides for a more exact match of the exchange energy for single determinant systems along with the correlation (and exchange) calculated from LDA theory in "hybrid" functionals. The most notable is the B3LYP functional, which is a combination of the Lee, Yang and Parr functional and the three-parameter model by Becke:

$$E_X^{B3LYP} = a_0 H_x^{HF} + (1 - a_0) E_x^{LDA} + a_x E_x^{B88} + (1 - a_c) E_C^{VWN} + a_c E_c^{LYP} \tag{A30}$$

The theoretical chemistry community developed density functional theory for finite molecular systems which involve molecules and cluster models that describe the catalytic systems. They use the same constructs used in many ab initio wavefunction methods, i.e. Gaussian or Slater basis sets. The solid-state physics community, on the other hand, developed density functional theory to describe bulk solid-state systems and infinite surfaces by using a supercell approach along with periodic basis functions, i.e. plane waves. Nearly all of our discussion has focused on finite molecular systems. In the next section we will describe in more detail infinite periodic systems." (Van Santen and Neurock, 2006)

APPENDIX B

Examples of Input Files for Gaussian'03 Computations

B1: Input File for Ethylene Adsorption on Ni_{13}(1 0 0) Surface

Table B.1 Input file for adsorption reaction

```
%chk=ni100-spe5-631-EthyAdsEG.chk
%mem=400MW
%nprocshared=2
# opt=(modredundant,maxcycle=1000) b3lyp/6-31g(d,p) nosymm
geom=connectivity scf=(maxcycle=1000,conver=4)

Title Card Required

0 5
 Ni                19.38200000    7.04800000    8.81000000
 Ni                19.38200000    8.81000000    7.04800000
 Ni                17.62000000    8.81000000    8.81000000
 Ni                19.38200000   10.57200000    8.81000000
 Ni                19.38200000    5.28600000   10.57200000
 Ni                17.62000000    7.04800000   10.57200000
 Ni                19.38200000    7.04800000   12.33400000
 Ni                19.38200000    8.81000000   10.57200000
 Ni                17.62000000    8.81000000   12.33400000
 Ni                17.62000000   10.57200000   10.57200000
 Ni                19.38200000   10.57200000   12.33400000
 Ni                19.38200000   12.33400000   10.57200000
 Ni                19.38200000    8.81000000   14.09600000
 H                 19.38200000    7.67900000    5.91700000
 H                 18.25100000    8.81000000    5.91700000
 H                 19.38200000    4.15500000    9.44100000
 H                 19.38200000    5.91700000    7.67900000
 H                 18.25100000    5.91700000    8.81000000
 H                 18.25100000    5.28600000    9.44100000
 H                 17.62000000    5.91700000    9.44100000
 H                 18.25100000    7.04800000    7.67900000
 H                 18.25100000    7.67900000    7.04800000
 H                 17.62000000    7.67900000    7.67900000
 H                 18.25100000    4.15500000   10.57200000
 H                 16.48900000    9.94100000   12.33400000
 H                 16.48900000   10.57200000   11.70300000
 H                 16.48900000   11.70300000   10.57200000
 H                 17.62000000   11.70300000   11.70300000
 H                 18.25100000   11.70300000   12.33400000
 H                 18.25100000   12.33400000   11.70300000
 H                 18.25100000   13.46500000   10.57200000
 H                 19.38200000   13.46500000   11.70300000
 H                 16.48900000    8.81000000   13.46500000
 H                 18.25100000    8.81000000   15.22700000
```

Table B.1 Cont'. Input file for adsorption reaction

```
H                  17.62000000    9.94100000   13.46500000
H                  18.25100000   10.57200000   13.46500000
H                  18.25100000    9.94100000   14.09600000
H                  19.38200000    9.94100000   15.22700000
H                  19.38200000   11.70300000   13.46500000
H                  19.38200000    4.15500000   11.70300000
H                  19.38200000    5.91700000   13.46500000
H                  19.38200000    7.67900000   15.22700000
H                  19.38200000    9.94100000    5.91700000
H                  19.38200000   11.70300000    7.67900000
H                  19.38200000   13.46500000    9.44100000
H                  18.25100000    5.28600000   11.70300000
H                  17.62000000    5.91700000   11.70300000
H                  18.25100000    5.91700000   12.33400000
H                  18.25100000    7.04800000   13.46500000
H                  17.62000000    7.67900000   13.46500000
H                  18.25100000    7.67900000   14.09600000
H                  18.25100000   11.70300000    8.81000000
H                  17.62000000   11.70300000    9.44100000
H                  18.25100000   12.33400000    9.44100000
H                  18.25100000    9.94100000    7.04800000
H                  17.62000000    9.94100000    7.67900000
H                  18.25100000   10.57200000    7.67900000
H                  16.48900000    7.67900000    8.81000000
H                  16.48900000    7.04800000    9.44100000
H                  16.48900000    8.81000000    7.67900000
H                  16.48900000    9.94100000    8.81000000
H                  16.48900000   10.57200000    9.44100000
H                  16.48900000    5.91700000   10.57200000
H                  16.48900000    7.04800000   11.70300000
H                  16.48900000    7.67900000   12.33400000
H                  16.48900000    8.81000000    9.94100000
H                  16.48900000    8.17900000   10.57200000
H                  16.48900000    8.81000000   11.20300000
H                  16.48900000    9.44100000   10.57200000
H                  21.14693152    8.56793818    9.08262263
C                  21.13769481    8.28810776   10.13259554
C                  21.14756862    9.19948984   11.10142353
H                  21.11995271    7.22314701   10.34795214
H                  21.13832500    8.91966417   12.15139428
H                  21.16531362   10.26444516   10.88607027

1
2
3
4
5
6
7
8
9
10
11
12
13
14
15
16
17
18
19
20
```

Table B.1 Cont'. Input file for adsorption reaction

```
 21
 22
 23
 24
 25
 26
 27
 28
 29
 30
 31
 32
 33
 34
 35
 36
 37
 38
 39
 40
 41
 42
 43
 44
 45
 46
 47
 48
 49
 50
 51
 52
 53
 54
 55
 56
 57
 58
 59
 60
 61
 62
 63
 64
 65
 66
 67
 68
 69
 70 71 1.0
 71 72 2.0 73 1.0
 72 74 1.0 75 1.0
 73
 74
 75

X 1 F
X 2 F
X 3 F
X 4 F
X 5 F
X 6 F
```

Table B.1 Cont'. Input file for adsorption reaction

```
X 7 F
X 8 F
X 9 F
X 10 F
X 11 F
X 12 F
X 13 F
X 14 F
X 15 F
X 16 F
X 17 F
X 18 F
X 19 F
X 20 F
X 21 F
X 22 F
X 23 F
X 24 F
X 25 F
X 26 F
X 27 F
X 28 F
X 29 F
X 30 F
X 31 F
X 32 F
X 33 F
X 34 F
X 35 F
X 36 F
X 37 F
X 38 F
X 39 F
X 40 F
X 41 F
X 42 F
X 43 F
X 44 F
X 45 F
X 46 F
X 47 F
X 48 F
X 49 F
X 50 F
X 51 F
X 52 F
X 53 F
X 54 F
X 55 F
X 56 F
X 57 F
X 58 F
X 59 F
X 60 F
X 61 F
X 62 F
X 63 F
X 64 F
X 65 F
X 66 F
X 67 F
X 68 F
X 69 F
```

B2: Input File for Equilibrium Geometry Calculation for the Rideal –I Type Ethylene Hydrogenation Reaction Mechanism:

For Step 3, $C_2H_5(ads) + H(ads) \rightarrow C_2H_6(ads)$ (4.3)

Table B.2. Input file for equilibrium geometry

```
%chk=EG-Ni13-h2.chk
%mem=450MW
%nproclinda=2
%nprocshared=4
# opt=maxcycle=1000 b3lyp/6-31g(d,p) nosymm geom=connectivity
scf=(maxcycle=1000,conver=4)

Title Card Required

0 7
 Ni                -0.75644700   -0.81634000   -1.34269500
 Ni                -0.60546000   -0.89706800    1.09086600
 Ni                 1.02610400    0.05943000   -0.19178900
 Ni                 1.04932400    2.36986600   -0.15856000
 Ni                 2.57516400    1.12218900   -1.44564000
 Ni                 0.53270900    1.08750000    1.78172700
 Ni                 2.71554400    1.13841400    0.92073800
 Ni                 1.73329700   -0.97953000    1.66124500
 Ni                 0.27262900    1.22187600   -2.03985600
 Ni                -1.00471100    1.12020100   -0.04686300
 Ni                 1.47629500   -0.83003100   -2.21477700
 Ni                 0.81595600   -2.18674700   -0.28181900
 Ni                 3.09378100   -0.97210000   -0.38464800
 H                  4.76127700   -2.65218200   -1.86913000
 C                  4.80306900   -1.85112900   -1.12988400
 H                  4.12546800   -1.02105800   -1.62914400
 C                  4.48793000   -2.38405600    0.28670600
 H                  4.36473700   -3.46831500    0.27122800
 H                  5.27419200   -2.11668900    0.99384800
 H                  5.78559900   -1.37837700   -1.15769300
 H                  3.51954500   -2.05056900    0.82644100

 1 3 1.0 9 1.0 10 1.0 11 1.0 12 1.0
 2 3 1.0 6 1.0 8 1.0 10 1.0 12 1.0
 3 4 1.0 5 1.0 6 1.0 7 1.0 8 1.0 9 1.0 10 1.0 11 1.0 12 1.0 13 1.0
 4 5 1.0 6 1.0 7 1.0 9 1.0 10 1.0
 5 7 1.0 9 1.0 11 1.0 13 1.0
 6 7 1.0 8 1.0 10 1.0
 7
 8
 9 10 1.0 11 1.0
 10
 11
 12
 13
 14 15 1.0
 15 17 1.0 20 1.0
 16
 17 18 1.0 19 1.0
 18
 19
 20
 21
```

B3: Input File for Transition State Geometry Calculation for the Rideal –I Type Ethylene Hydrogenation Reaction Mechanism:

For Step 3, $C_2H_5(ads) + H(ads) \rightarrow C_2H_6(ads)$ (4.3)

Table B.3. Input file for transition state geometry

```
%chk=Transition-state.chk
%mem=1500MW
%nprocshared=8
# opt=(newton,maxcycle=1000,ts,noeigentest,calcfc,loose)
b3lyp/6-31g(d,p) nosymm geom=connectivity
scf=(XQC,maxcycle=3000,conver=6)

Title Card Required

0 7
 Ni                -0.60985400   -1.16223400   -1.09364200
 Ni                 0.02932000   -1.27092400    1.18062700
 Ni                 1.11399800    0.05144400   -0.28272800
 Ni                 0.78657300    2.32176400   -0.03658400
 Ni                 2.16214100    1.45098000   -1.72212200
 Ni                 0.89707400    0.86108700    1.81797900
 Ni                 2.85902100    1.34175500    0.54472000
 Ni                 2.45583100   -0.87208900    1.36813500
 Ni                -0.18568200    1.08326800   -1.83561400
 Ni                -0.95463400    0.73210900    0.35062200
 Ni                 1.30808900   -0.70983500   -2.41204700
 Ni                 1.54672200   -2.21787900   -0.40753800
 Ni                 3.21706700   -0.54868800   -0.93335800
 H                  5.11987200   -2.85117200   -1.46797900
 C                  4.91123900   -1.99325400   -0.82727300
 H                  4.80229200   -1.12316300   -1.54778600
 C                  3.68738900   -2.26372800    0.09775900
 H                  3.24905800   -3.24898500   -0.26308500
 H                  4.02789800   -2.53504200    1.10498100
 H                  5.80024400   -1.74563300   -0.24624700
 H                  3.82234300   -0.78449700    0.55148100

 1 2 1.0 3 1.0 9 1.0 10 1.0 11 1.0
 2 3 1.0 6 1.0 10 1.0 12 1.0
 3 4 1.0 5 1.0 6 1.0 7 1.0 8 1.0 9 1.0 10 1.0 11 1.0 12 1.0 13 1.0
 4 5 1.0 6 1.0 7 1.0 9 1.0 10 1.0
 5 7 1.0 9 1.0 11 1.0 13 1.0
 6 7 1.0 8 1.0 10 1.0
 7 8 1.0 13 1.0
 8 12 1.0
 9 10 1.0 11 1.0
 10
 11 13 1.0
 12 13 1.0
 13
 14 15 1.0
 15 17 1.0 20 1.0
 16
 17 19 1.0
 18
 19
 20
 21
```